LIGO Laboratory / LIGO Scientific Collaboration

LIGO-T070062-02-D *ADVANCED LIGO* 8/10/07

AOS: Stray Light Control (SLC) Conceptual Design

Michael Smith

Distribution of this document:
LIGO Science Collaboration

This is an internal working note
of the LIGO Project.

California Institute of Technology
LIGO Project – MS 18-34
1200 E. California Blvd.
Pasadena, CA 91125
Phone (626) 395-2129
Fax (626) 304-9834
E-mail: info@ligo.caltech.edu

Massachusetts Institute of Technology
LIGO Project – NW22-295
185 Albany St
Cambridge, MA 02139
Phone (617) 253-4824
Fax (617) 253-7014
E-mail: info@ligo.mit.edu

LIGO Hanford Observatory
P.O. Box 1970
Mail Stop S9-02
Richland, WA 99352
Phone 509-372-8106
Fax 509-372-8137

LIGO Livingston Observatory
P.O. Box 940
Livingston, LA 70754
Phone 225-686-3100
Fax 225-686-7189

http://www.ligo.caltech.edu/

Table of Contents

Table of Tables

Table of Figures

Abstract

This document will present the conceptual design for the AOS Stray Light Control subsystem for ADLIGO.

1 Introduction

1.1 Purpose

The purpose of this document is to present a conceptual design that meets the SLC Design requirements. Primary requirements are derived ("flowed-down") from the LIGO principal science requirements. Secondary requirements, which govern Detector performance through interactions between AOS and other Detector subsystems, have been allocated by Detector Systems Engineering.

1.2 Scope

This document will present conceptual designs for the Stray Light Control (SLC) subsystem of AOS under the following assumptions: 1) the recycling cavity is assumed to be marginally stable; 2) all wedge angles for the core optics components are vertical.

1.2.1 Stray Light Control

A block diagram showing the principal scattering sources of the AOS System is shown in Figure 1.

AOS is responsible for controlling and reducing the phase noise due to scattered light injected into the IFO mode to acceptable levels; except for scattering that occurs in the IO section, which is defined as everything prior to the IO baffle on HAM3, and everything beyond the Brewster's window viewports between HAM5 and HAM6.

The Stray Light Control subsystem will corroborate with the Systems group on the choice of COC wedge angles for producing PO beams.

The Stray Light Control subsystem will provide an ETM telescope baffle to block the excess light transmitted through the ETM that exceeds the clear aperture of the ETM telescope.

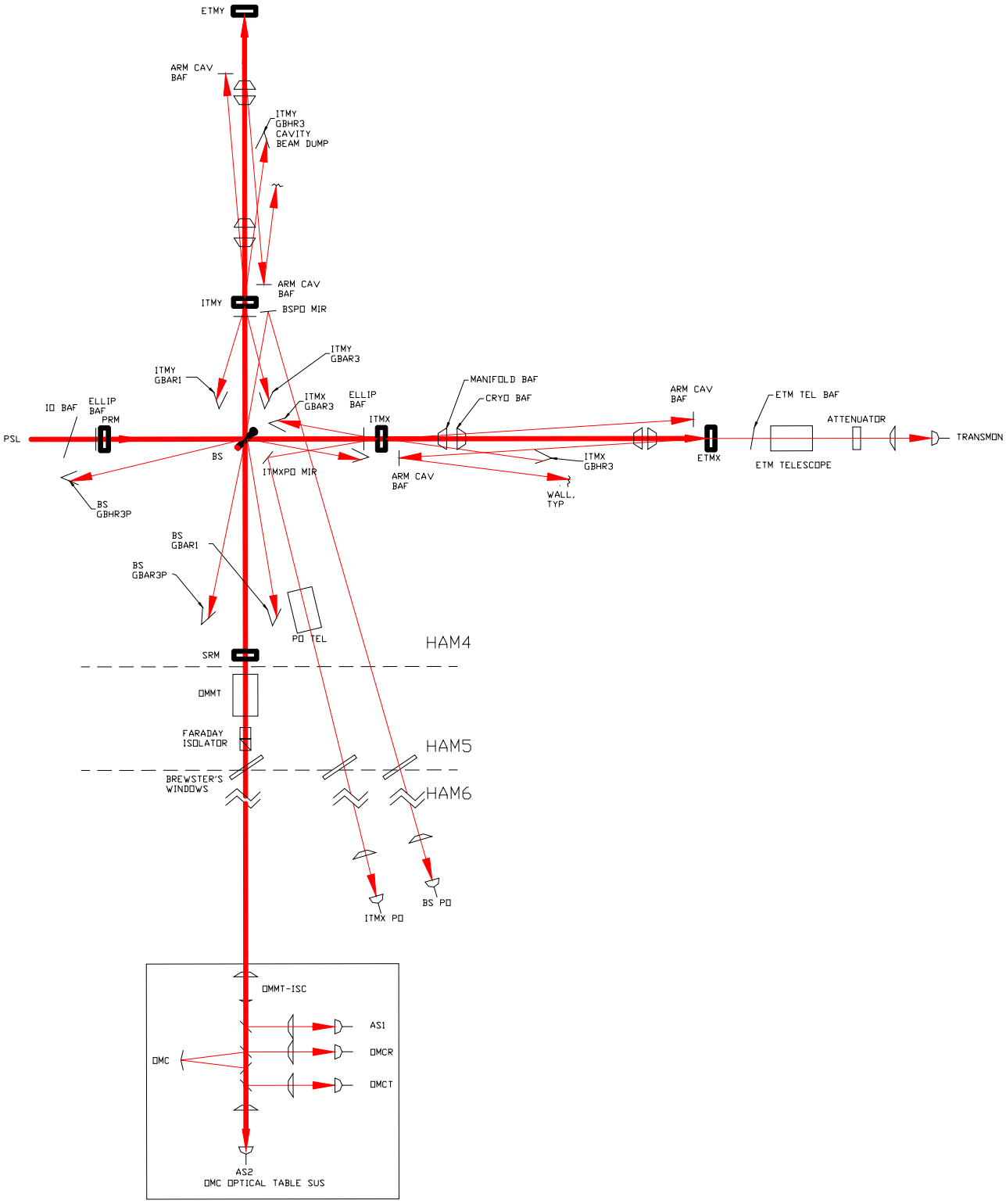

Figure 1: AOS System Block Diagram

1.3 Definitions

1.4 Acronyms

AOS - Auxiliary Optics Support

AR - Antireflection mirror coating

AS - anti-symmetric port signal

ASC - Alignment Sensing and Control

BS - Beam Splitter

BSC - Beam Splitter Chamber

CDS – Computer Data Systems

ETMx, ETMy - End Test Mass in the interferometer ‘X’ or ‘Y’ arm

HAM - Horizontal Access Module

HR – Hi-reflectance mirror coating

IFO - LIGO interferometer

IO - Input Optics

ISC- Interferometer Sensing and Control

ITMx, ITMy - Input Test Mass in the interferometer ‘X’ or ‘Y’ arm

LIGO - Laser Interferometer Gravity Wave Observatory

LSC - Length Sensing and Control

LVEA-vacuum equipment area

mm – millimeter

MMT – mode matching telescope

mrad – milliradian

MTBF – mean time before failure

NA – not applicable

nm – nanometer

OSEM – sensor/actuator head

PO - Pick-off

p-p, peak to peak

ppm - parts per million

PRM – Power Recycling Mirror

p-v, peak to valley

Q – quality factor

QPD – quadrant photo diode

RH – relative humidity

rms - root-mean-square

rtHz – square root Hertz

SLC – Stray Light Control

SOS – Small Optic Suspension

SRD - Science Requirements Document

SRM – Signal Recycling Mirror

SW – Solid Works

TBD - To Be Determined

W - Watt

WFS – wave front sensor

1.5 Applicable Documents

1.5.1 LIGO Documents

1. T980027-00, Baffling Requirements for the 4K and 2K IFO
2. Rai Weiss, BRDF data, 9/20/95
3. E980131-A, Component Specification, Faraday Isolator, 20 mm
4. T060013-02, Inputs to Beam Tube Scattering and Optical Surface Roughness Requirement Analysis for Advanced LIGO (table2)
5. E950111-A LIGO Naming Convention
6. E960022-B LIGO Vacuum Compatibility, Cleaning Methods and Qualification Procedures
7. E990303-03 Seismic Isolation Subsystem Design Requirements Document
8. L970061-00-D Guidance for Seismic Component Cleaning, Baking, and Shipping Preparation
9. LIGO-T960065-03 Seismic Isolation Design Requirements Document
10. M060056-06 Advanced LIGO Reference Design
11. M060062-00 HAM Single-stage Isolation Baseline Option Review Report
12. M950046-F LIGO Project System Safety Management Plan
13. MIL-C-104B
14. Robert Schofield (11/17/06 LHO ILOG)
15. T010076-01 Optical Layout for Advanced LIGO
16. T040126-A Baffle Furnace Bake Procedure

17. T060073-00 Transfer Functions of Injected Noise
18. T060360-02 PO Mirror Assembly & Telescope, and OMMT Conceptual Design Requirements
19. T920004-00 Estimation of Special Optical Properties of a Triangular Ring Cavity
20. T960151-02 Large and Small Optics Suspension Electronics Design Requirements
21. T980104-00 COS Final Design
22. T070003-00 Backscattering from the AS Port: A Comparison of P. Fritschel's Estimate and AOS T060263.
23. T070061-00 AOS: Stray Light Control (SLC) Design Requirements

1.5.2 Non-LIGO Documents

2 Catalog of SLC Design Requirements

The requirements for the SLC subsystem are derived in T070061-00 AOS: Stray Light Control (SLC) Design Requirements and are referenced below by paragraph number.

1. 4.2 Noise Requirements
2. 4.2.1 Direct Requirements
3. 4.2.2 Implied Requirement for Scattering Surfaces
4. 4.3 Faraday Isolator Requirements
5. 4.4 IO Baffle Requirement
6. 4.5 Cryopump Baffle Requirement
7. 4.6 BSC Chamber Components
8. 4.7 Clear Aperture Requirements
9. 4.8 Generic Requirements
10. 4.8.1 Mechanical Characteristics & Standards
11. 4.8.2 Electrical Characteristics & Standards
12. 4.8.3 Vacuum Compatibility Requirements
13. 4.8.4 Acoustic Requirements
14. 4.8.5 Earthquake Requirements
15. 4.8.6 Operating Environment
16. 4.8.7 Quality Assurance
17. 4.8.8 Reliability
18. 4.8.9 Maintainability
19. 4.8.10 Documentation
20. 4.8.11 Transportability
21. 4.8.11 Safety

3 Stray Light Control Conceptual Design Characteristics

3.1 COC Wedge Angle Determination

The COC wedge angles determine the separation between the main beam in the recycling cavity and the ghost beams that will either be intercepted with a pick-off mirror, or dumped inside a cavity beam dump.

3.1.1 Beam Profile in Recycling Cavity

The Beam cross section within the recycling cavity is non-Gaussian, and is determined in the vertical direction by the clear aperture of the PRM, 245 mm, and in the horizontal direction by the clear aperture of the BS, 370 mm diameter by 60 mm thick. The beam profile is approximately an ellipse with the horizontal semi-diameter of 107.1 mm and the vertical semi-diameter of 122.5 mm.

3.1.2 Minimum Size of the Ghost Beam

The minimum size of the primary ghost beams from the ITM and BS that must be intercepted is determined by calculating the scattered light noise from the fraction of the ghost beam that is not intercepted, which will be assumed to hit the chamber wall and scatter into the mode of the recycling cavity thereby causing phase noise.

Using the scattered light noise model described in Appendix A—Scattered Light Noise Theory, it was determined that a 100ppm un-dumped fraction of these ghost beams that scatter from the vacuum chamber walls cause an acceptable amount of scattered light displacement noise. Therefore, the fraction of the ghost beam power that misses the beam dumps will be limited to < 100ppm.

3.1.2.1 Power in the Recycling Cavity Beam

The total power in the elliptically apodized Gaussian beam of the recycling cavity is given by

$$P_{rc} := 4 \cdot \int_0^b \int_0^{a \cdot \sqrt{1 - \frac{y^2}{b^2}}} P(x,y)\, dx\, dy$$

Where the Gaussian function,

$$P(x,y) := 2 \cdot \frac{P_0}{\pi \cdot w^2} \cdot e^{-2 \cdot \left(\frac{x^2 + y^2}{w^2} \right)}$$

has been integrated out to the boundaries of an ellipse with semi-minor and semi-major diameters a and b respectively.

The total power in the elliptical recycling cavity beam will be calculated using the following parameters:

Gaussian beam radius, mm	$w := 60$
elliptical baffle minor semi-axis, mm	$a := 107.1$
elliptical baffle major semi-axis, mm	$b := \frac{245}{2}$
Gaussian power parameter	$P_{0rc} := 1.0542 \times 10^3$

Then,

$$P_{rc} = 1.0535 \times 10^3$$

which agrees with the specified power in one arm of the recycling cavity.

3.1.2.2 Fractional Ghost Beam Power Caught by Beam Dump and Pick-off Mirror

The total power captured by a beam dump with a half-width, a, and a half-height, h, is given by

$$P_{bd}(h) := 4 \cdot \int_0^h \int_0^{a \cdot \sqrt{1 - \frac{y^2}{b^2}}} P(x, y)\, dx\, dy$$

The fraction of the total power captured by the beam dump is given by

$$f_{bd}(h) := \frac{P_{bd}(h)}{P_{rc}}$$

And, the fractional power missing the beam dump, which will be scattered by the vacuum chamber, is

$$f_{mbd}(h) := 1 - f_{bd}(h)$$

This function is plotted in Figure 2. With a half-height of 115 mm and a half-width of 107.1 mm for the beam dumps and PO mirrors, the un-dumped power fraction will be approximately 50 ppm, which is acceptable

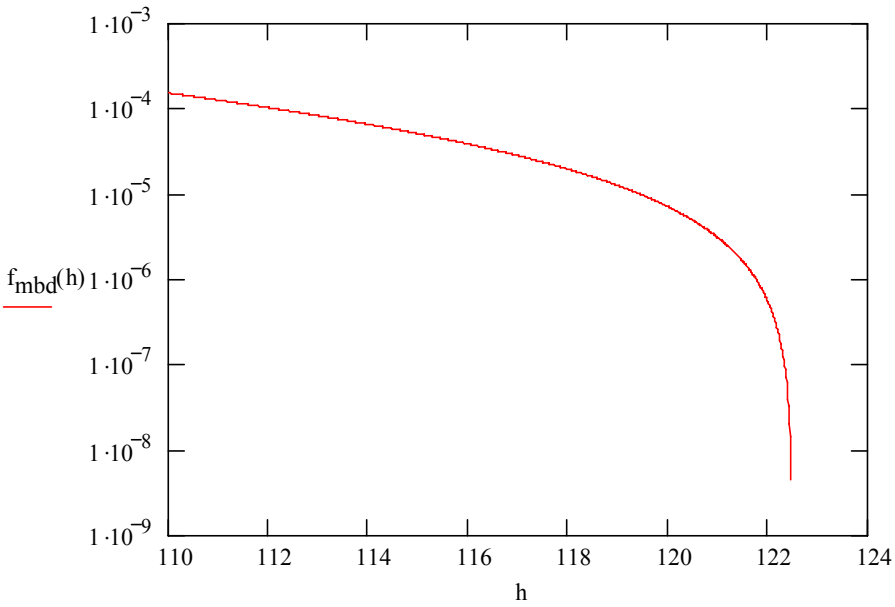

Figure 2: Ghost beam power missing the Beam Dump

3.1.2.3 Positioning Tolerance of Beam Dump and PO Mirror

If the beam dump is not centered, but is displaced vertically by an amount δ, the total power captured with the beam dump will be given by

$$P_{bd}(h,\delta) := 2\cdot\int_{-h+\delta}^{h+\delta}\int_{0}^{a\cdot\sqrt{1-\frac{y^2}{b^2}}} I(x,y)\,dx\,dy$$

The fractional power missing the displaced beam dump, with a 115 mm vertical-height beam dump, is shown in Figure 3.

The un-dumped power fraction will be < 100ppm provided the beam dump is positioned within +/- 6 mm.

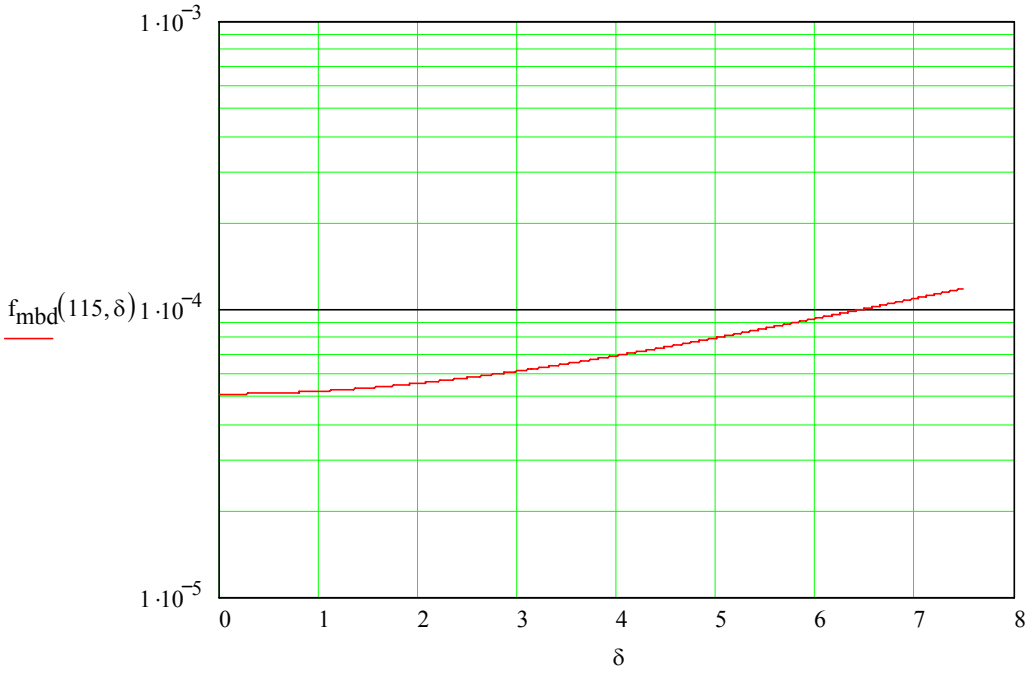

Figure 3: Positioning tolerance of PO mirror or Beam Dump

3.1.2.4 Beam Dump and PO mirror Aperture

Based on this analysis, the clear aperture for the PO mirrors and beam dumps will be either an ellipse or a rectangle with half-width, a = 108 mm, and half-height, h = 115 mm.

3.1.3 Wedge Angles for Unfolded IFO

3.1.3.1 BS Wedge Angle

The BS wedge angle determines the clearance between the vertical edge of the recycling cavity beam and the bottom of the BSPO Mirror, as illustrated in the ZEMAX layout in Figure 4.

The BS Wedge is chosen to be 1.66 deg. The clearance between the recycling cavity beam and the BSPO mirror is 163 mm.

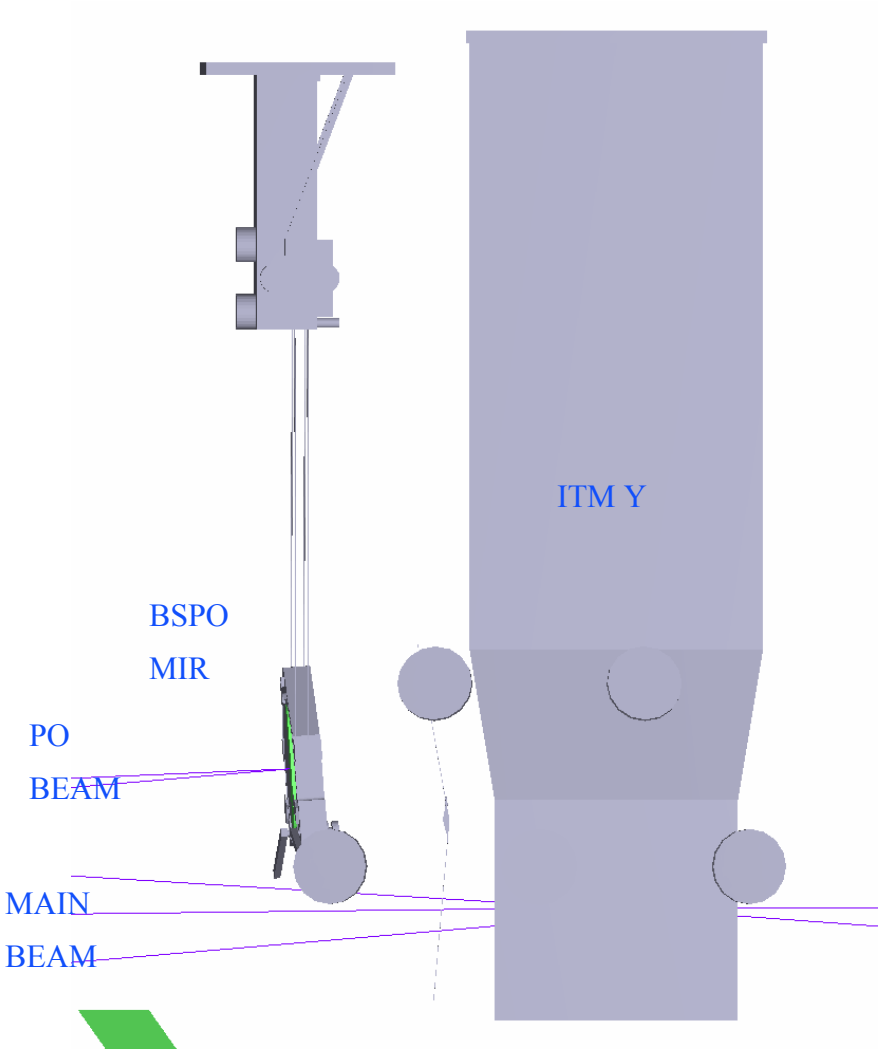

Figure 4: BS PO Beam Clearance

3.1.3.2 ITM Wedge Angle

The ITM wedge angle determines the clearance between the vertical edge of the recycling cavity beam and the bottom of the ITMX PO Mirror.

The ITM wedge is chosen to be 1.45 deg. The clearance between the recycling cavity beam and the ITMX PO mirror will be 122 mm.

3.1.3.3 CP Wedge Angle

The CP wedge angle determines the height of the main beam at the PRM mirror.

The CP wedge is chosen to be 0.61 deg. The height of the beam at the PRM will be the same height as the MMT3--global -156.6 mm, with a table clearance of 15.9 mm. The global height of the BS will be the same as the PRM.

3.1.3.4 PRM Wedge Angle

The PRM wedge will be minimal. A 5 arc minute wedge (0.08 deg) was chosen to eliminate coherence effects between the two faces of the mirror.

3.1.3.5 SRM Wedge Angle

The SRM wedge will be minimal. A 5 arc minute wedge (0.08 deg) was chosen to eliminate coherence effects between the two faces of the mirror.

3.1.3.6 ETM Wedge Angle

The ETM wedge will be large enough to allow the first transmitted ghost beam to be dumped on the ETM Transmitted Beam optical table. A 10 arc minute wedge (0.167) was chosen.

3.1.3.7 COC Wedge Angle Summary

Table 1: COC Wedge Angles, Unfolded IFO

Mirror	Wedge Angle, deg	Orientation	Direction	Symmetry
MMT3	0.5	vertical	either side	AR side
PRM	0.08	vertical	thin side up	either side
SRM	0.08	vertical	thin side up	either side
BS	1.66	vertical	thin side down	symmetric
ITM	1.45	vertical	thin side up	AR side
CP	0.61	vertical	thin side up	symmetric
ETM	0.167	vertical	thin side down	AR side
ETM RM	0.167	vertical	thin side up	either side

3.1.4 Wedge Angles for Folded IFO

TBD

3.2 Stray Light Control Performance Characteristics

3.2.1 Scattered Light Sources

The AOS scattered light sources that contribute to the total scattered light displacement noise are listed in Table 1, together with the incident power and the scattered power. The AOS scattered light requirement was taken to be 1/14 of the ADLIGO Science Requirement, which is 50% of the total scattered light noise budget.

Table 2: Scattered Light Source, Incident Power and Scattered Power

SCATTERING SOURCE	INCIDENT POWER, W	SCATTERED POWER, W
Faraday_Power	1.35E-01	7.37E-10
AC_Baffle_Power	7.33E+00	2.00E-18
AC_Baffle_Edge_Power	3.50E-02	9.58E-19
AC_Baffle_Refl_Power	7.33E-02	2.00E-20
AS_Brewster_Power	1.35E-01	1.10E-16
ITMX_PO_Brewster_Power	3.16E-01	7.73E-17
BS_PO_Brewster_Power	1.58E-01	9.67E-18
Cryo_Baffle_Power	2.77E+00	7.56E-18
Cryo_Baffle_Refl_Power	2.77E-02	7.56E-21
ITMY_GBAR1_BD_Power	3.16E-01	2.58E-16
ITMY_GBAR1_Undump_Power	9.48E-09	7.73E-22
ITMY_GBAR1_BD_Refl_Power	4.74E-07	1.93E-22
ITM_GBAR3_BD_Power	6.25E-01	5.05E-16
ITM_GBAR3_Undump_Power	1.86E-08	1.50E-21
ITM_GBAR3_BD_Refl_Power	9.28E-07	3.75E-22
ITM_GBAR4_Power	1.87E-04	4.50E-21
ITM_GBHR3_BD_Power	3.14E-03	6.41E-23
ITM_GBHR3_Undump_Power	4.69E-13	9.57E-31
ITM_GBHR3_BD_Refl_Power	2.34E-11	2.39E-31
ITM_GBHR4_Power	9.38E-07	2.87E-30
BS_GBAR3X_BD_Power	1.58E-01	6.44E-17
BS_GBAR3X_Undump_Power	1.18E-09	4.83E-23
BS_GBAR3X_Refl_Power	5.92E-08	1.21E-23
BS_GBAR4X_Power	2.37E-05	1.45E-22
BS_GBAR1_BD_Power	3.16E-01	2.58E-16
BS_GBAR1_Undump_Power"	3.16E-05	2.58E-18
BS_GBAR1_Refl_Power	1.58E-03	6.45E-19
ITM_Ellip_Baffle_Power	1.40E+00	2.57E-15
ITM_Ellip_Baffle_Refl_Power	1.40E-03	2.57E-20
ITM_Ellip_Baffle_Edge_Power	1.80E-02	3.31E-16
PRM_Ellip_Baffle_Power	1.25E-07	3.43E-23
Cryo_Baffle_Edge_Power	7.39E-02	2.02E-18

AS_Brewster_Refl_Power	5.40E-05	3.52E-19
ETM_Tel_Baffle_Power	2.11E+00	1.16E-16
ETM_Tel_Baffle_Refl_Power	5.29E-03	7.28E-22
ETM_Tel_Baffle_Edge_Power	9.76E-03	5.38E-19
Manifold_Wall_Wide_Angle_Power	7.22E-01	3.96E-21
Manifold_Spoolpiece_Wide_Angle_Power	8.60E-03	1.11E-16
Manifold_Baffle_Wide_Angle_Power	8.60E-03	1.18E-24
BS_GBHR4X_Power	2.37E-05	7.25E-23
BS_GBAR3P_BD_Power	3.16E-01	1.29E-16
BS_GBAR3P_Undump_Power	2.37E-09	4.83E-23
BS_GBAR3P_Refl_Power	1.18E-07	1.21E-24
BS_GBHR3P_BD_Power	3.16E-01	1.29E-16
BS_GBHR3P_Undump_Power	2.37E-09	9.66E-23
BS_GBHR3P_Refl_Power	1.18E-07	2.42E-23
OMMT2_Power	1.35E-01	3.30E-11
AS_Brewster_Refl_Power	5.40E-05	3.52E-19

3.2.2 Summary of Scattered Light Displacement Noise

A summary of the scattered light displacement noise with all the AOS noise sources mitigated, except for the Brewster's Window noise is shown in Figure 5. The Scattered Light Noise Requirement is not met at all frequencies.

Removing the Brewster's Window meets the Scattered Light Noise Requirement, 4.2.1 Direct Requirements, at all frequencies, as shown in Figure 6.

3.2.3 Output Faraday Isolator

The Faraday Isolators that were used for Initial LIGO will be re-used for ADLIGO with a modification to preserve the in-line beam direction.

The scattered light model indicates that the Output Faraday Isolator must be suspended in order to reduce the scattered light noise from the optical surfaces. The optical surfaces are all in a vertical plane, so no motion isolation is required in the vertical direction. A conceptual drawing of the modified Faraday Isolator suspended with a modified LOS structure is shown in Figure 7.

The pitch and yaw pointing angles of the Output Faraday Isolator will be pre-set during initial alignment. A remotely controlled Picomotor will provide a small amount of pitch motion to misalign a possible glint of the IFO output beam from the optical surfaces of the Faraday Isolator.

3.2.3.1 Faraday Isolator Forward Transmissivity

The measured transmissivity of the Initial LIGO Output Faraday Isolator is 98%.

This meets the requirement 4.3 Faraday Isolator Requirements.

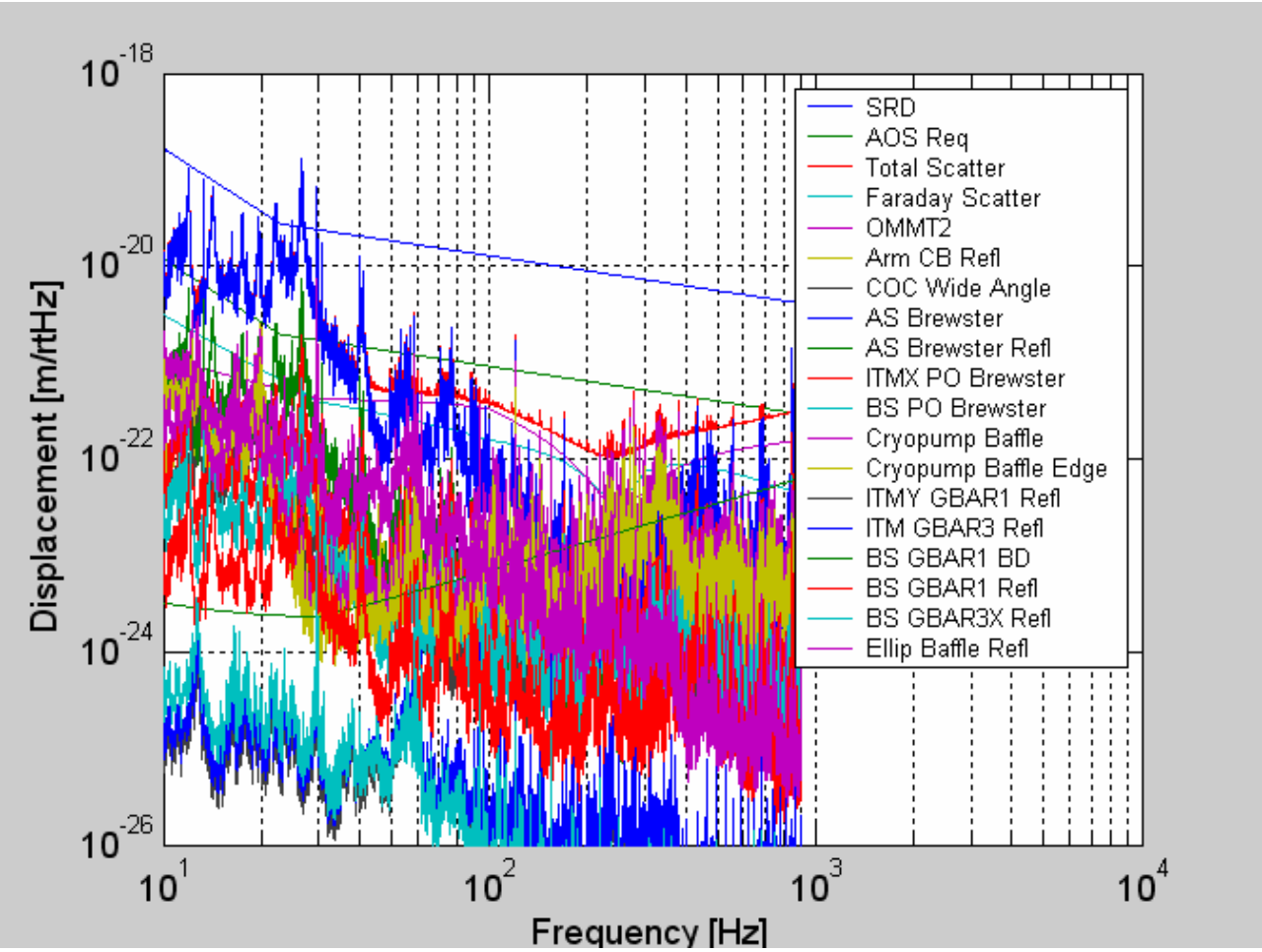

Figure 5: Scattered Light Displacement Noise, Brewster's Windows in Place

3.2.3.2 Faraday Isolator Reverse Transmissivity

The measured reverse power transmission of the Initial LIGO Output Faraday Isolator is < 0.0001.

This meets the requirement 4.3 Faraday Isolator Requirements.

3.2.3.3 BRDF of Faraday Surfaces

The Output Faraday Isolator has four calcite prism surfaces and one TGG crystal surface on the entrance side. These surfaces will scatter light back toward the antisymmetric port of the IFO. The light scattered by the additional surfaces beyond the Faraday rotator magnet will be attenuated by the reverse transmissivity of the Faraday Isolator and will be ignored.

The BRDF of the TGG surface was estimated using the fractal back-scattering model proposed by R. Weiss; see T920004-00 Estimation of Special Optical Properties of a Triangular Ring Cavity, for incidence angles between 1E-4 and 1E-1 radians.

$$BRDF(\theta) := \frac{\alpha}{\theta^2}$$

where

$$\alpha := 1.5 \cdot 10^{-3} \cdot S$$

and S is the total integrated scattering loss of the surface.

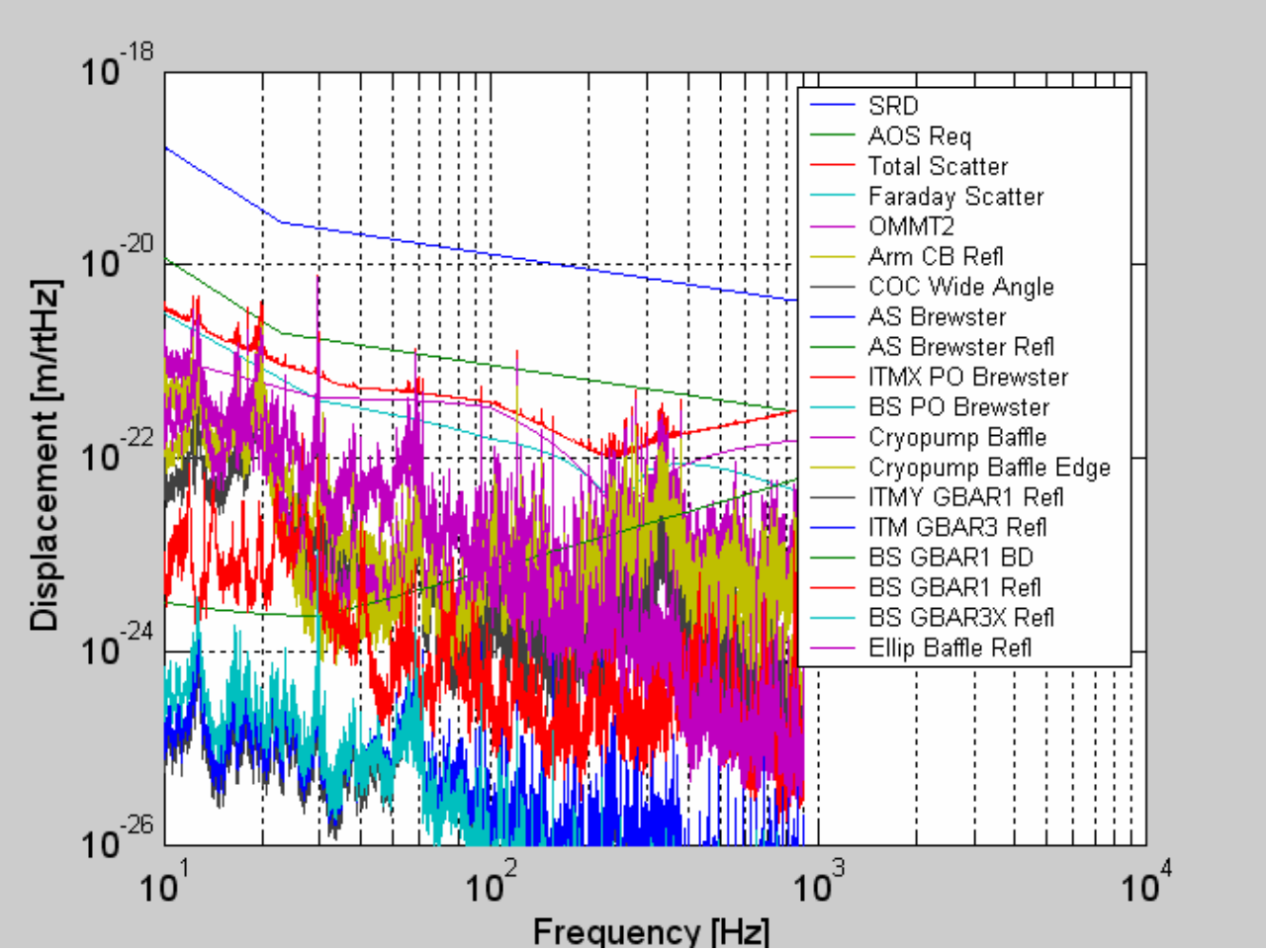

Figure 6: Scattered Light Displacement Noise, Brewster's Windows Removed

Assuming an incidence angle on the Faraday Isolator surfaces of 1.7E-2 rad (1 deg) and a total scattering loss per surface of 100 ppm, the estimated BRDF is 5E-4 sr^{-1}.

It was assumed that the calcite prisms have a similar BRDF, and that the scattered light noise injected into the IFO will add in phase.

3.2.3.4 Output Faraday Isolator Suspension

The Output Faraday Isolator will be suspended by a modified LOS as shown in Figure 7. The length of the pendulum is estimated to be 0.4 m. Elastomeric damping elements will be provided at the tops and bottoms of the four-wire suspension, with an assumed damping Q < 1000.

The suspension frame will be mounted to the HAM optical table, with the motion requirement shown in Figure 8.

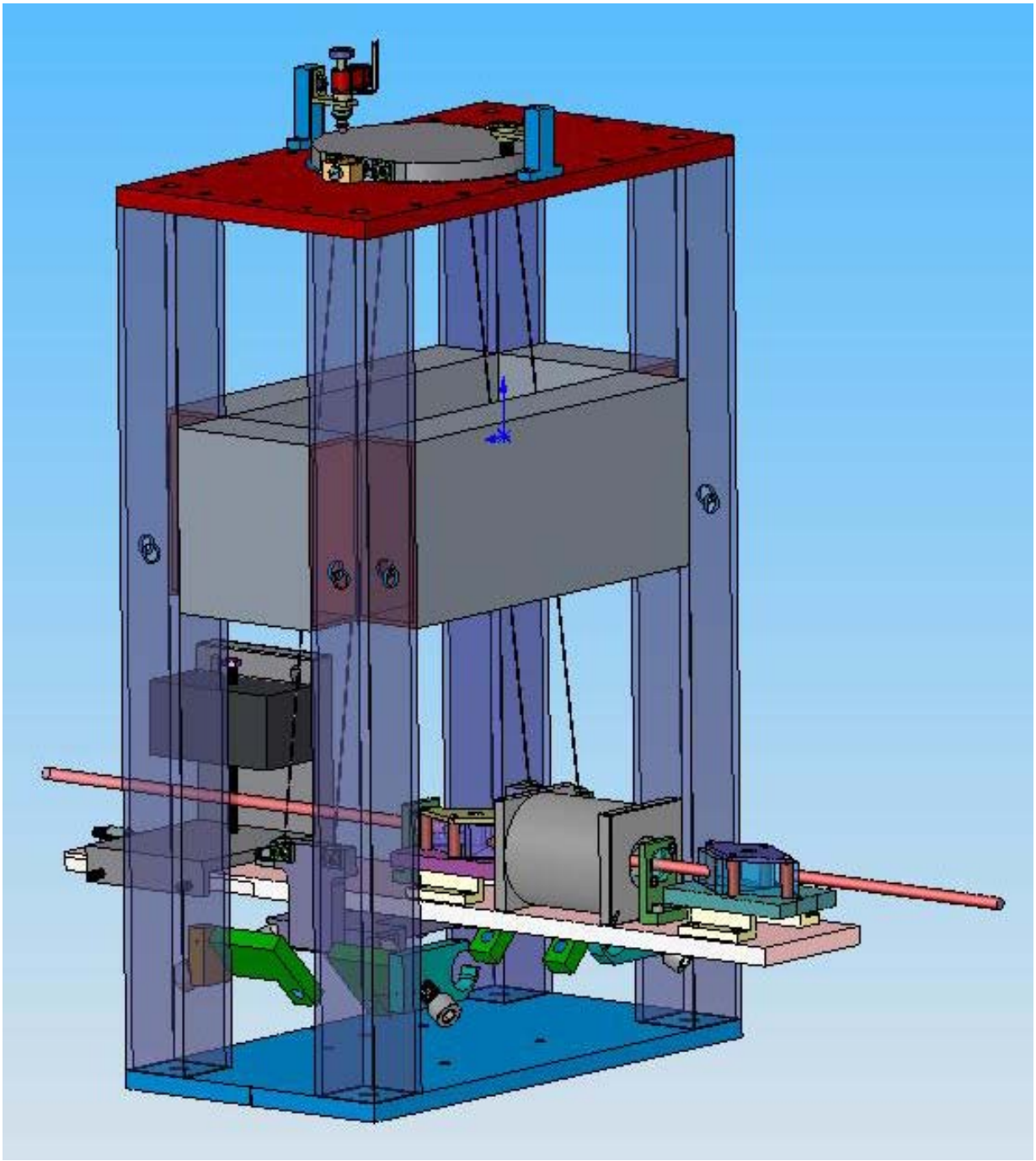

Figure 7: Initial LIGO Output Faraday Isolator Parts Suspended in a Modified LOS

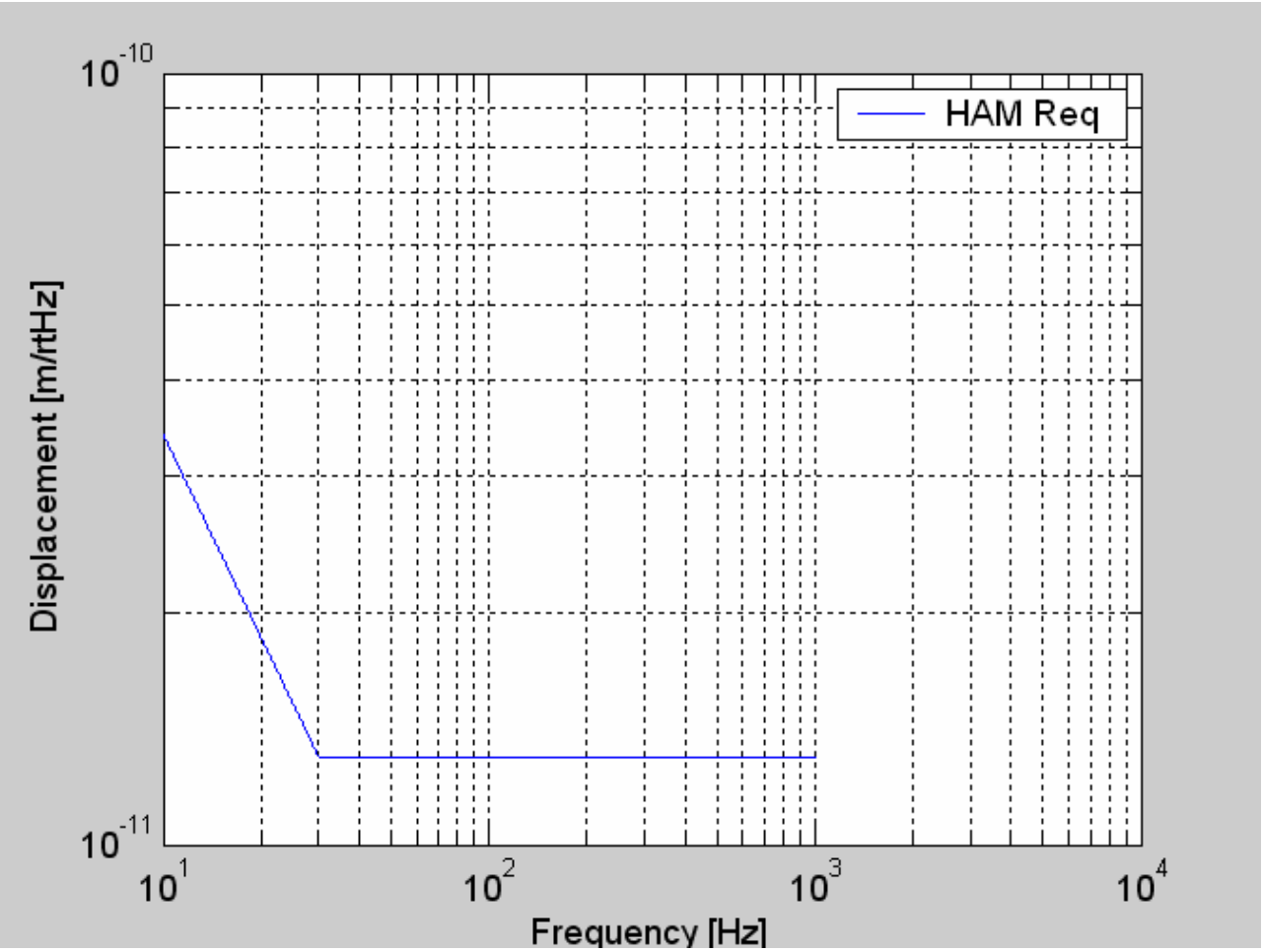

Figure 8: HAM optics table Seismic Motion Requirement

The minimum Output Faraday Isolator motion attenuation requirements were determined using the scattered light model, assuming five surfaces with BRDF of 5E-4 sr^{-1}, and are shown in Figure 9, together with a calculated simple pendulum transfer function.

3.2.3.5 Scattered Light Displacement Noise of Suspended Output Faraday Isolator

The scattered light displacement noise caused by the suspended Output Faraday Isolator is shown in Figure 10.

3.2.3.6 Stay Clear Diameter

The clear aperture of the Faraday Isolator is 20 mm diameter. The OMMT will have a beam reduction ratio of 28.9, which will create an elliptical beam profile at the entrance to the Faraday Isolator with vertical diameter = 8.5 mm and horizontal diameter = 7.4 mm. The clear aperture of the Faraday Isolator will be pre-aligned within 2 mm of the beam centerline by referencing its position to the center of the ITM.

This meets the requirement 4.7 Clear Aperture Requirements

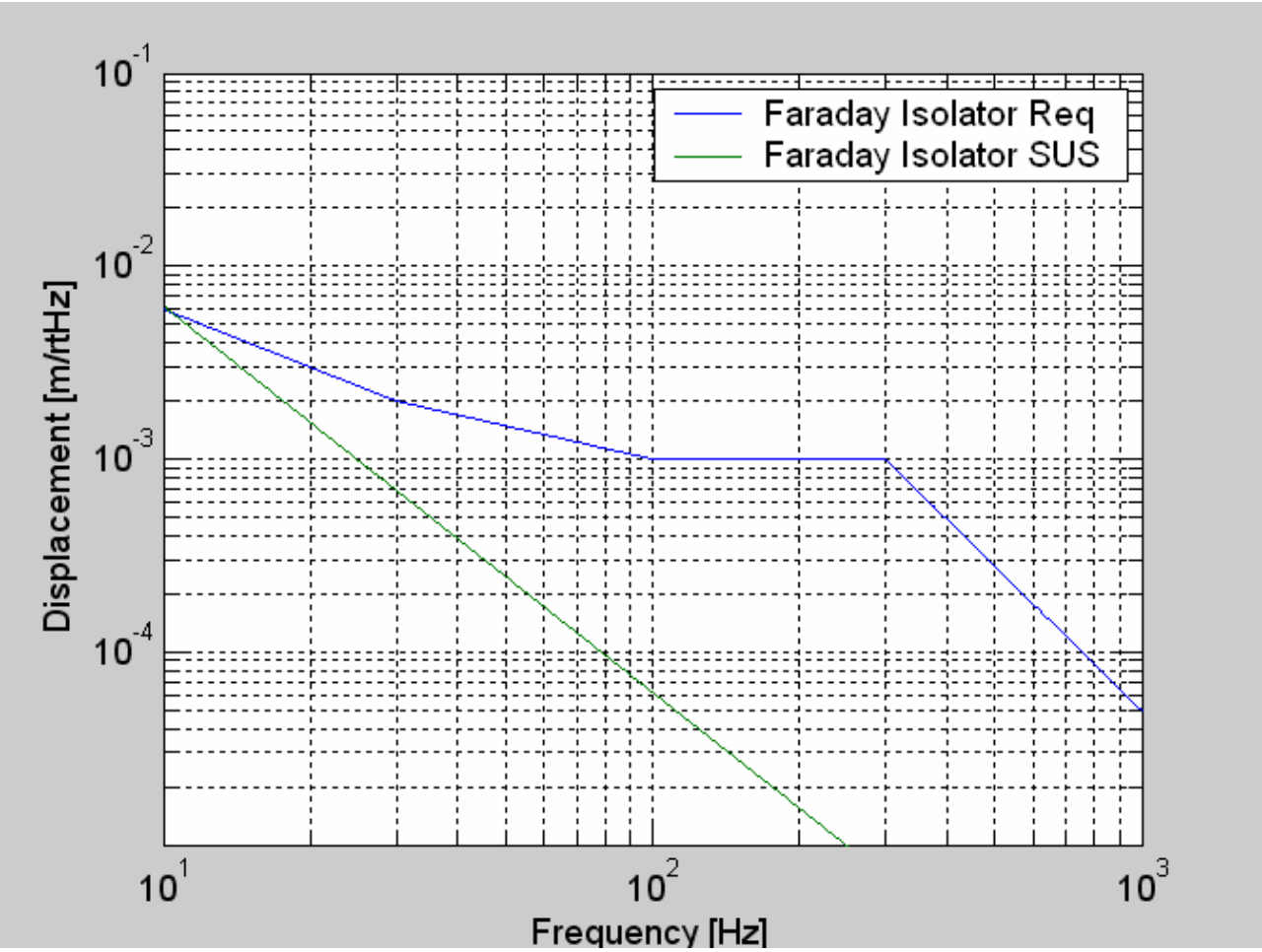

Figure 9: Output Faraday Isolator SUS Amplitude Response

3.2.4 Arm Cavity Baffle

3.2.4.1 Incident Power on Arm Cavity Baffle

The power scattered from the far COC mirror, at the opposite end of the arm cavity, into the annular region bounded by the outer radius of the near COC and the inside radius of the Cryopump Baffle will be incident on the Arm Cavity Baffle. It is given by

$$P_{acb} := P_a \cdot \int_{\theta_{itm}}^{\theta_{cp}} 2 \cdot \pi \cdot \theta \cdot BRDF_1(\theta)\, d\theta$$

The Initial LIGO pathfinder COC CSIRO, surface 2, S/N 2 was used to estimate the BRDF. See T980027-00, Baffling Requirements for the 4K and 2K IFO.

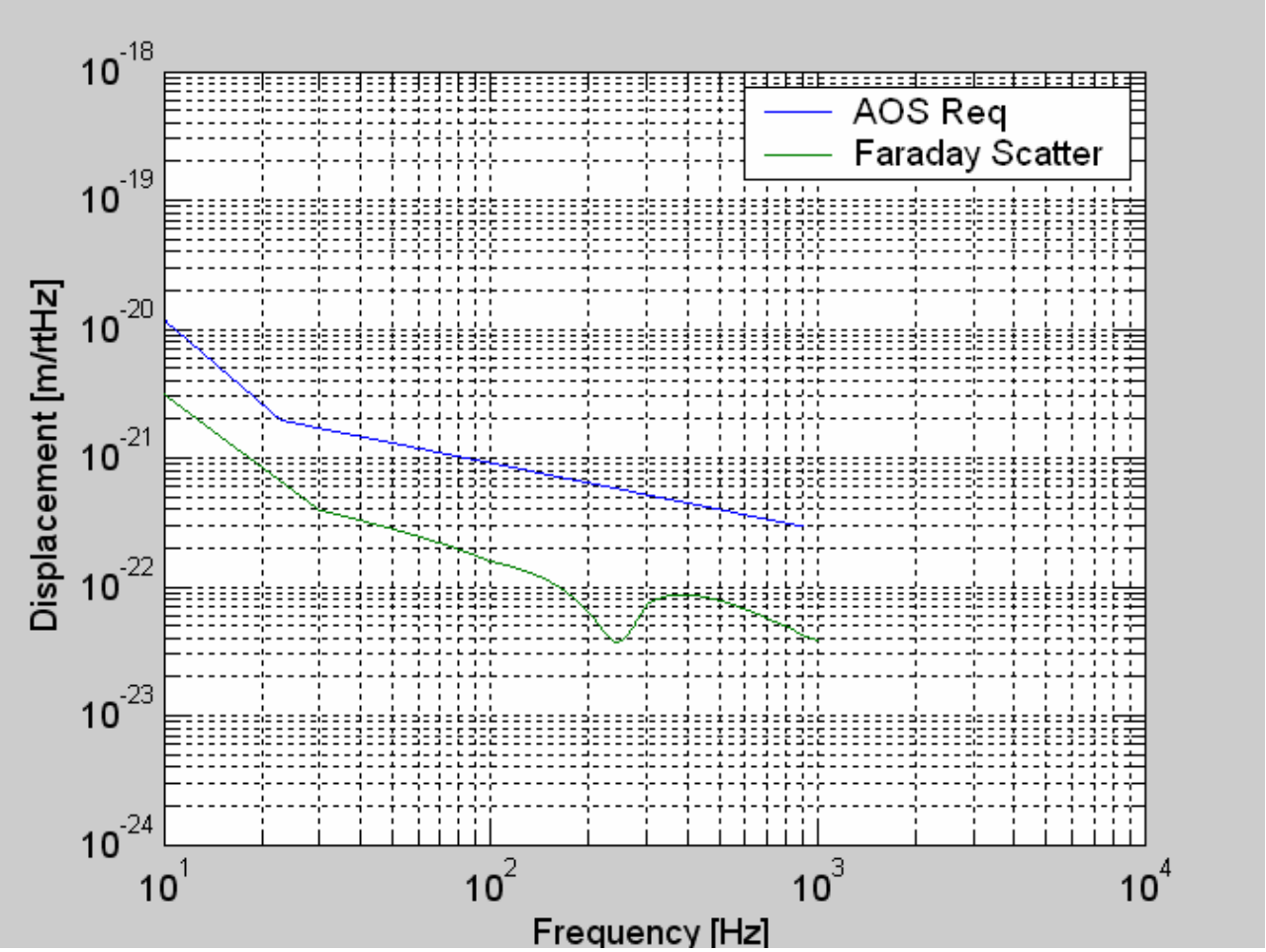

Figure 10: Scattered Light Displacement Noise from Suspended Faraday Isolator

$$BRDF_1(\theta) := \frac{2755.12}{\left(1 + 8.50787 \cdot 10^8 \cdot \theta^2\right)^{1.23597}}$$

Where θ_{itm} is 4.25 E-5 rad

θ_{cp} is 9.612 E-5 rad

and, P_a is the arm power 8.339 E5 W

P_{acb} = 7.4 W

3.2.4.2 Arm Cavity Baffle Motion

3.2.4.2.1 HEPI Displacement

The Arm Cavity Baffle shown in Figure 11 will be suspended with a single pendulum from Stage "0" HEPI support ring of the BSC optical table adjacent to the HR side of the ITM and ETM. Earthquake stops will be mounted to the BSC vacuum enclosure.

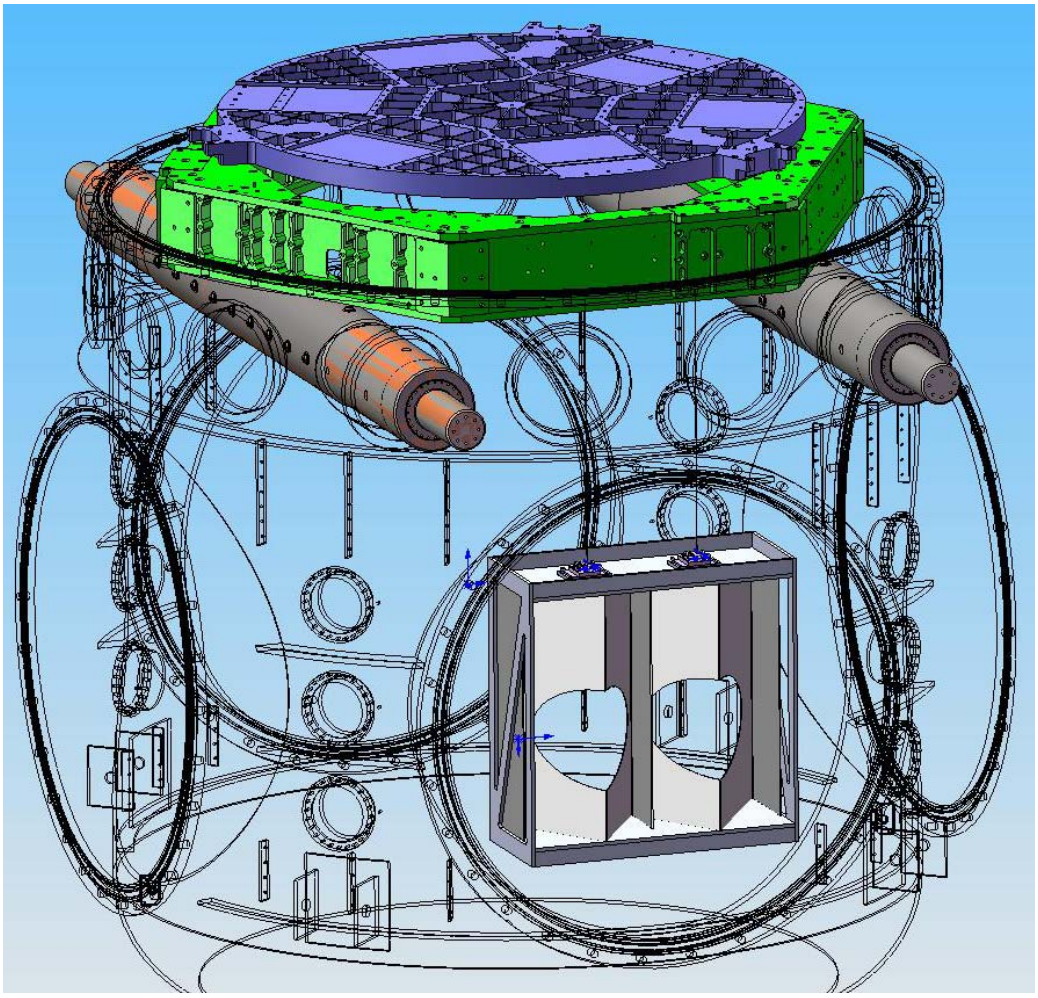

Figure 11: Suspended Arm Cavity Baffle

We will assume that the x-displacement spectrum of the BSC HEPI isolation system is described by Brian Lantz in the SEI elog entry ID: 596, 3/14/06, as shown in Figure 12.

3.2.4.2.2 Minimum Arm Cavity Baffle Motion Requirements

With an assumed BRDF of 0.001 sr^-1, the scattered light model indicates that the Arm Cavity Baffle requires 0.1 attenuation at 10 Hz, and no motion attenuation for frequencies > 30 Hz, as shown in Figure 13.

3.2.4.2.3 Arm Cavity Baffle Suspension Transfer Functions

The pitch, roll, and yaw resonances of the two-wire Arm Cavity Baffle suspension were estimated using a Matlab model developed by the SUS group, and are all around 1 Hz, as shown in Figure 14, Figure 15, and Figure 16. With these transfer functions, the relative motion will be attenuated by a factor >10 for frequencies > 10 Hz, and will exceed the requirement.

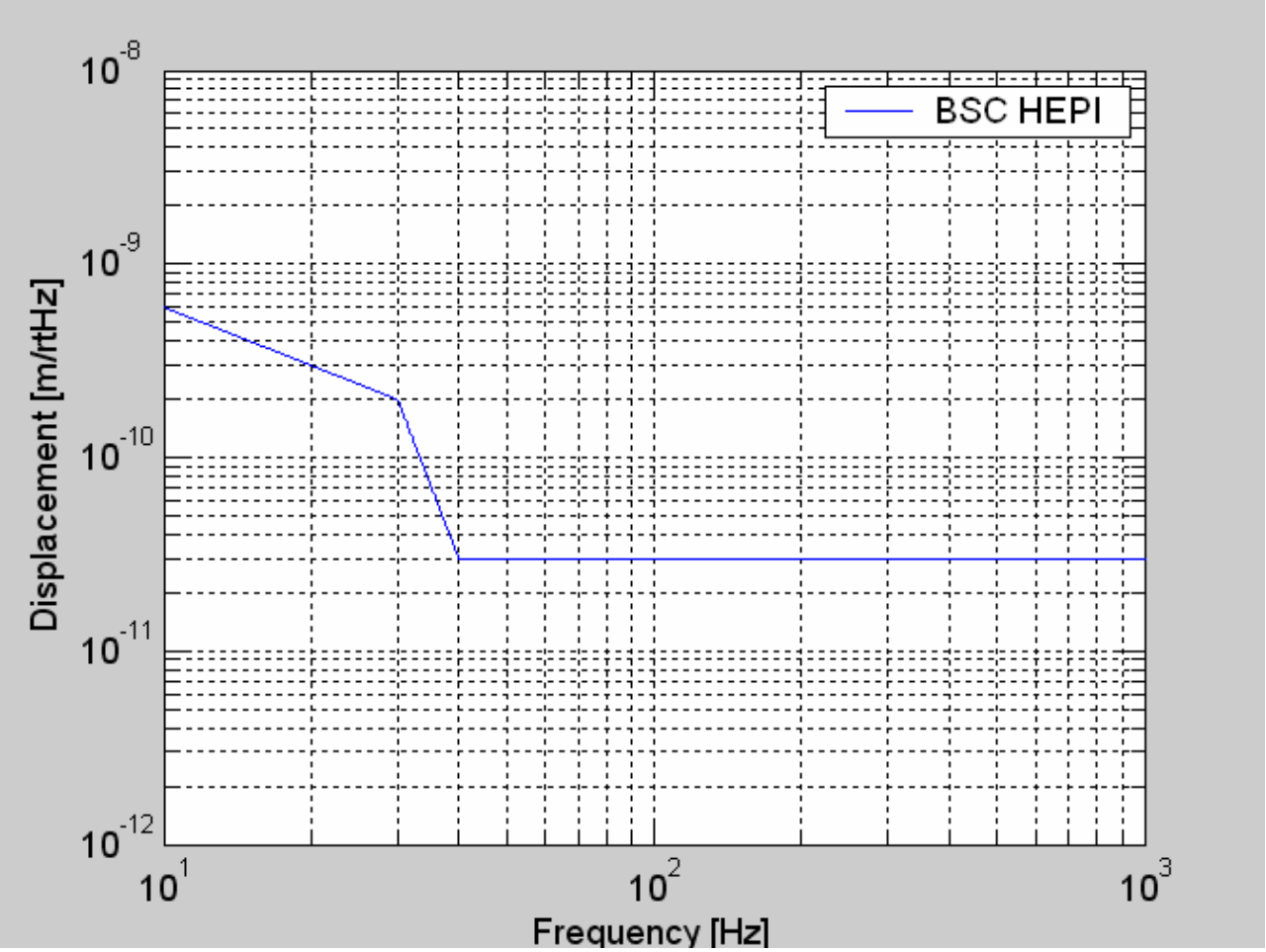

Figure 12: BSC HEPI Motion Spectrum

The hole in the baffle for the IFO beam extends in the longitudinal direction because of the tilt angle of the vertical baffle surfaces. The scattering surfaces of the exposed, rough edges of the baffle hole will exhibit a longitudinal motion due to coupling from the vertical motion. The average vertical-to-horizontal coupling factor is estimated to be 0.6.

Vertical springs will attach to the suspension wires to provide a vertical resonance around 1 Hz, shown by the green curves in the figures, which will reduce the vertical motion by a factor >10 and the coupled-longitudinal motion by a factor >17 @ frequencies > 10Hz.

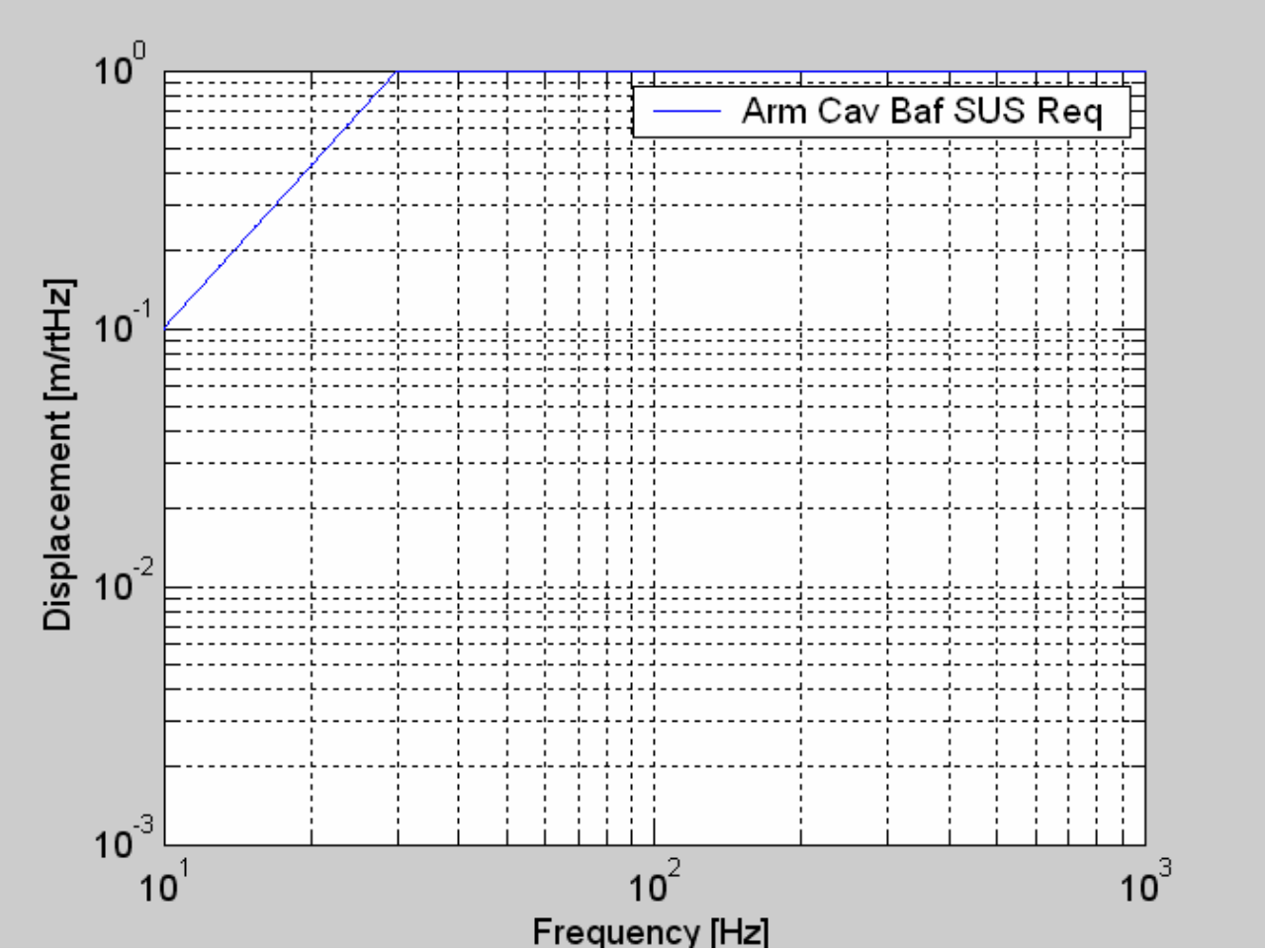

Figure 13: Arm Cavity Baffle Attenuation, Minimum Requirement

3.2.4.3 Arm Cavity Baffle Surface BRDF

The Arm Cavity Baffle will be constructed of black glass with the surface inclined at an incidence angle 56 deg and is estimated to have a BRDF < 0.001 sr^{-1}.

3.2.4.4 Arm Cavity Edge BRDF

The exposed surface of the edges of the holes cut in the Arm Cavity Baffle for passage of the IFO main beams will scatter light into the IFO mode. The scattered light calculation assumed a BRDF = 0.1 sr^-1.

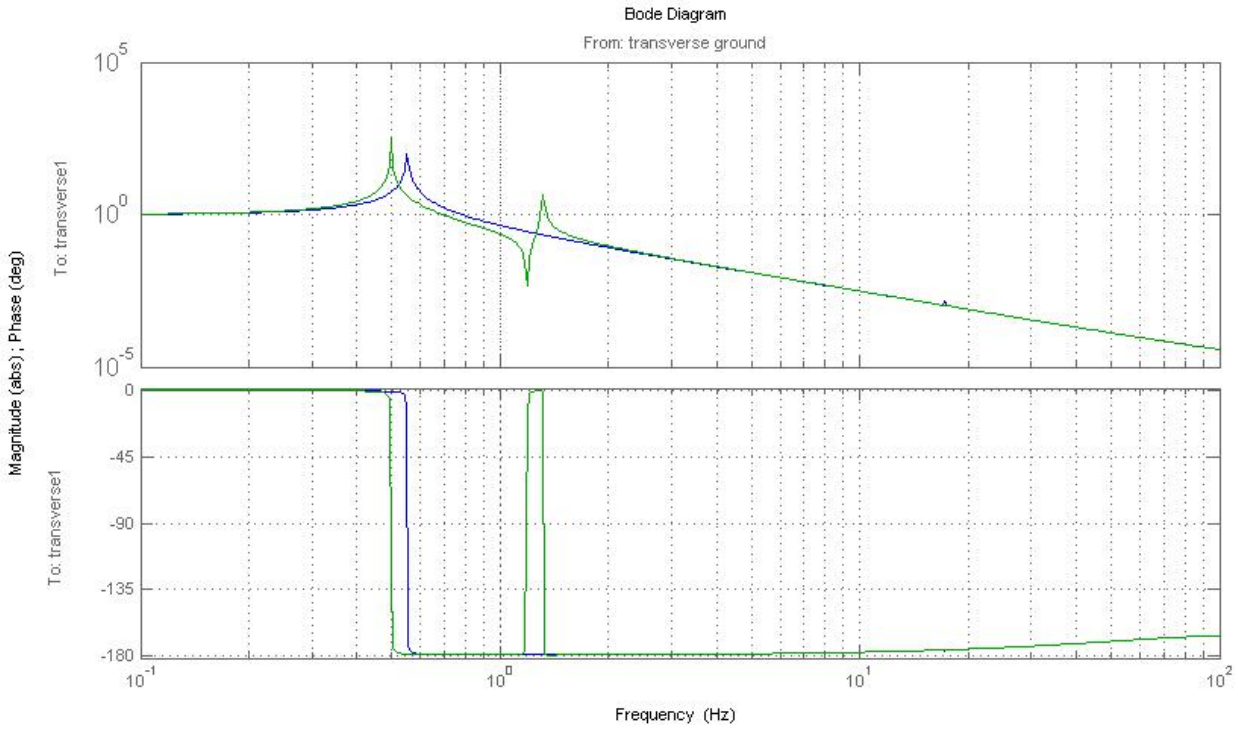

Figure 14: Transverse Transfer Function, ACB SUS

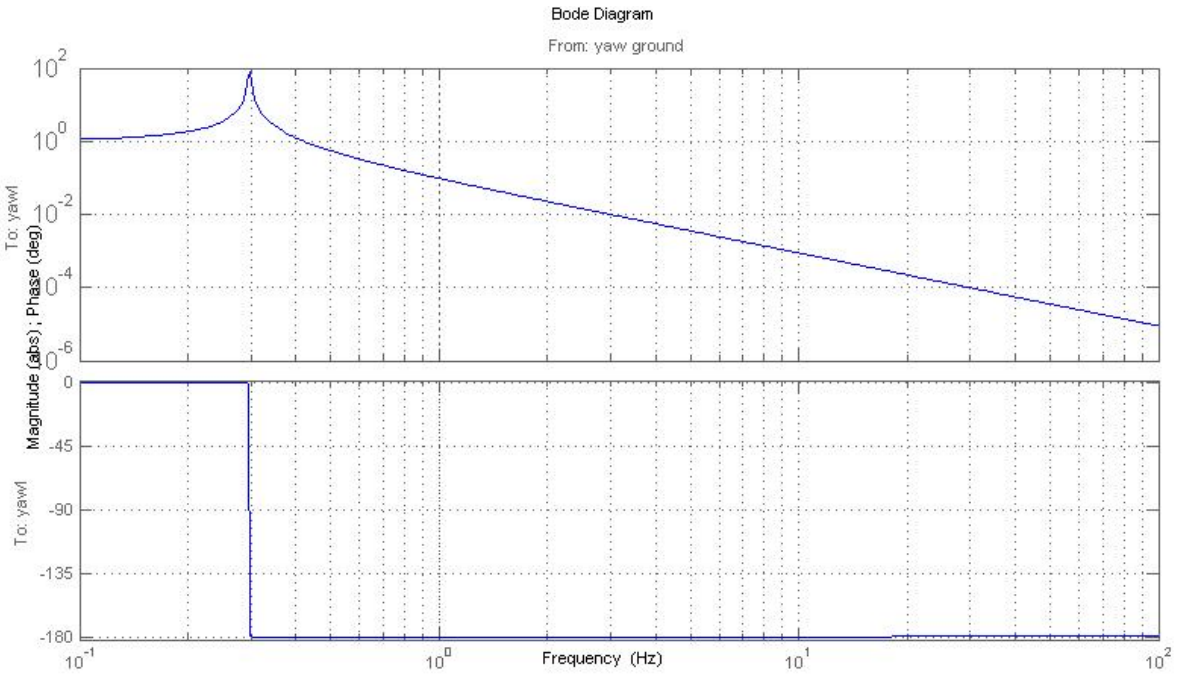

Figure 15: Yaw Transfer Function, ACB SUS

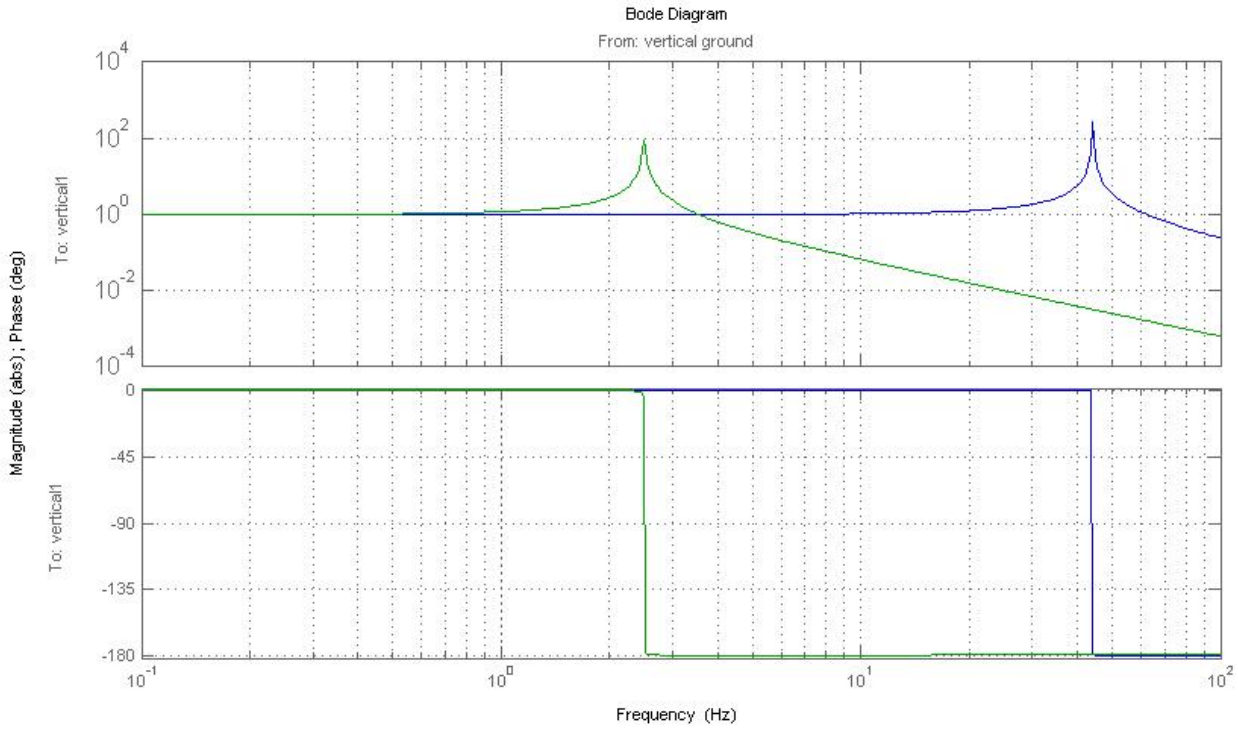

Figure 16: Vertical Transfer Function, ACB SUS

3.2.4.5 Arm Cavity Baffle Reflectivity

The light that is not absorbed by the Arm Cavity Baffle will reflect from the baffle surface onto the inside walls of the vacuum manifold, where it will scatter from the manifold, reflect again from the Arm Cavity Baffle, and enter the IFO mode at the far COC.

The scattered light model was used to calculate the requirement for the reflectivity of the Arm Cavity Baffle. Assuming a BRDF of the vacuum manifold wall of 0.025 at an incidence angle of 40 deg, the reflectivity of the Arm Cavity Baffle must is < 1%.

This low reflectivity will be obtained by using multiple reflections from uncoated black glass inclined near Brewster's angle.

3.2.4.6 Seismic Motion of the Vacuum Manifold

The light that reflects from the Arm Cavity Baffle will scatter from the vacuum manifold, which has the seismic motion shown in Figure 17. See Robert Schofield (11/17/06 LHO ILOG).

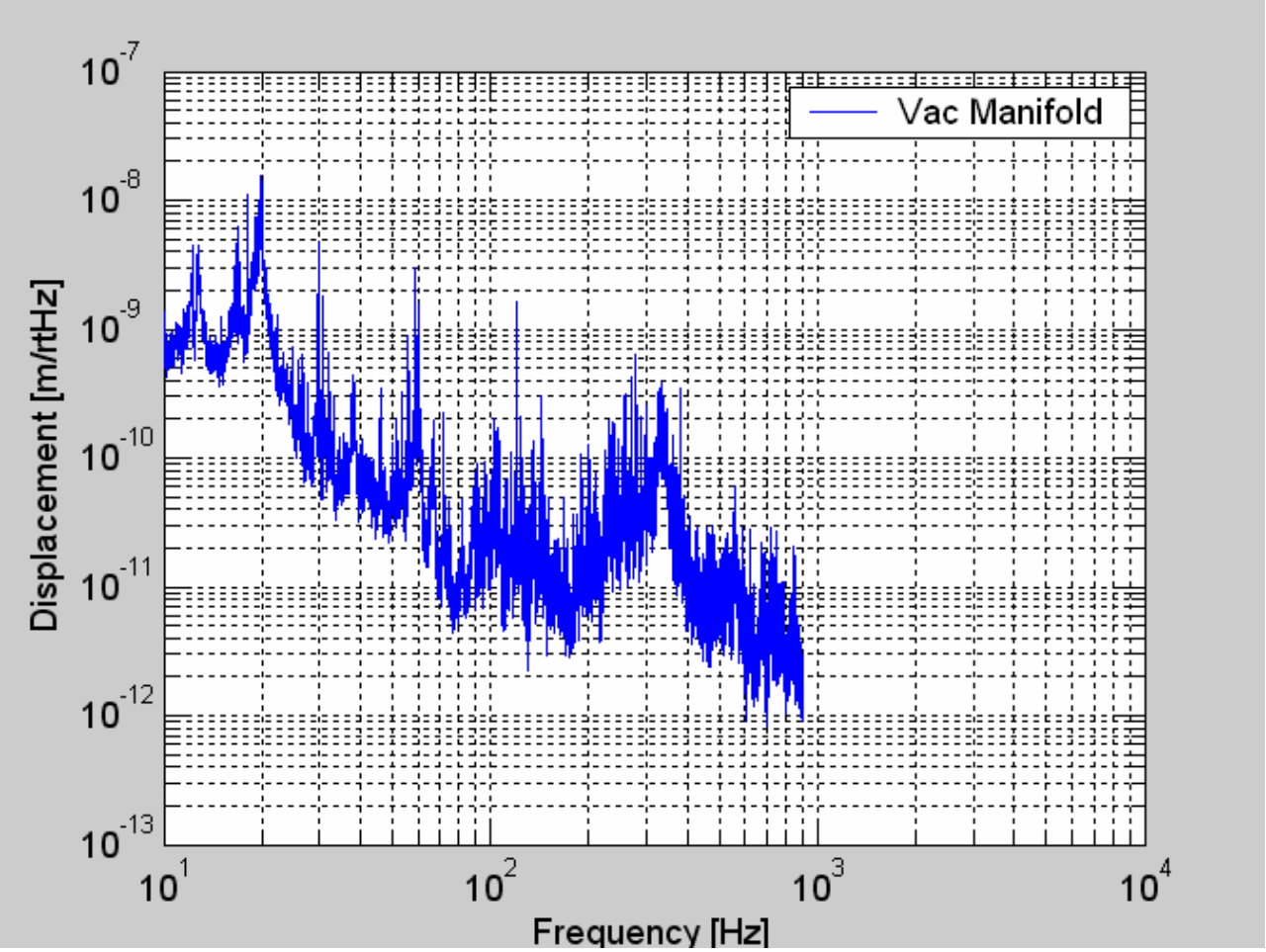

Figure 17: Seismic motion of vacuum manifold

3.2.4.7 Scattered Light Displacement Noise of Suspended Arm Cavity Baffle

The light that scatters directly from the surface and from the edges of the beam holes of the suspended Arm Cavity Baffle has a phase noise caused by the seismic motion of the HEPI support structure attenuated by the transfer function of the Arm Cavity Baffle suspension.

The light that reflects from the baffle and subsequently scatters from the vacuum manifold walls will have a phase noise caused by the seismic motion of the walls. The vacuum manifold is assumed to have a BRDF = 0.1 sr^-1

The maximum scattered light noise from these three sources was calculated using the scattered light model and is shown in Figure 18. The actual suspension of the Arm Cavity Baffle will reduce the displacement noise due to direct scatter by the baffle surface significantly, and the dominant noise source is expected to be the reflected light from the Arm Cavity Baffle that scatters from the vacuum manifold walls.

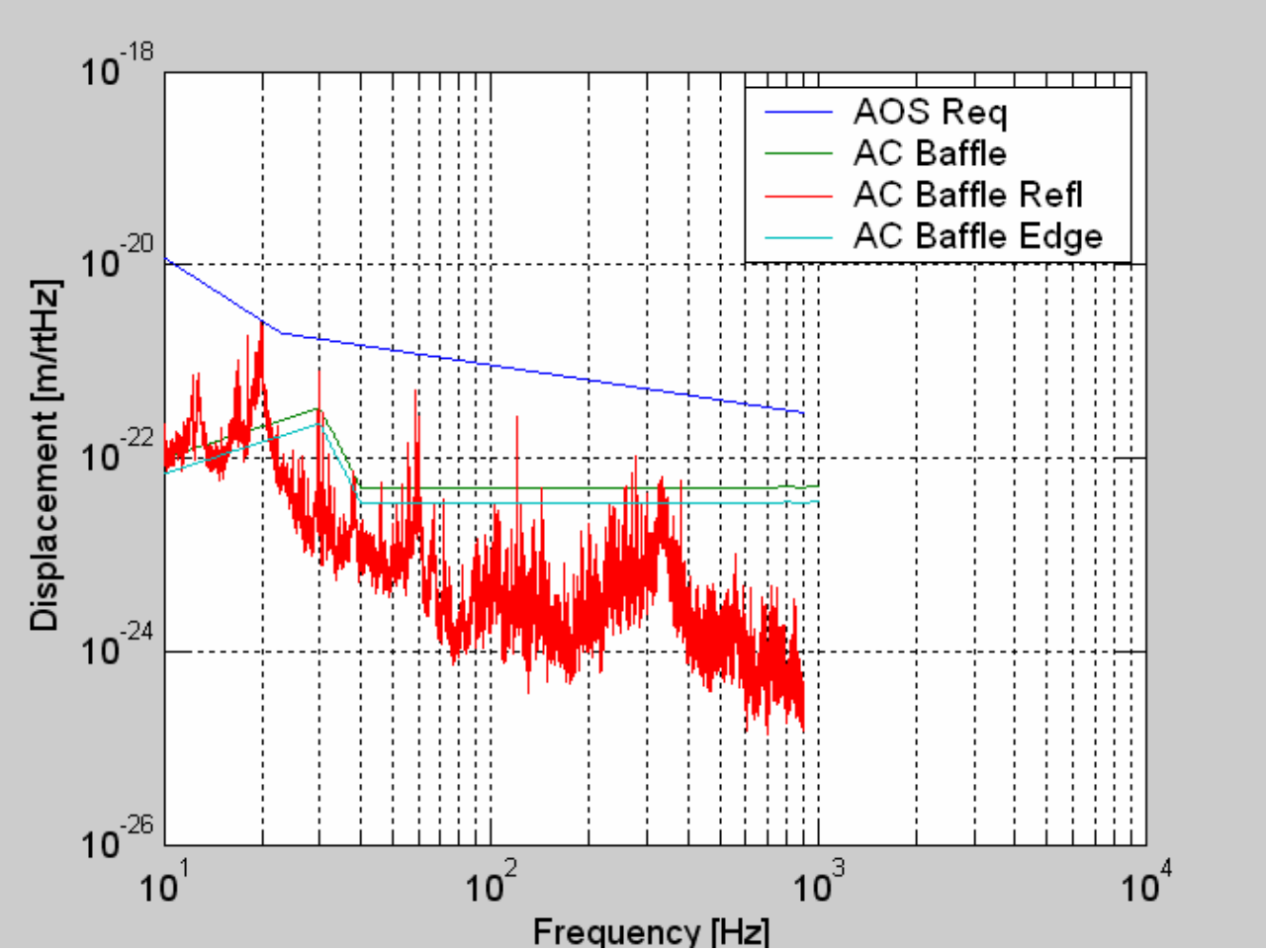

Figure 18: Arm Cavity Baffle Scattered Light Displacement Noise

3.2.4.8 Fringe Wrapping of Arm Cavity Baffle Displacement Noise

The Arm Cavity Baffle has a vertical bounce resonance at approximately 2.3 Hz. The displacement noise at the odd harmonics of the motion due to fringe wrapping was calculated using the fringe wrap model, see Fringe-Wrapping in Appendix A—Scattered Light Noise Theory, assuming a simple pendulum function with a Q = 1000 at the resonant frequency. The fringe wrapping does not cause excessive noise above 10 Hz, as shown in Figure 19.

3.2.4.9 Stay Clear Diameter

The clear aperture of the Arm Cavity Baffle is 346 mm diameter, which is larger than the diameter of the ITM and ETM COC. The clear aperture will be pre-aligned by referencing its position to the center of the HR surface of the COC in the quad suspension frame within 4 mm.

This meets the requirement 4.7 Clear Aperture Requirements.

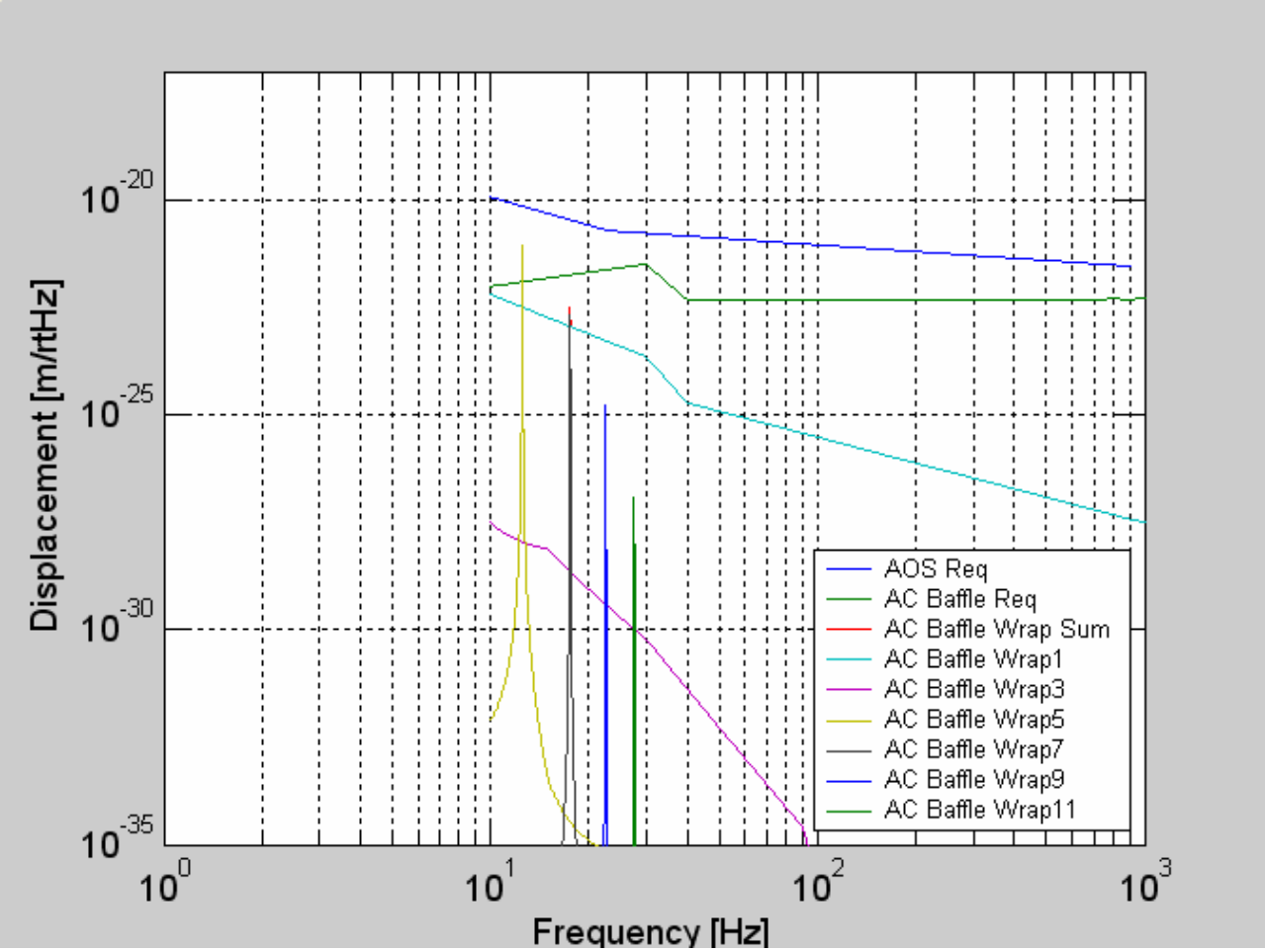

Figure 19: Arm Cavity Baffle Scattered Light Displacement Noise Caused by Fringe-wrapping

3.2.5 Elliptical Baffle

3.2.5.1 ITM Elliptical Baffle

A conceptual drawing of the suspended ITM Elliptical Baffle is shown in Figure 20.

3.2.5.1.1 ITM Elliptical Baffle Seismic Attenuation

The ITM elliptical baffle will be suspended with a single pendulum from the HEPI support ring adjacent to the AR side of the ITM. Earthquake stops will be mounted to the chamber walls.

The required motion attenuation of the Elliptical Baffle is shown in Figure 21.

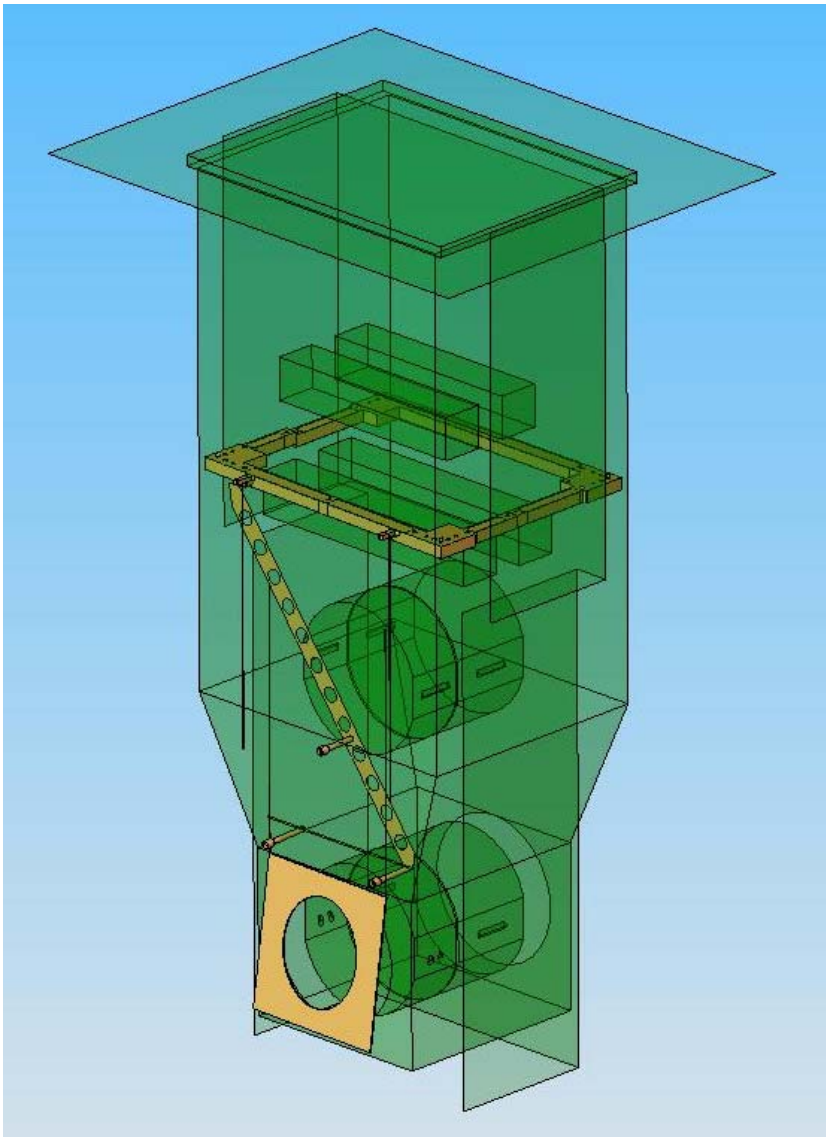

Figure 20: Suspended Elliptical Baffle

3.2.5.1.2 ITM Elliptical Baffle Reflectivity

The light that is not absorbed by the ITM Elliptical Baffle will reflect from the baffle surface onto the insides of the vacuum chamber. There, it will scatter from the wall, reflect again from the ITM Elliptical Baffle, and enter the IFO mode at the far COC.

The scattered light model determined that the reflectivity of the ITM Elliptical Baffle must be < 0.001.

This low reflectivity will be obtained by using a single sheet of black glass with a high efficiency AR coating.

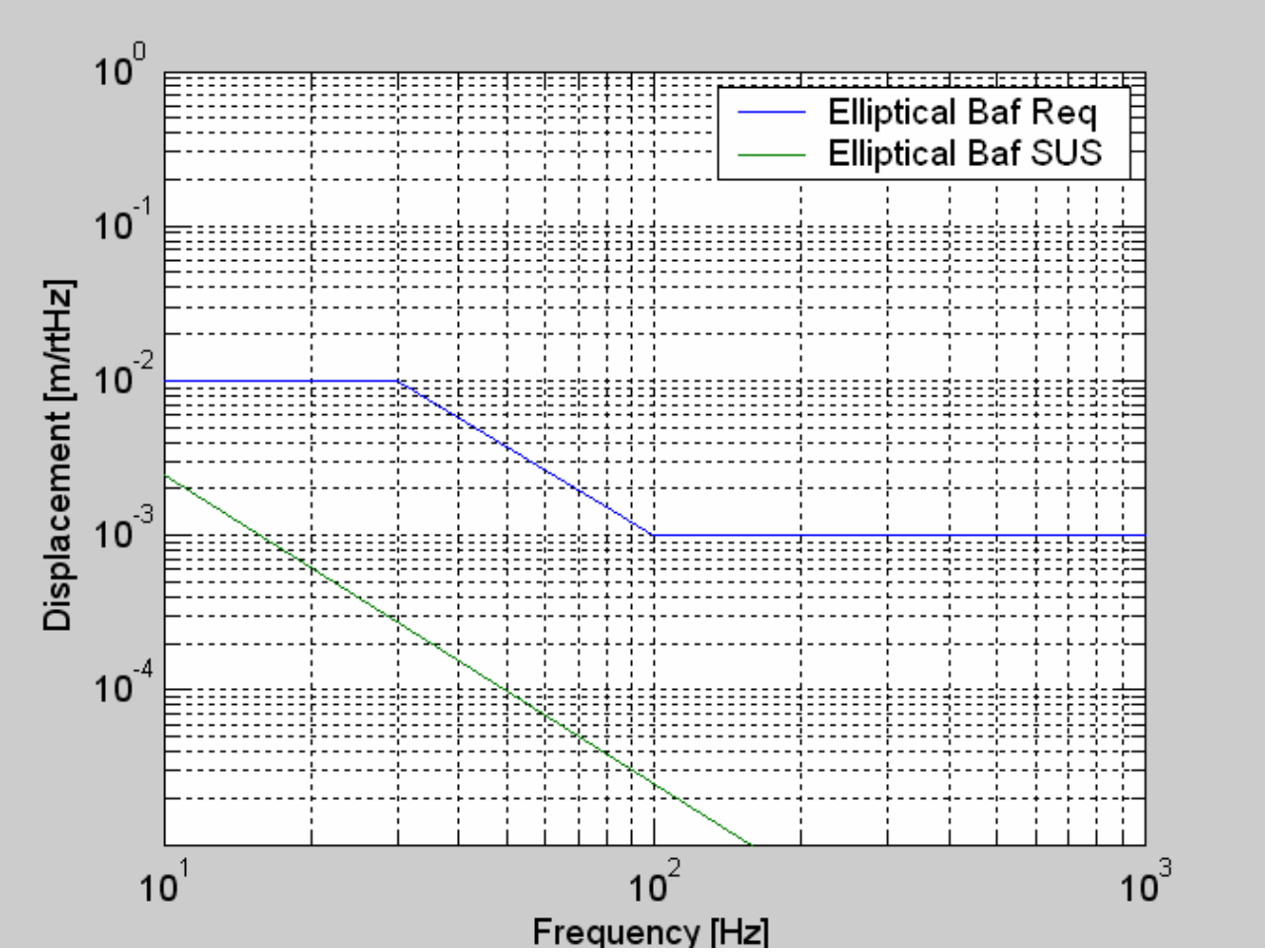

Figure 21: Elliptical Baffle SUS Amplitude Response

3.2.5.1.3 Seismic Motion of the Vacuum Chamber

The seismic motion of the vacuum chamber is shown in Figure 22. See Robert Schofield (11/17/06 LHO ILOG).

3.2.5.1.4 Scattered Light Displacement Noise of Suspended Elliptical Baffle

The light that scatters directly from the surface and from the edges of the beam hole of the suspended Elliptical Baffle has a phase noise caused by the seismic motion of the HEPI support ring attenuated by the transfer function of the Elliptical Baffle suspension, which is shown in Figure 21.

The light that reflects from the baffle and subsequently scatters will have a phase noise caused by the seismic motion of the chamber walls.

The vacuum chamber walls are assumed to have a BRDF = 0.1 sr^-1. The Elliptical Baffle surface BRDF < 0.01 sr^-1. The Elliptical Baffle edge BRDF = 0.1 sr^-1.

The scattered light displacement noise from these three sources is shown in Figure 23.

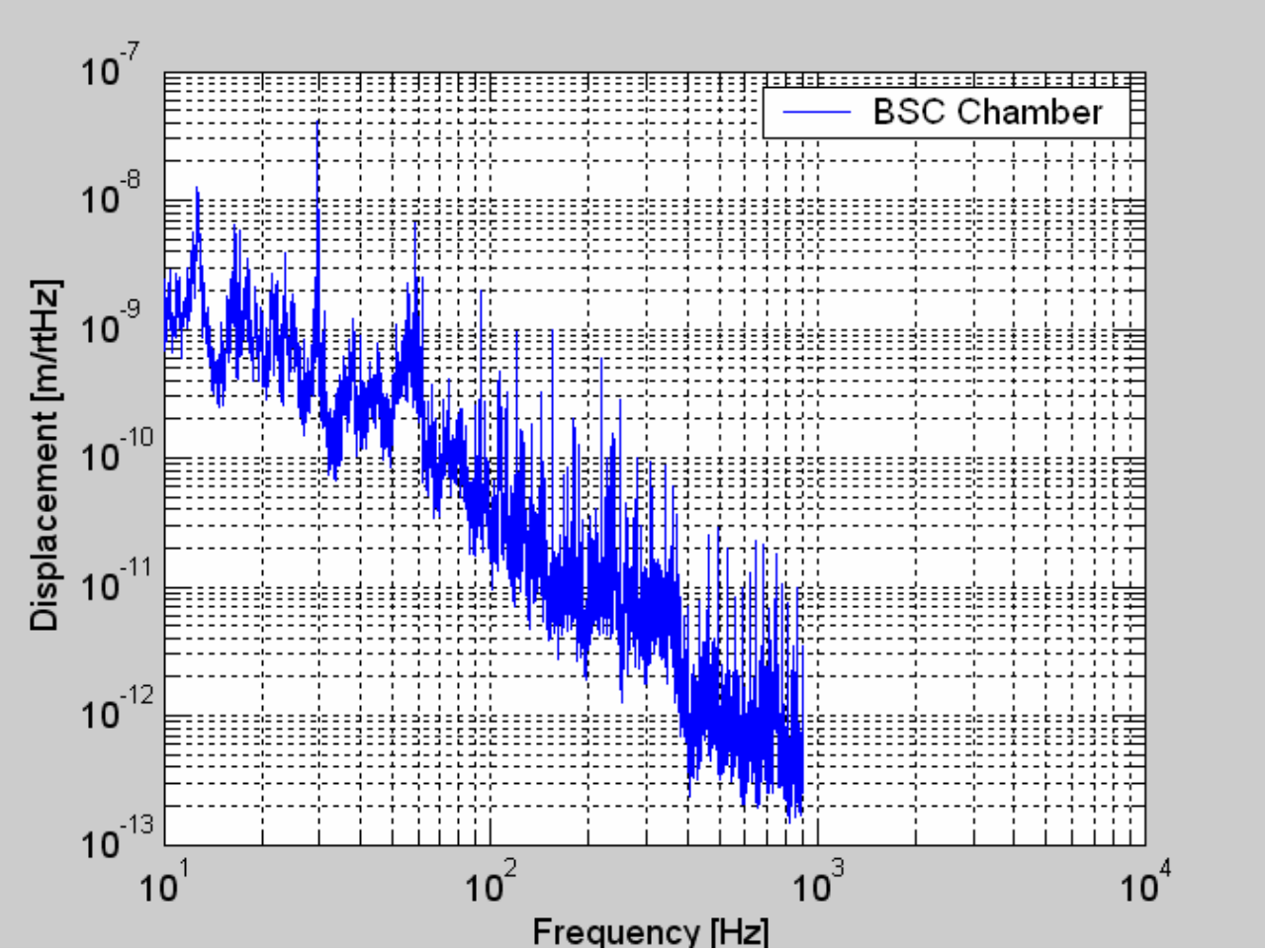

Figure 22: Seismic motion of BSC chamber

3.2.5.1.5 Stay Clear Diameter

The clear aperture of the Elliptical Baffle is 218 mm horizontal diameter and 249 mm vertical diameter. This is 2 mm larger on all sides than the limiting aperture that is determined by the vertical clear aperture of the PRM and the horizontal clear aperture of the BS, which define the size and shape of the beam in the recycling cavity. The Elliptical Baffle will be aligned within 2 mm of the beam center.

This meets the requirement 4.7 Clear Aperture Requirements.

3.2.5.2 PRM Elliptical Baffle

The PRM Elliptical Baffle will mount to the modified LOS structure on the AR side of the PRM.

3.2.5.2.1 Motion of PRM Elliptical Baffle

The seismic motion will be the same as the HAM optical table shown in Figure 8.

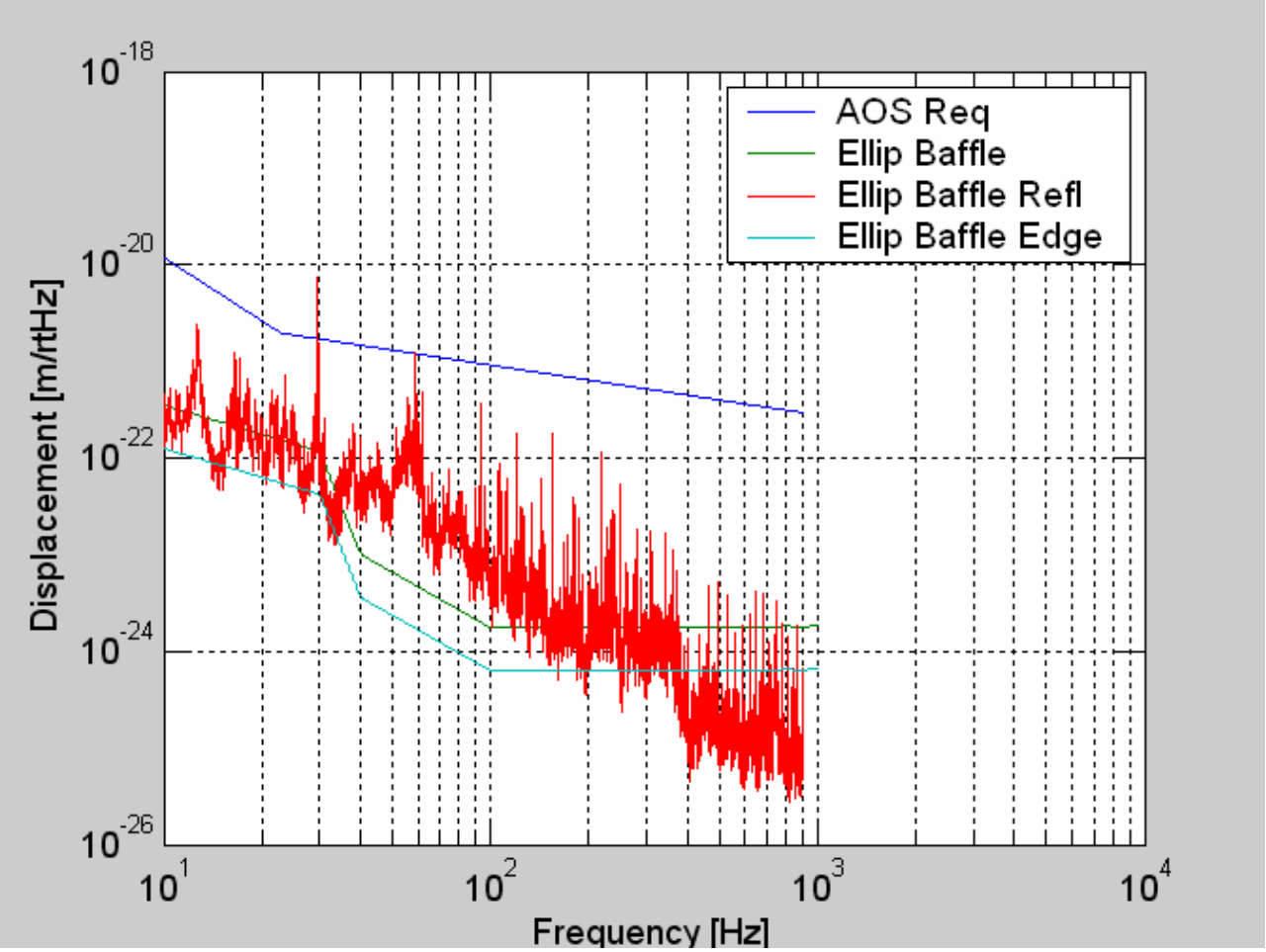

Figure 23: Elliptical Baffle Scattered Light Displacement Noise

3.2.5.2.2 Power Hitting the PRM Elliptical Baffle from IO Side

The irradiance of the IO Gaussian beam incident on the PRM Elliptical Baffle is given by

$$I_{PSL}(x,y) := 2\cdot\frac{P_{0psl}}{\pi\cdot w^2}\cdot e^{-2\cdot\left(\frac{x^2+y^2}{w^2}\right)}$$

where P_{0psl} is the total power in the IO beam, and w= 0.060 m is the Gaussian beam radius. The power passing through the hole in the elliptical baffle is given by

$$P_{all} := 4\cdot\int_0^b\int_0^{a\cdot\sqrt{1-\frac{y^2}{b^2}}} I_{PSL}(x,y)\,dx\,dy$$

The power that hits the elliptical baffle is given by

$$P_{prmellbaf} := P_{psl} - P_{el}$$

With a total power input = 125 W, the power hitting the elliptical baffle is = 0.084 W. Approximately 80 % of this power will be absorbed by the baffle, and the remaining 20% will reflect from the angled baffle onto the inside of the IO beam tube.

3.2.5.2.3 Scattered Light Displacement Noise of PRM Elliptical Baffle

The symmetric port beam that emerges from the PR mirror passes freely through the PRM Elliptical baffle because the baffle determines the extent of the beam in the recycling cavity. A negligible fraction of the symmetric port beam will be scattered by the baffle toward the power recycling cavity.

Assuming that 1ppm fraction of the symmetric port beam is scattered by the PRM elliptical baffle and a BRDF = 0.1, the scattered light displacement noise is shown in Figure 24.

3.2.5.2.4 Stay Clear Diameter

The clear aperture of the Elliptical Baffle is 218 mm horizontal diameter and 249 mm vertical diameter. This is 2 mm larger on all sides than the limiting aperture that is determined by the vertical clear aperture of the PRM and the horizontal clear aperture of the BS, which define the size and shape of the beam in the recycling cavity. The Elliptical Baffle will be aligned within 2 mm of the beam center.

3.2.6 Manifold Baffle

3.2.6.1 Wide Angle Scatter from COC

The wide-angle scatter from point defects on the ITM and ETM will hit the vacuum manifold wall that attaches to the BSC chamber and the spool-piece flange leading to the cryopump at the end of the manifold.

The manifold wall will scatter light back toward the IFO mode area on the surface of the COC, which will subsequently re-scatter that light into the IFO mode.

Some of the wide-angle light from the COC will hit the right-angled cylindrical “corner” where the manifold joins the flat surface of the spool-piece flange. This “corner” will act as an efficient retro-reflector that will return a large fraction of the incident light back to the COC.

A manifold baffle, shown in Figure 25, will hide the “corner” and avoid the retro-reflection.

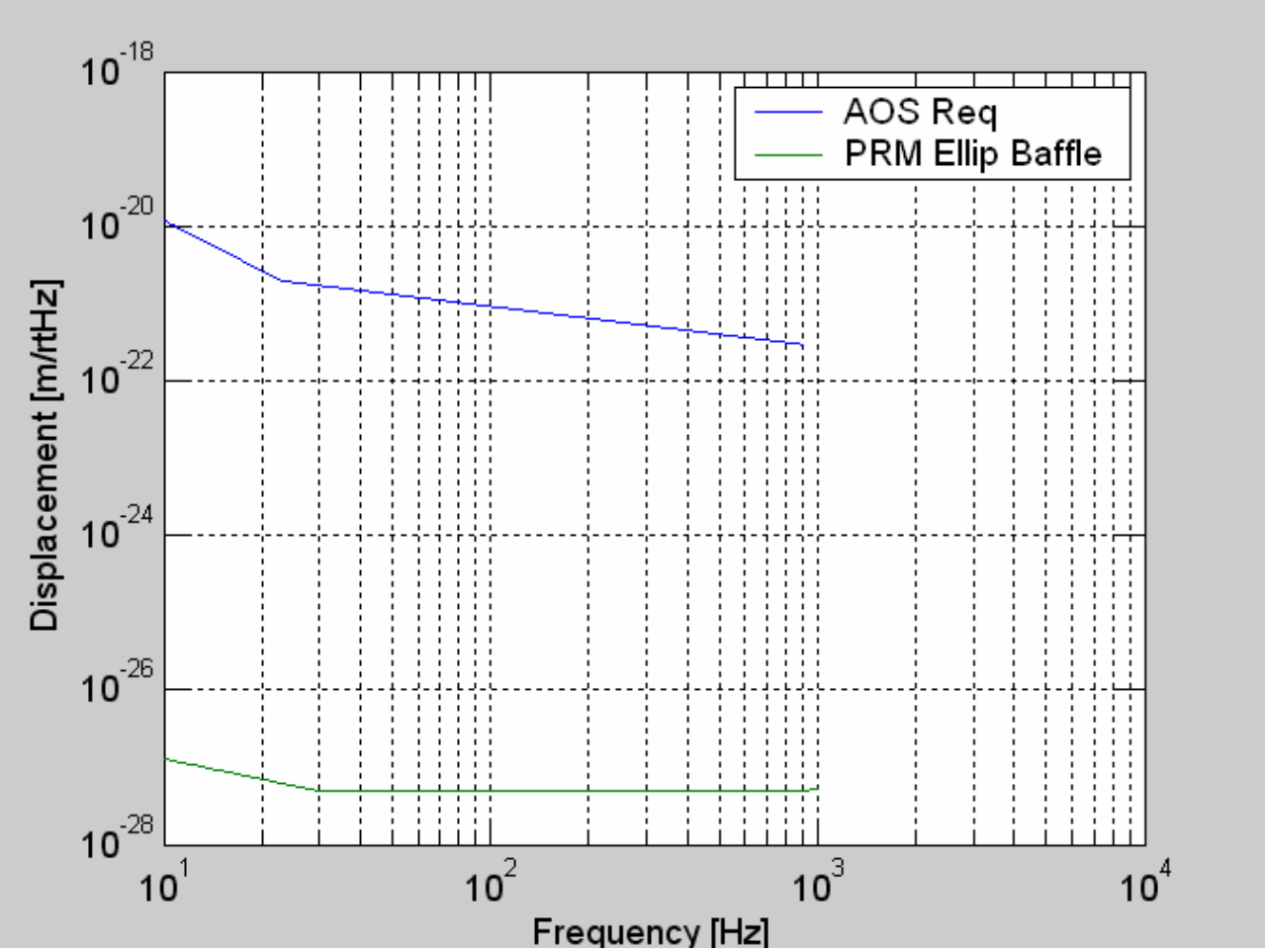

Figure 24: Scattered Light Displacement Noise of PRM Elliptical Baffle

3.2.6.1.1 Seismic Motion of Manifold Baffle

The manifold wall and the Manifold Baffle have the motion spectrum of the manifold, as shown in Figure 17.

A preliminary FEA vibration analysis shows that the first resonance of the Manifold Baffle occurs at approximately 120 Hz. The Q is expected to be <1000, so the motion will be acceptable.

3.2.6.1.2 Scattered Light Displacement Noise of Wide-angle COC Scattering

The wide-angle scattered light from the COC mirror was assumed to have a Lambertian distribution with total integrated scattered power equal to 15ppm fraction of the circulating power in the arm cavity. Much of this scattered light will be intercepted by the proximity of the arm cavity baffle, and some of the light will pass through the beam holes in the Arm Cavity Baffle and hit the walls.

The calculated displacement noise spectrum from light scattered into the IFO mode from three sources: 1) light scattering from the manifold wall, 2) light retro-reflecting from the spool-piece

flange surface at the end of the baffle, and 3) light scattered from a manifold baffle blocking the spool-piece flange corner, is shown in Figure 26.

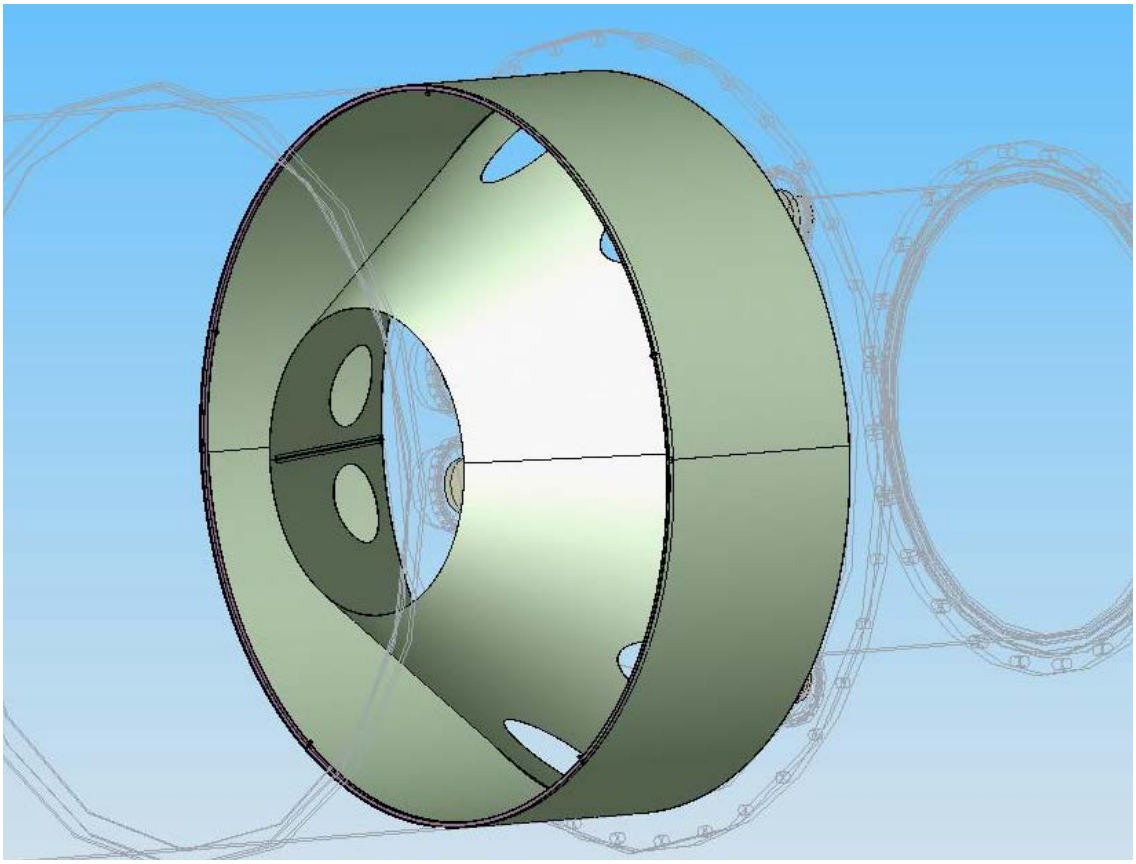

Figure 25: Manifold Baffle

The diffuse scatter by the manifold wall is acceptable, but may be problematical at low frequencies if the scattered power ratio is > 15 ppm;

The retro-reflected light from the spool-piece will cause excessive noise, as shown by the cyan curve. However, this excessive displacement noise can be reduced to a negligible level by blocking the corner of the spool-piece flange /manifold with the conical manifold baffle, as shown by the red curve.

3.2.7 Brewster's Window

Brewster's Windows for the AS beam, the ITMX PO beam, and the BS PO beam will be mounted to the HAM6 Septum Plate, which is mounted to the flange of the HAM chamber, as shown in Figure 27. The compressible bellows between the Septum Plate assembly and the mounting flange of HAM 6 allows the Brewster's Windows to be removed without moving any other vacuum enclosures.

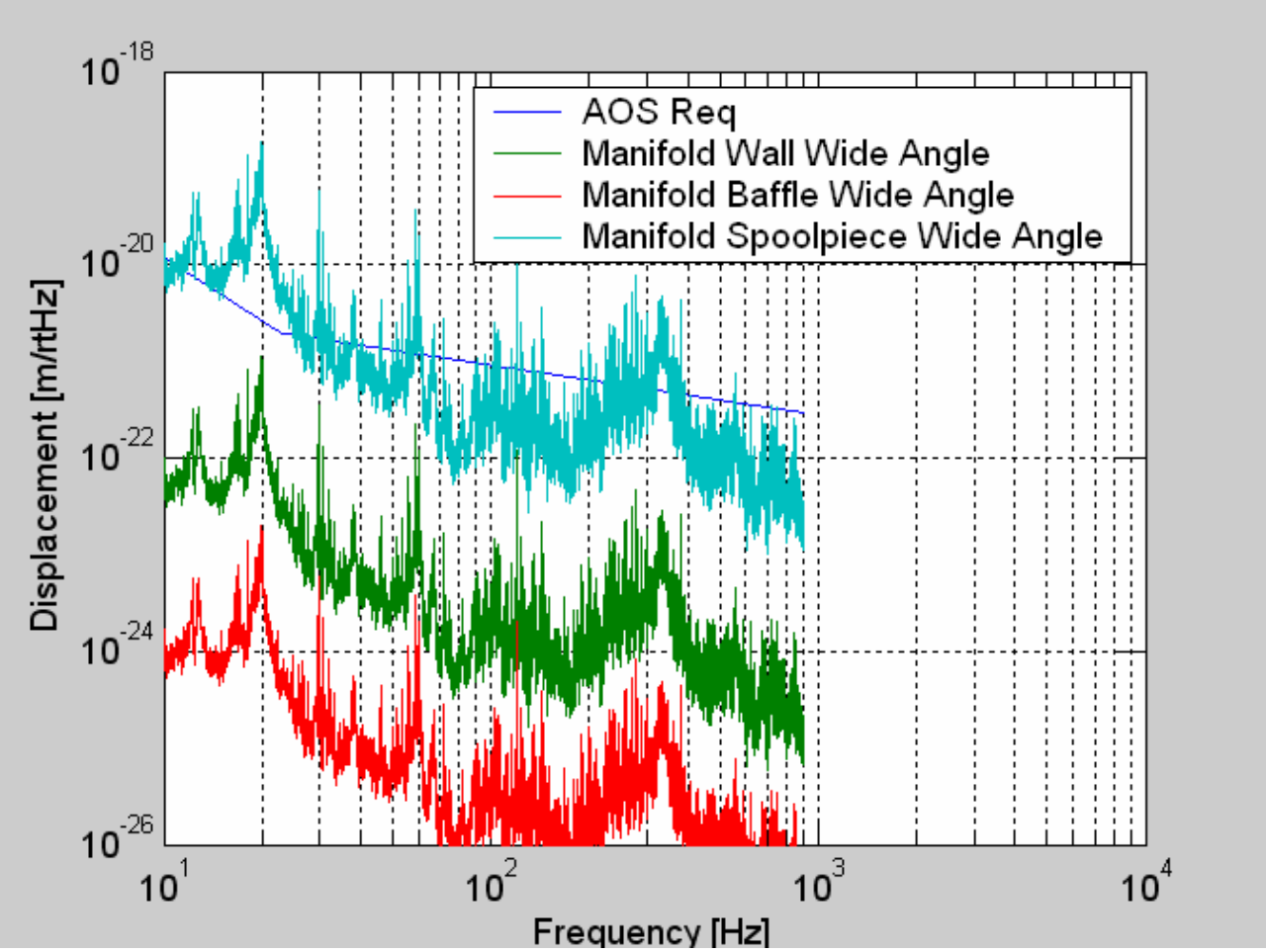

Figure 26:Wide-Angle COC Scattered Light Displacement Noise

3.2.7.1 Brewster's Window BRDF

The BRDF of the Brewster's Window was estimated using the fractal back-scattering model proposed by R. Weiss; see T920004-00 Estimation of Special Optical Properties of a Triangular Ring Cavity, for incidence angles > 0.1 rad.

$$BRDF_{56} := \frac{\alpha}{0.98^2}$$

Where

$$\alpha := 1.5 \cdot 10^{-3} \cdot S$$

and S is the total integrated scattering loss of the surface.

The incidence angle on the Brewster's Window is 56 degrees. The total scattering loss per surface is estimated to be 40 ppm.

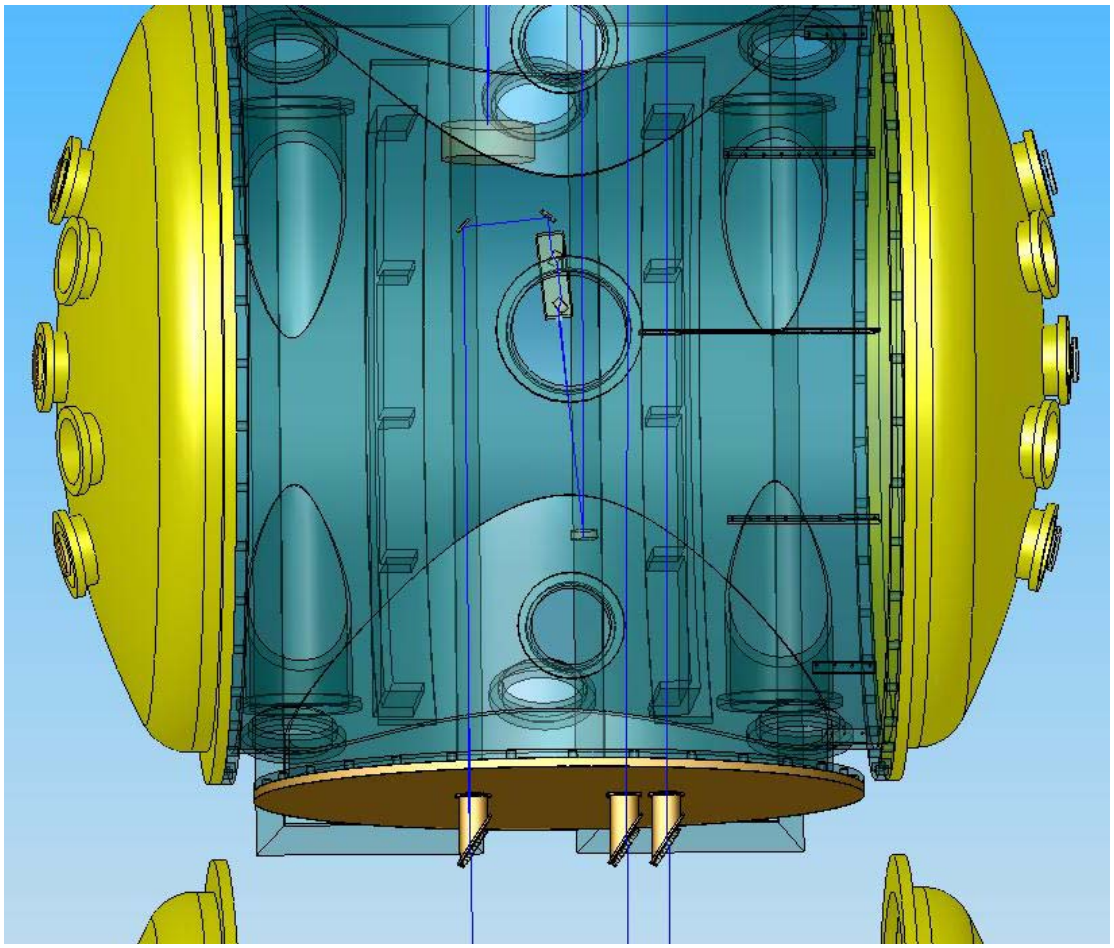

Figure 27: AS Brewster's Window Mount

The calculated BRDF is 6E-6 sr^{-1}. A corroborating data point is the specification for a super polished mirror in the Newport catalog: BRDF < 3E-6 sr^{-1} @ 56 deg incidence. The BRDF of an uncoated window may be lower than the value for a mirror surface.

3.2.7.2 Seismic Motion of the Brewster's Windows

The Brewster' Windows are mounted directly the HAM Plenum, and will have the displacement spectrum of the HAM6 flange, as shown in Figure 28. See Robert Schofield (11/17/06 LHO ILOG).

3.2.7.3 Scattered Light Displacement Noise of Brewster's Window

The AS beam, the ITMX PO beam, and the BS PO beam all scatter from Brewster's windows that move with the displacement spectrum of the HAM6 flange. With an assumed BRDF of 5E-6 for two Brewster's window surfaces, the scattered light displacement noise from the Brewster's windows is shown in Figure 29. The scattered light noise from the AS Brewster's beam exceeds the AOS requirement and also the ADLIGO Science requirement.

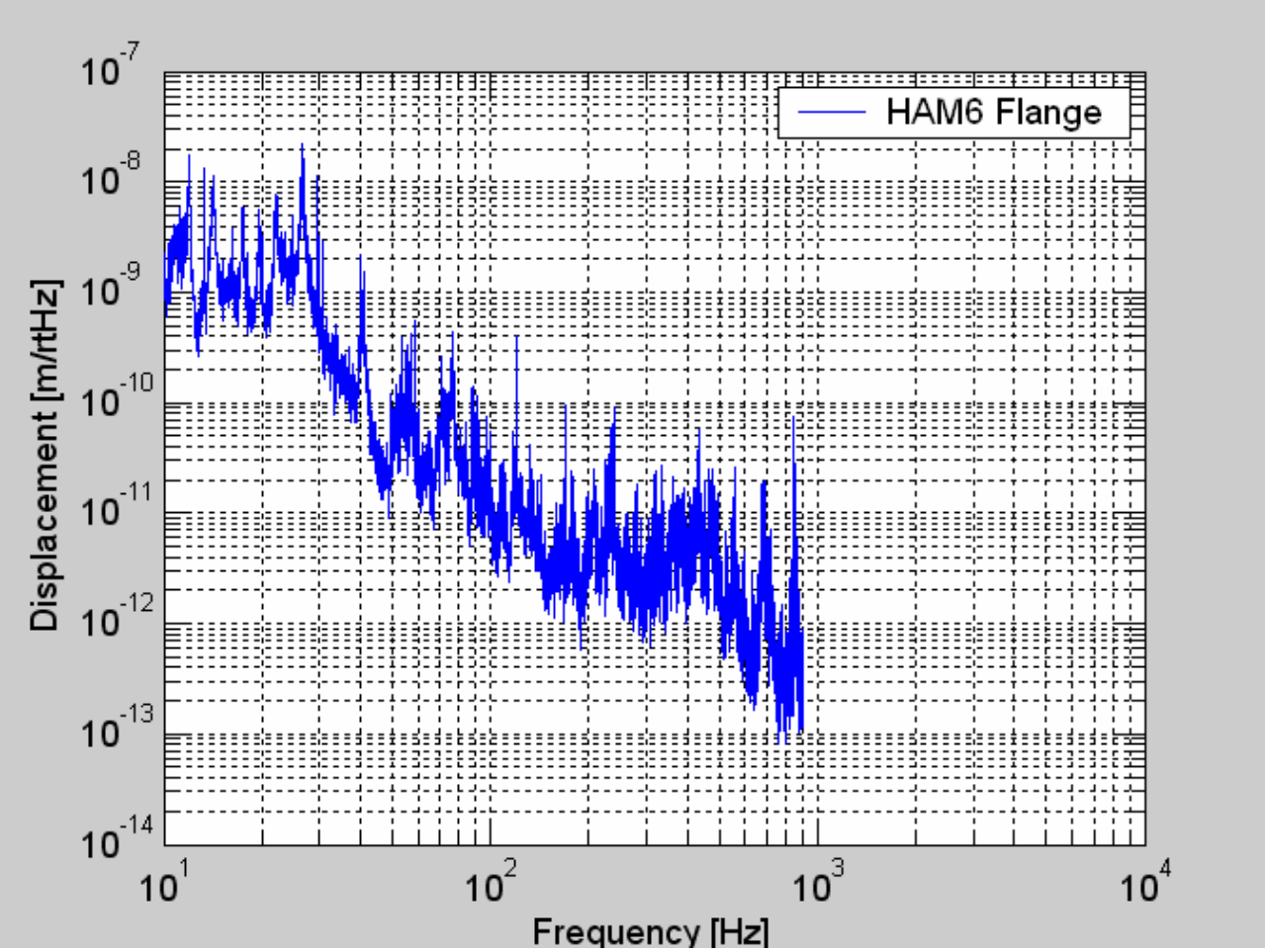

Figure 28: Displacement Spectrum of HAM 6 Flange

3.2.7.3.1 Reflected Light from AS Brewster's Window

The light that reflects from the two surfaces of the AS Brewster's window will hit the insides of the window nozzle. Then, it will scatter from the nozzle, reflect again from the Brewster's Window, and enter the IFO mode.

The reflectivity of the window at Brewster's angle for p-polarized light is given by the Fresnel equation

$$R(\theta) := \left(\frac{n^2 \cdot \cos\left(\theta \cdot \frac{\pi}{180}\right) - \sqrt{n^2 - \sin\left(\theta \cdot \frac{\pi}{180}\right)^2}}{n^2 \cdot \cos\left(\theta \cdot \frac{\pi}{180}\right) + \sqrt{n^2 - \sin\left(\theta \cdot \frac{\pi}{180}\right)^2}} \right)^2$$

Brewster's angle, at which the reflectivity vanishes, is equal to 55.4 deg, for a fused silica window with n = 1.445.

If the incident beam on the Brewster's window differs by ±2 deg from Brewster's angle, the reflectivity will vary from

$$R(\theta_{Brew}+2) = 4.2E\text{-}4 \text{ to } R(\theta_{Brew}-2) = 3.5E\text{-}4$$

The scattered light model was used to calculate the scattering from the reflected light that hits the window nozzle, assuming a BRDF of the nozzle of 0.1 sr^-1, and the reflectivity of the Brewster's Window R = 4E-4. The results shown in Figure 29, indicate that the reflected light displacement noise is an order of magnitude less than the direct scattered light from the AS Brewster's window and is not a dominant noise source.

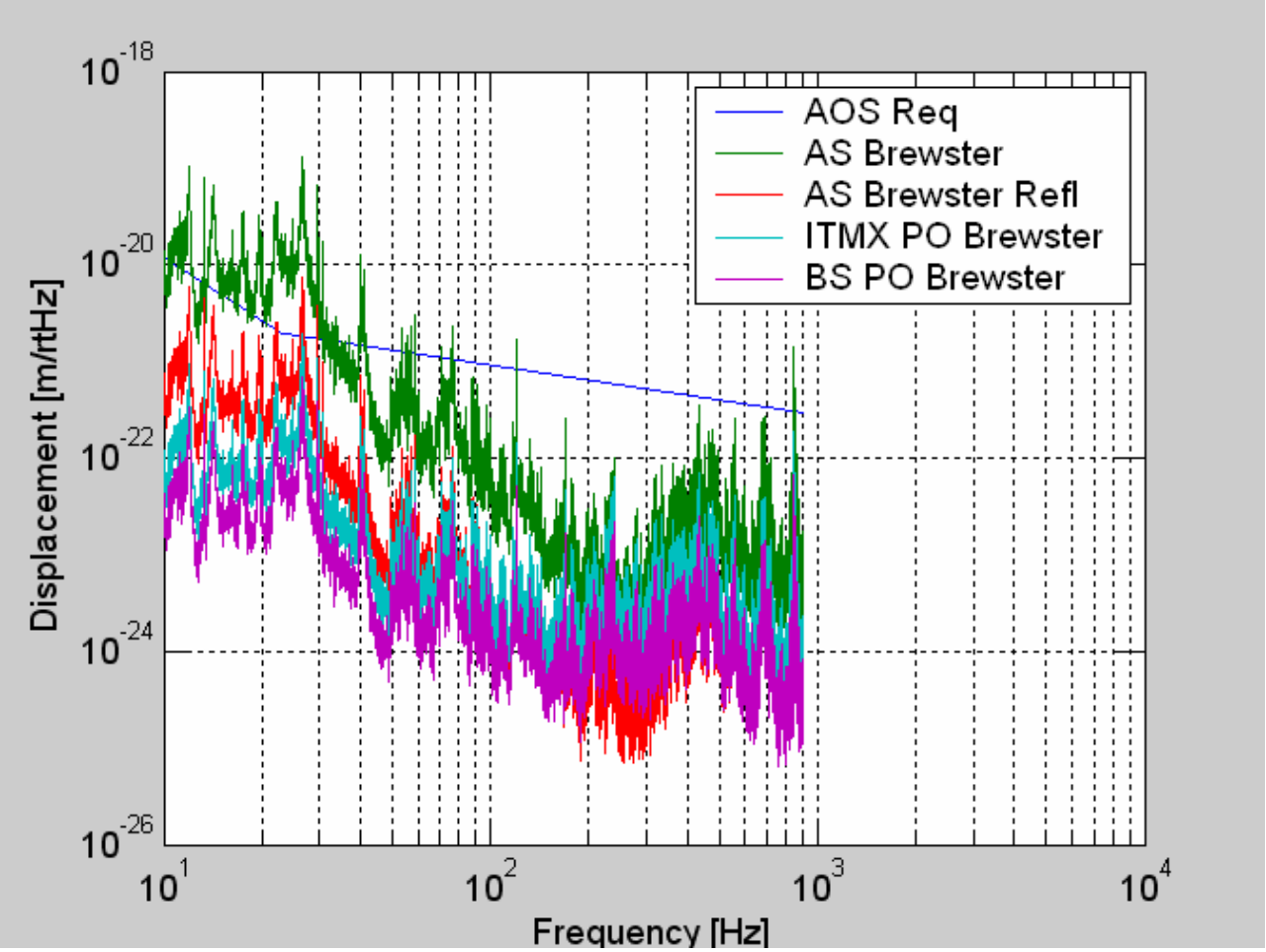

Figure 29: Brewster's Window Scattered Light Displacement noise

3.2.7.4 Brewster's Window Removal

The Brewster's Window is mounted to the nozzle piece with o-rings and a capture flange, and the nozzle piece is mounted independently to the HAM Plenum. Therefore, the nozzle piece can be removed by venting HAM5, with access from the adjoining vented HAM6 chamber, without removing the blanking flange.

When the Brewster's Windows are removed, the total scattered light displacement noise meets the AOS requirement, as shown in Figure 6.

3.2.7.4.1 Stay Clear Diameter

The clear aperture of the Brewster's Window is > 60 mm diameter. The OMMT, the BS PO TEL, and the ITMX PO TEL have beam reduction ratios of 28.9, which will create an elliptical beam profile at the Brewster's Windows with vertical diameter = 8.5 mm and horizontal diameter = 7.4 mm.

This meets the requirement 4.7 Clear Aperture Requirements

3.2.8 Output Mode Matching Telescope, OMMT

OMMT2 mirror has a reduced spot size, and therefore will be the dominant scattering source of the OMMT.

3.2.8.1 Motion of OMMT2

The OMMT2 mirror is suspended from an SOS that is mounted to the HAM 4 optical table. The longitudinal attenuation of the SOS will be modeled as a single pendulum with a resonance at 1 Hz, see T000134-00, Dynamical Properties of LIGO Single Loop Suspended Mirrors. The minimum suspension requirement was calculated using the scattered light model, with an assumed BRDF = 3E-3, as described in 3.2.8.2. As seen in Figure 30, the SOS suspension exceeds the minimum requirements.

3.2.8.2 BRDF of OMMT2

The BRDF of the OMMT2 will be estimated using the fractal back-scattering model proposed by R. Weiss; see T920004-00 Estimation of Special Optical Properties of a Triangular Ring Cavity, for incidence angles 1E-4 <θ > 0.1 rad. We will assume a total scattering loss of 500 ppm, and a scattering angle of 0.016 rad.

$$\mathrm{BRDF}_{500}(\theta) := \frac{7.444 \times 10^{-7}}{\theta^{2}}$$

$$\mathrm{BRDF}_{500}(0.016) = 2.908 \times 10^{-3}$$

3.2.8.3 Scattered Light Displacement Noise of OMMT

The scattered light displacement noise was calculated using the scattered light model, with a BRDF = 3E-3 and the minimum suspension requirement for the OMMT2 mirror. The displacement noise does not exceed the AOS requirements, as shown in Figure 31.

These results show that the surface figure and micro-roughness of the OMMT mirrors can be of ordinary commercial quality, with a total scattering loss as high as 500 ppm. Super-polished mirrors are not required for the OMMT.

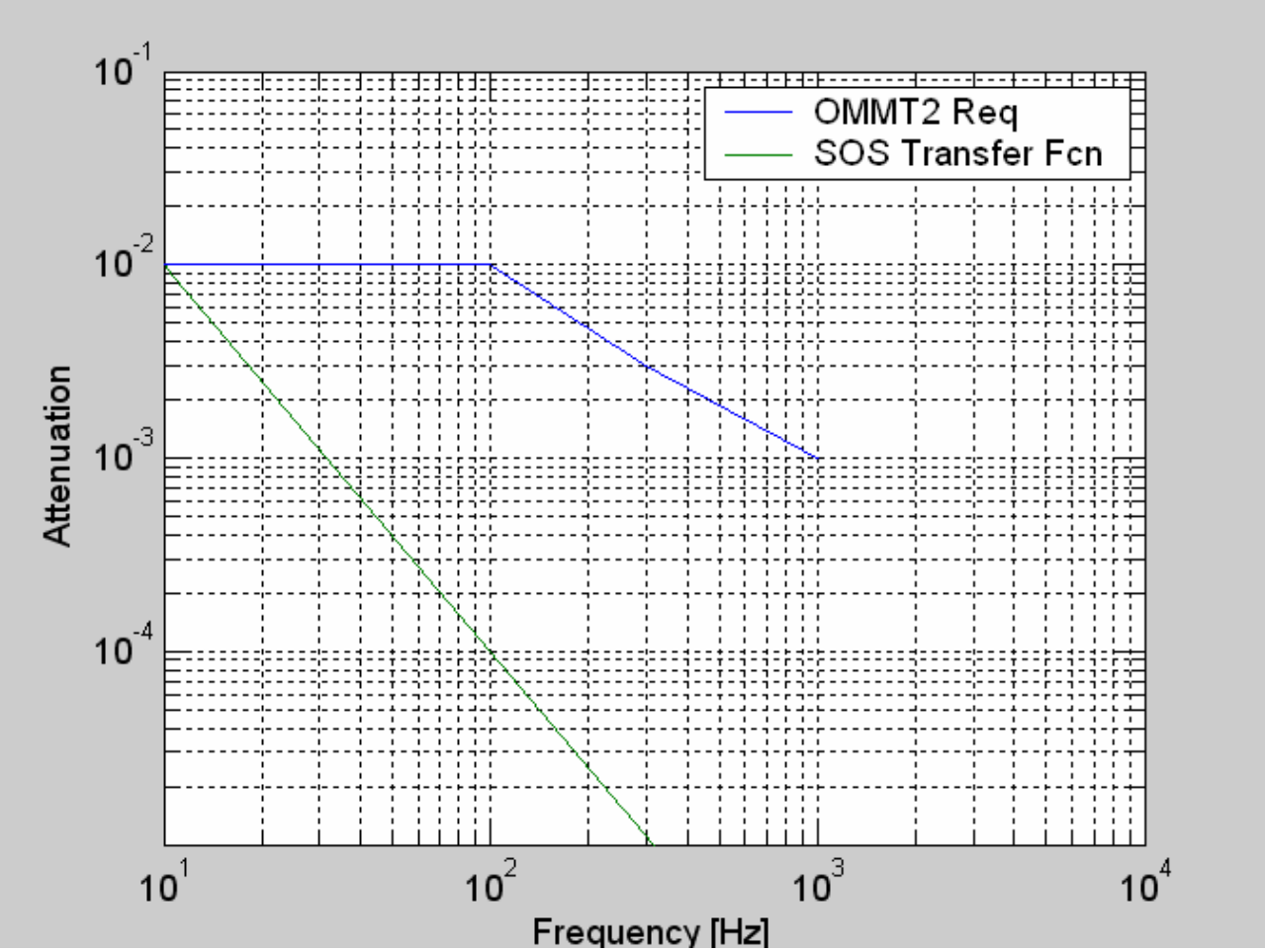

Figure 30: OMMT2 Suspension Requirements

3.2.9 CAVITY BEAM DUMPS

The Cavity Beam dump has a rectangular clear aperture, 218 mm horizontal by 249 mm vertical.

The vertical walls will be made of black glass, fastened between top and bottom metal plates.

3.2.9.1 Un-Dumped Cavity Beam Dump Beam

The Cavity Beam Dumps will be centered within 6 mm of the center of the recycling cavity beam. Less than 100E-6 fraction of the ghost beam power will miss the Cavity Beam Dump and will hit the chamber walls, as described in 3.1.2.3.

3.2.9.2 BSC Mounted Cavity Beam Dumps

A concept for the suspending the Cavity Beam Dump inside the BSC chamber is shown in Figure 32. It is a single pendulum suspended by wires that mount to the HEPI stage “0” support structure.

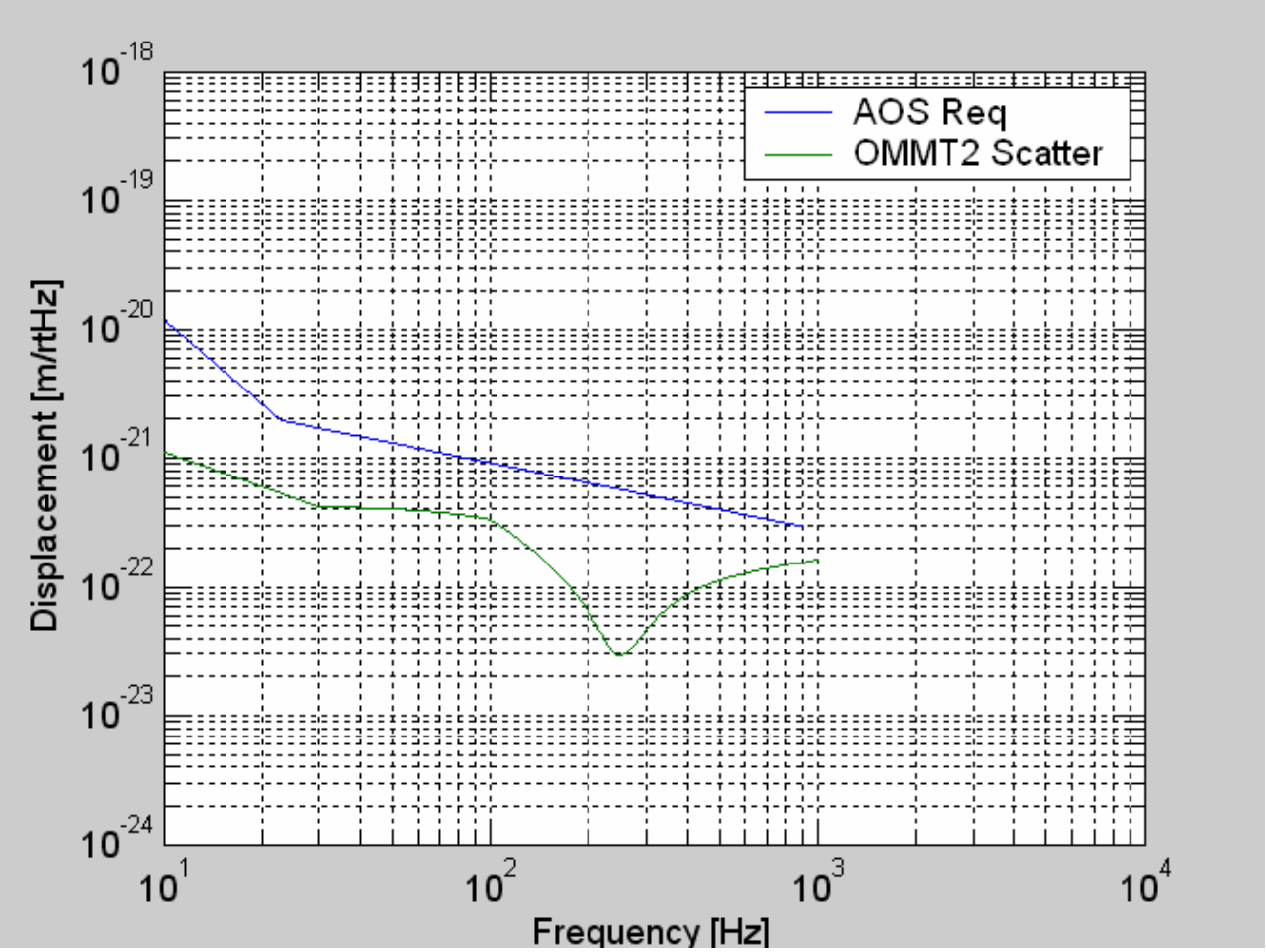

Figure 31: OMMT2 Scattered Light Displacement Noise

3.2.9.2.1 BSC Cavity Beam Dump Seismic Attenuation

3.2.9.2.1.1 Minimum Attenuation Requirement

The longitudinal attenuation of the Cavity Beam Dump will be modeled as a single pendulum with a resonance at 0.5 Hz. The minimum suspension requirement was calculated using the scattered light model, with an assumed BRDF = 0.001. The Cavity Beam Dump suspension exceeds the minimum requirements, as shown in Figure 33.

3.2.9.2.1.2 Damping

The suspended Cavity Beam Dump will be damped with a Q < 1000 by means of elastomeric damping elements surrounding the suspension wires near the top and bottom attachment points.

3.2.9.3 HAM Chamber Mounted Cavity Beam Dumps

The BSAR3P and BSHR3P Cavity Beam Dumps will mount directly to the HAM optical table and will not have an addition suspension.

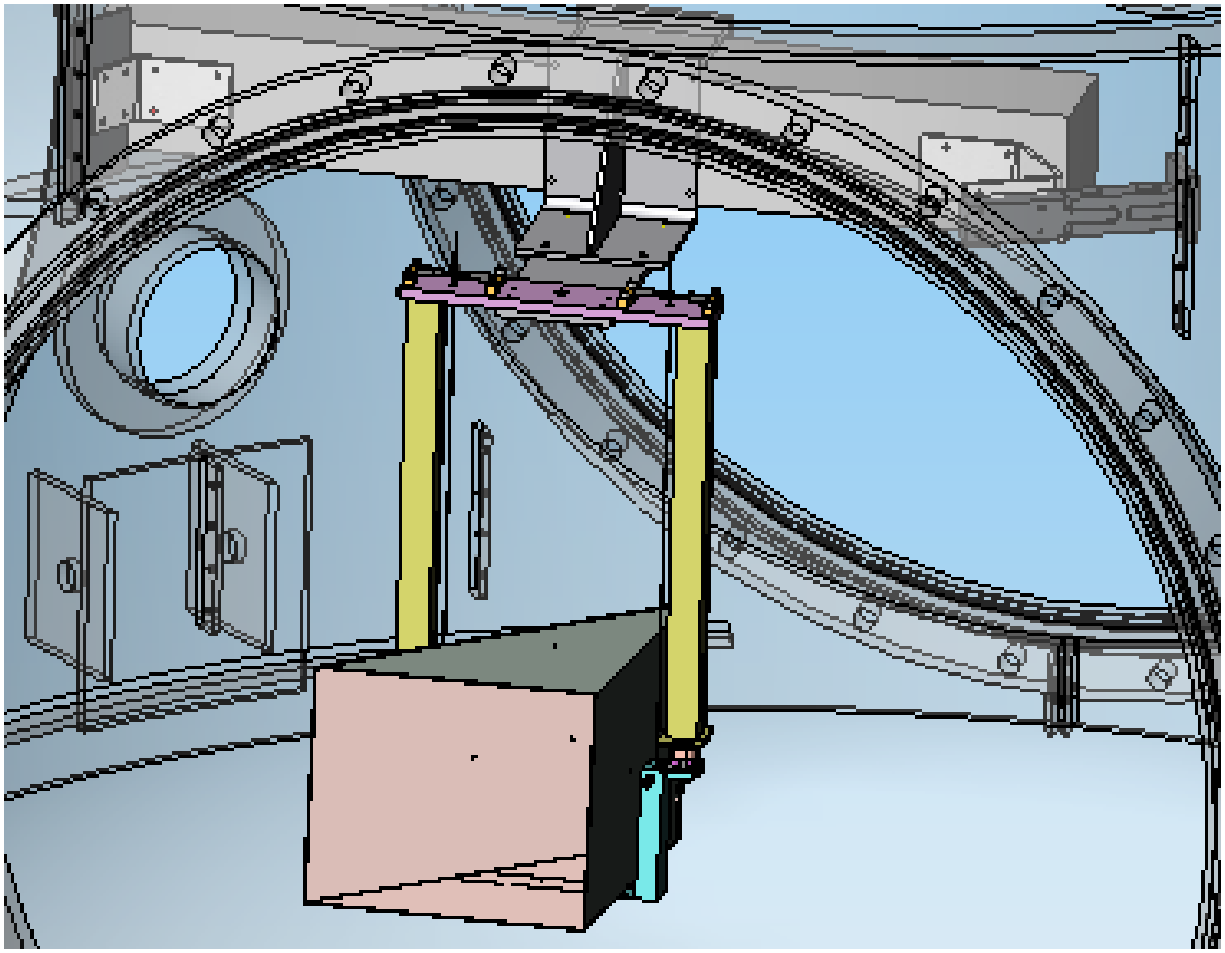

Figure 32: Suspended Cavity Beam Dump Concept

3.2.9.4 Cavity Beam Dump BRDF

The Cavity Beam Dump surfaces will be constructed of black glass with a BRDF < 0.001 sr^-1, and a net reflectivity < 0.005.

3.2.9.5 Scattered Light Displacement Noise of Ghost Beams

3.2.9.5.1 ITMY GBAR1

The ITMY GBAR1 Beam Dump is suspended from the HEPI stage "0" support structure. Most of the ghost beam light will be absorbed and scattered from the beam dump. Less than 100E-6 fraction of the ghost beam will miss the beam dump and scatter from the chamber wall. Some of the light that enters the beam dump will reflect, scatter from the wall, then reflect again from the beam dump surface and enter the mode of the IFO.

The scattered light displacement noise from these sources is shown in Figure 34.

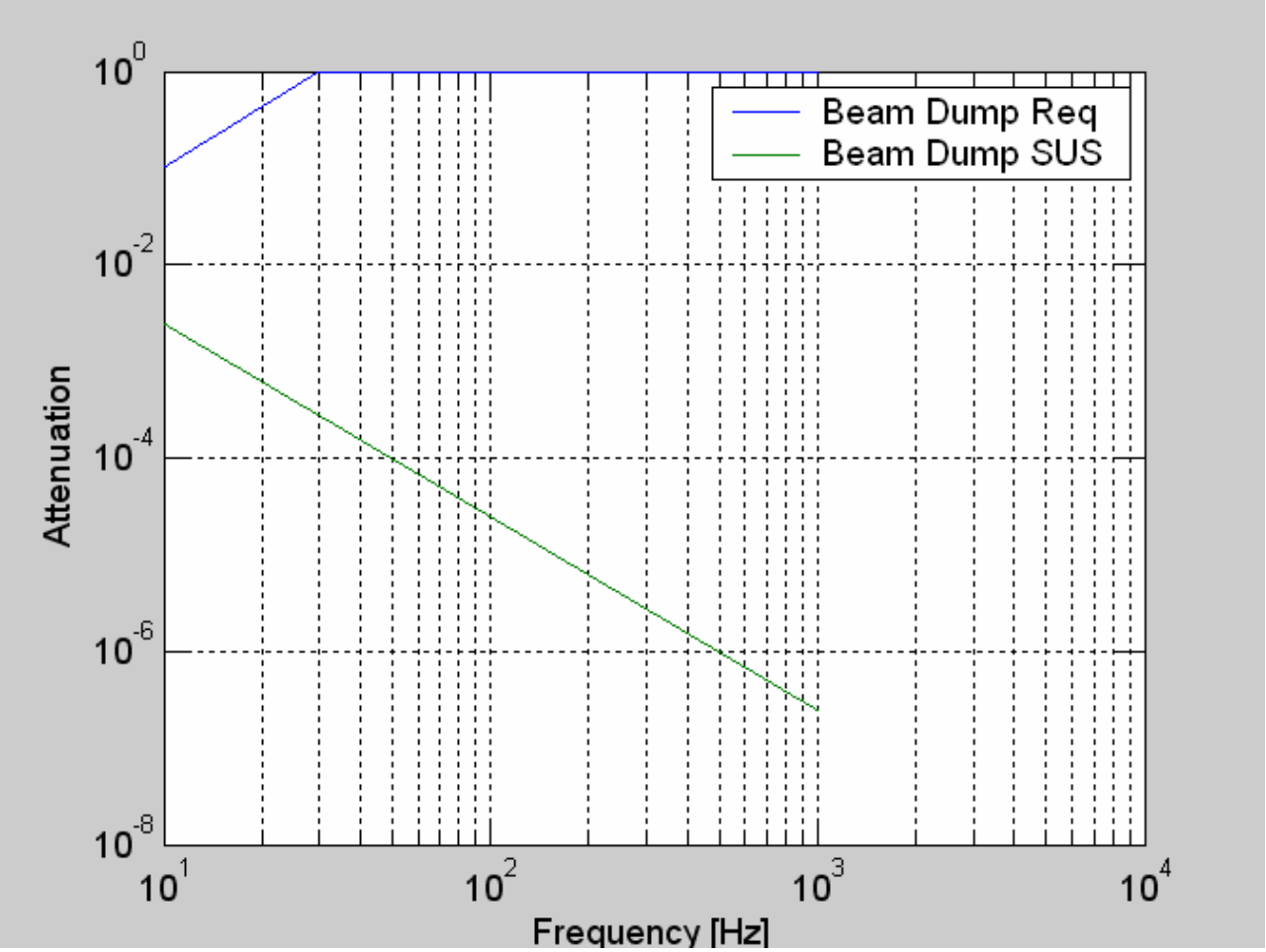

Figure 33: Cavity Beam Dump Suspension Attenuation

3.2.9.5.2 ITMY GBAR3

The ITMY GBAR3 Beam Dump is suspended from the HEPI stage "0" support structure. Most of the ghost beam light will be absorbed and scattered from the beam dump. Less than 100E-6 fraction of the ghost beam will miss the beam dump and scatter from the chamber wall. Some of the light that enters the beam dump will reflect, scatter from the wall, then reflect again from the beam dump surface and enter the mode of the IFO. The scattered light displacement noise from these sources is shown in Figure 35.

3.2.9.5.3 Fringe-wrapping of ITM GBAR3 Beam Dump Displacement Noise

The Beam Dump has a pendulum resonance at around 0.8 Hz. The displacement noise at the odd harmonics of the motion due to fringe wrapping was calculated using the fringe wrap model, assuming a simple pendulum function with Q = 1000 at the resonant frequency. The fringe wrapping does not cause excessive noise above 10 Hz, as shown in Figure 36.

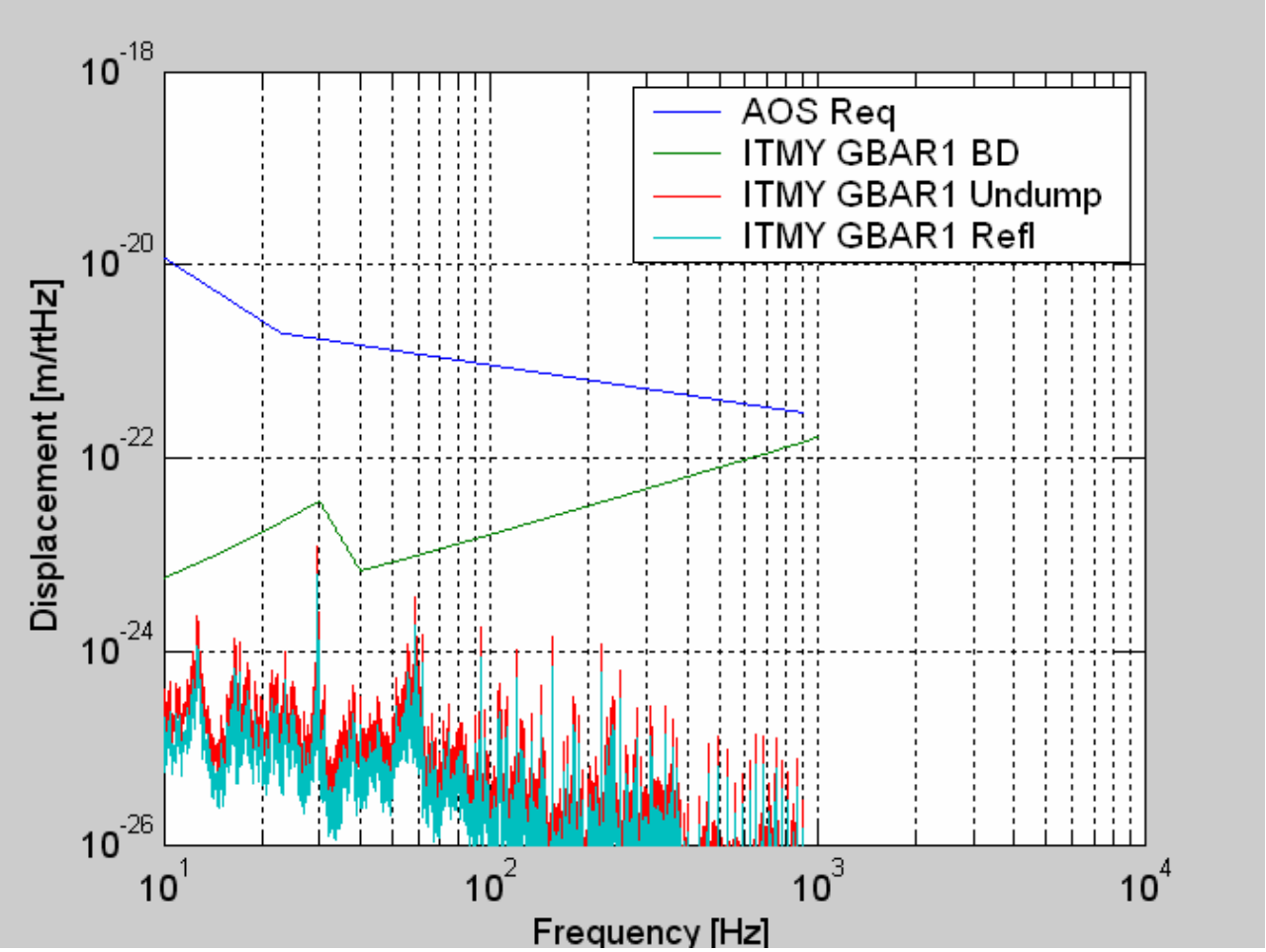

Figure 34: ITMY GBAR1 Beam Dump Scattered Light Displacement Noise

3.2.9.5.4 ITM GBHR3

The ITM GBHR3 Beam Dump is suspended from the HEPI stage "0" support structure. Most of the ghost beam light will be absorbed and scattered from the beam dump. Less than 100E-6 fraction of the ghost beam will miss the beam dump and scatter from the chamber wall. Some of the light that enters the beam dump will reflect, scatter from the wall, then reflect again from the beam dump surface and enter the mode of the IFO. The scattered light displacement noise from these sources is shown in Figure 37.

3.2.9.5.5 Folded ITM GBHR3

The folded ITM GBHR3 ghost beam will hit the walls of the manifold and scatter back into the IFO mode. The scattered light displacement noise is shown in Figure 38.

3.2.9.5.6 BS GBAR1

The BS GBAR1 Beam Dump is mounted to the HAM optical table. Most of the ghost beam light will be absorbed and scattered from the beam dump. Less than 100E-6 fraction of the ghost beam

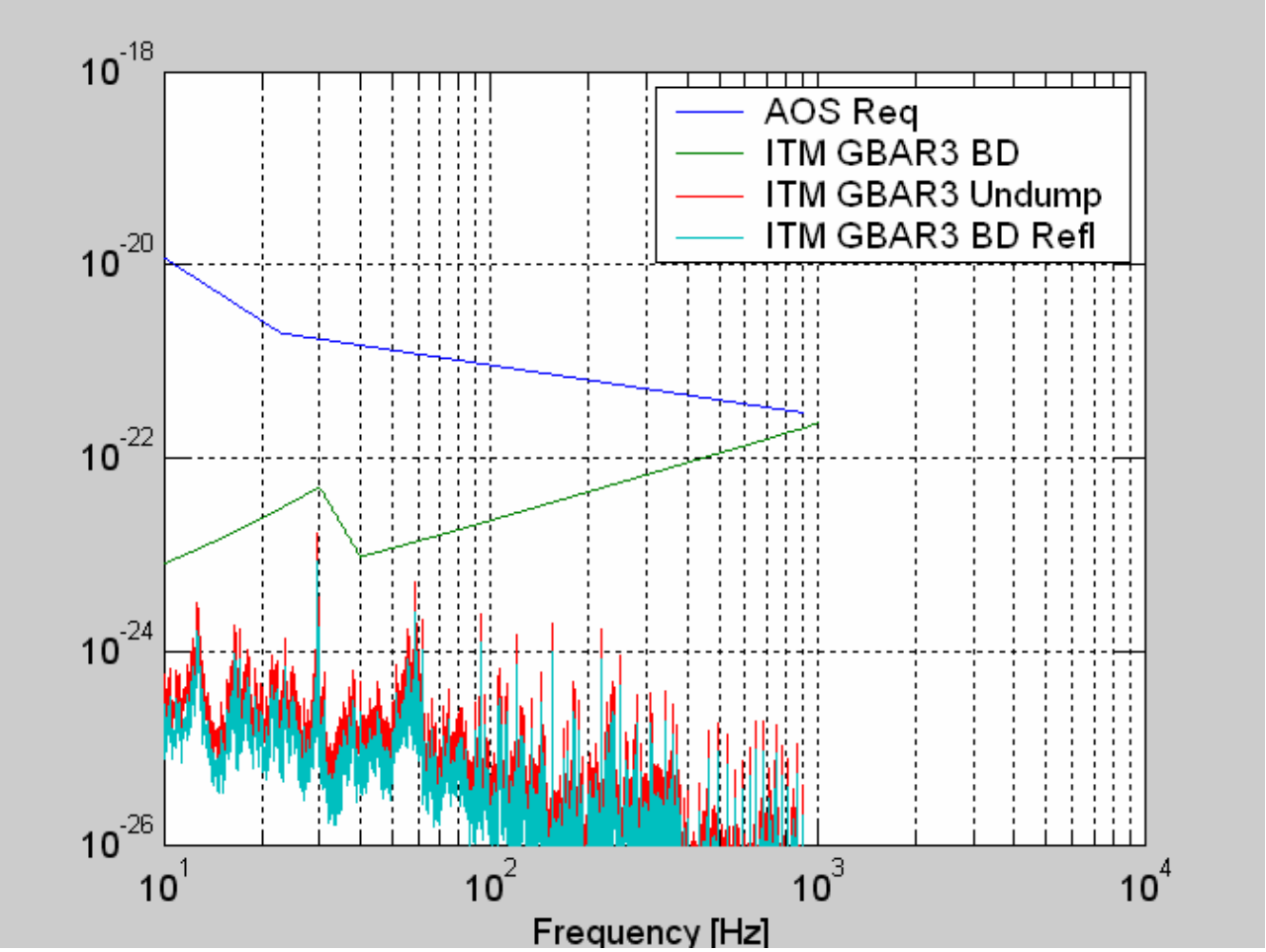

Figure 35: ITM GBAR3 Beam Dump Scattered Light Displacement Noise

will miss the beam dump and scatter from the chamber wall. Some of the light that enters the beam dump will reflect, scatter from the wall, then reflect again from the beam dump surface and enter the mode of the IFO. The scattered light displacement noise from these sources is shown in Figure 39.

3.2.9.5.7 BS GBAR3X

The BS GBAR3X Beam Dump is suspended from the HEPI stage "0" support structure. Most of the ghost beam light will be absorbed and scattered from the beam dump. Less than 100E-6 fraction of the ghost beam will miss the beam dump and scatter from the chamber wall. Some of the light that enters the beam dump will reflect, scatter from the wall, then reflect again from the beam dump surface and enter the mode of the IFO. The scattered light displacement noise from these sources is shown in Figure 40.

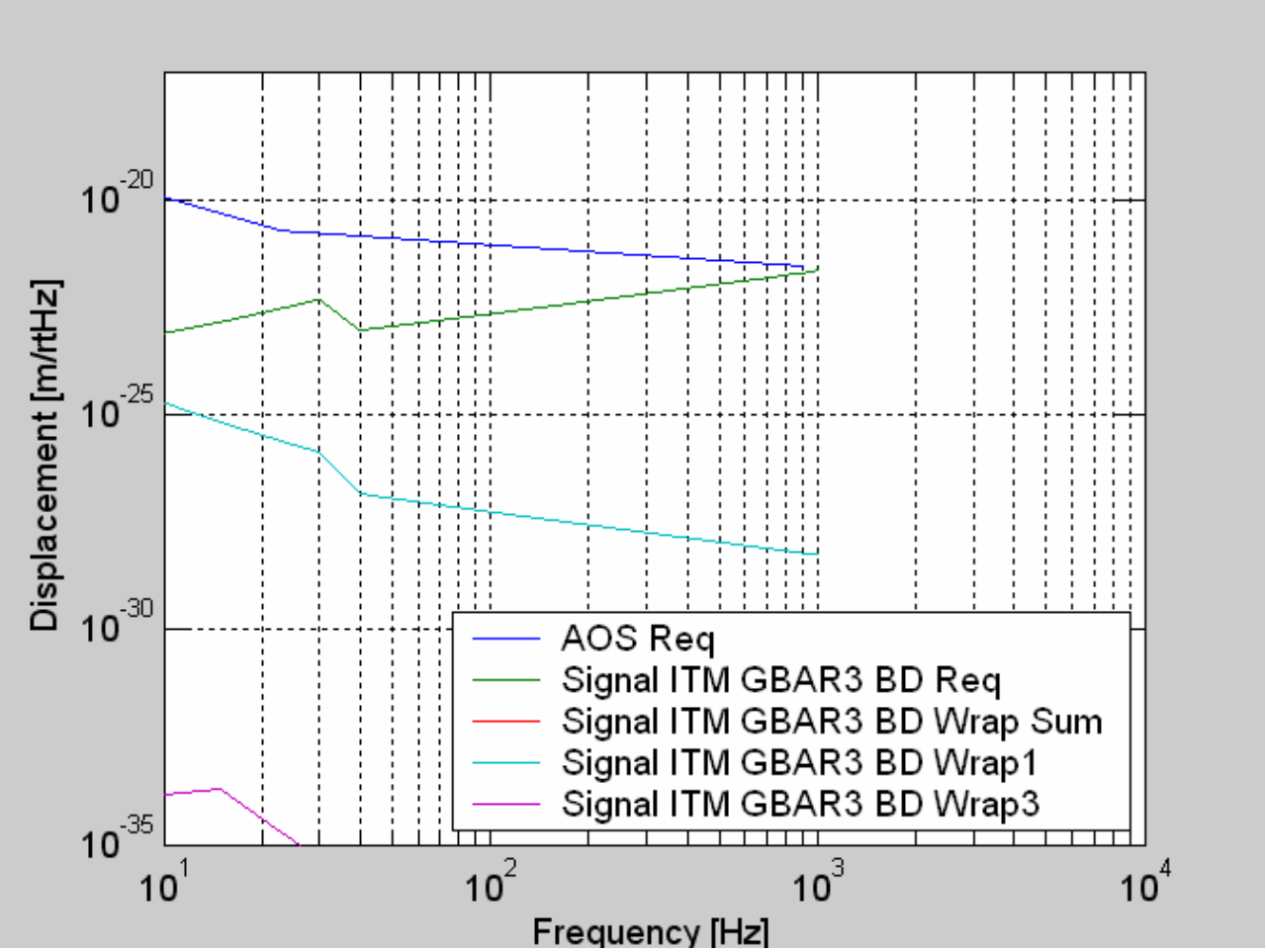

Figure 36: ITM GBAR3 BD Scattered Light Displacement Noise Caused by Fringe-wrapping

3.2.9.5.8 BS GBAR3P

The BS GBAR3P is mounted directly to the HAM optical table. Most of the ghost beam light will be absorbed and scattered from the beam dump. Less than 100E-6 fraction of the ghost beam will miss the beam dump and scatter from the chamber wall. Some of the light that enters the beam dump will reflect, scatter from the wall, then reflect again from the beam dump surface and enter the mode of the IFO. The scattered light displacement noise from these sources is shown in Figure 41.

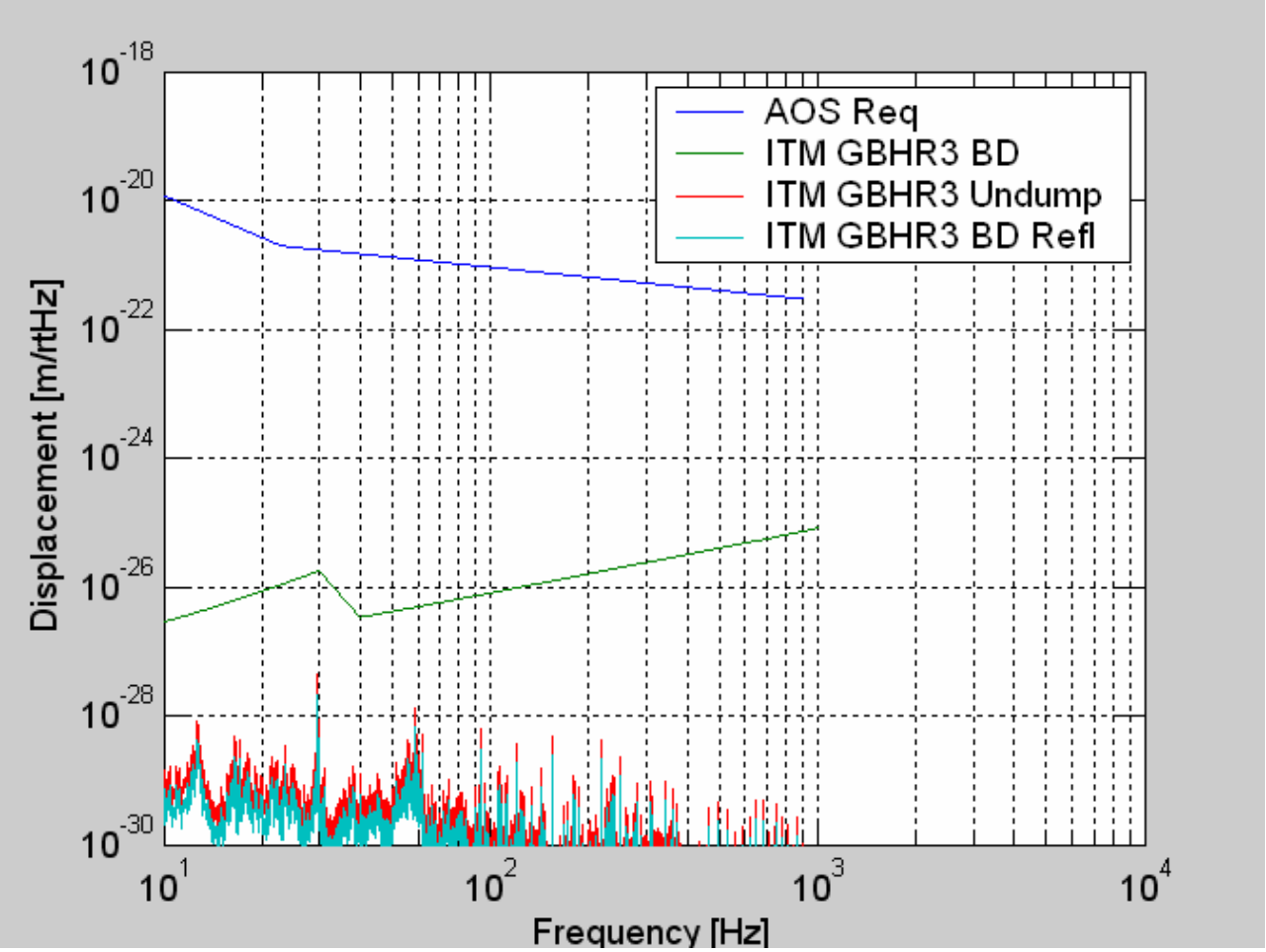

Figure 37: ITM GBHR3 Beam Dump Scattered Light Displacement Noise

3.2.9.5.9 BS GBHR3P

The BS GBHR3P Beam Dump is mounted directly to the HAM optical table. Most of the ghost beam light will be absorbed and scattered from the beam dump. Less than 100E-6 fraction of the ghost beam will miss the beam dump and scatter from the chamber wall. Some of the light that enters the beam dump will reflect, scatter from the wall, then reflect again from the beam dump surface and enter the mode of the IFO. The scattered light displacement noise from these sources is shown in Figure 42.

3.2.9.5.10 ITM GBAR4, ITM GBHR4, BS GBAR4X

The second order ghost beams, ITM GBAR4, ITM GBHR4, BS GBAR4X, and BS GBHR4X will be allowed to hit the walls and scatter. This scattered light will not contribute a significant scattered light displacement noise, as shown in Figure 43.

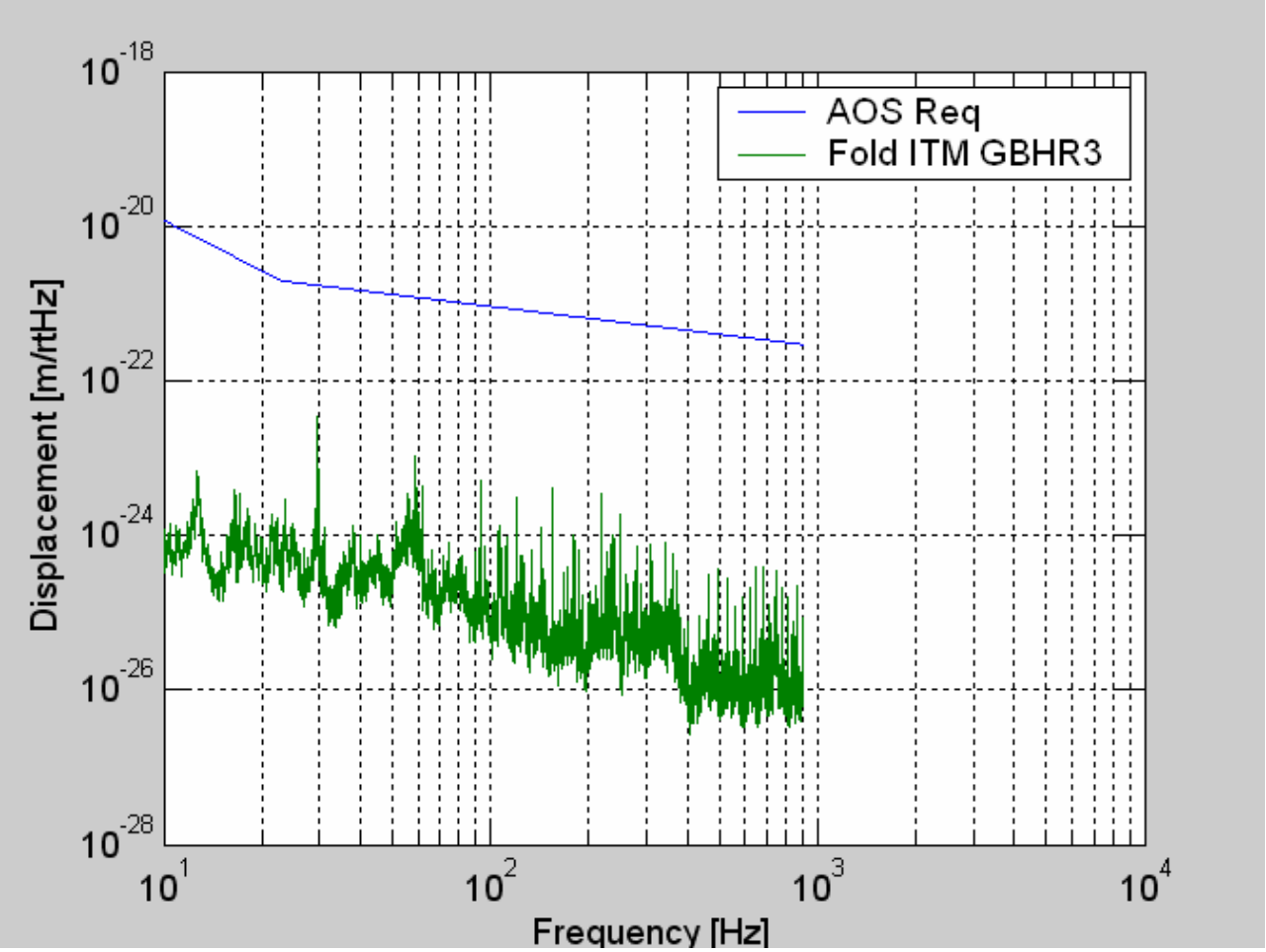

Figure 38: Folded ITM GBHR3 Scattered Light Displacement Noise

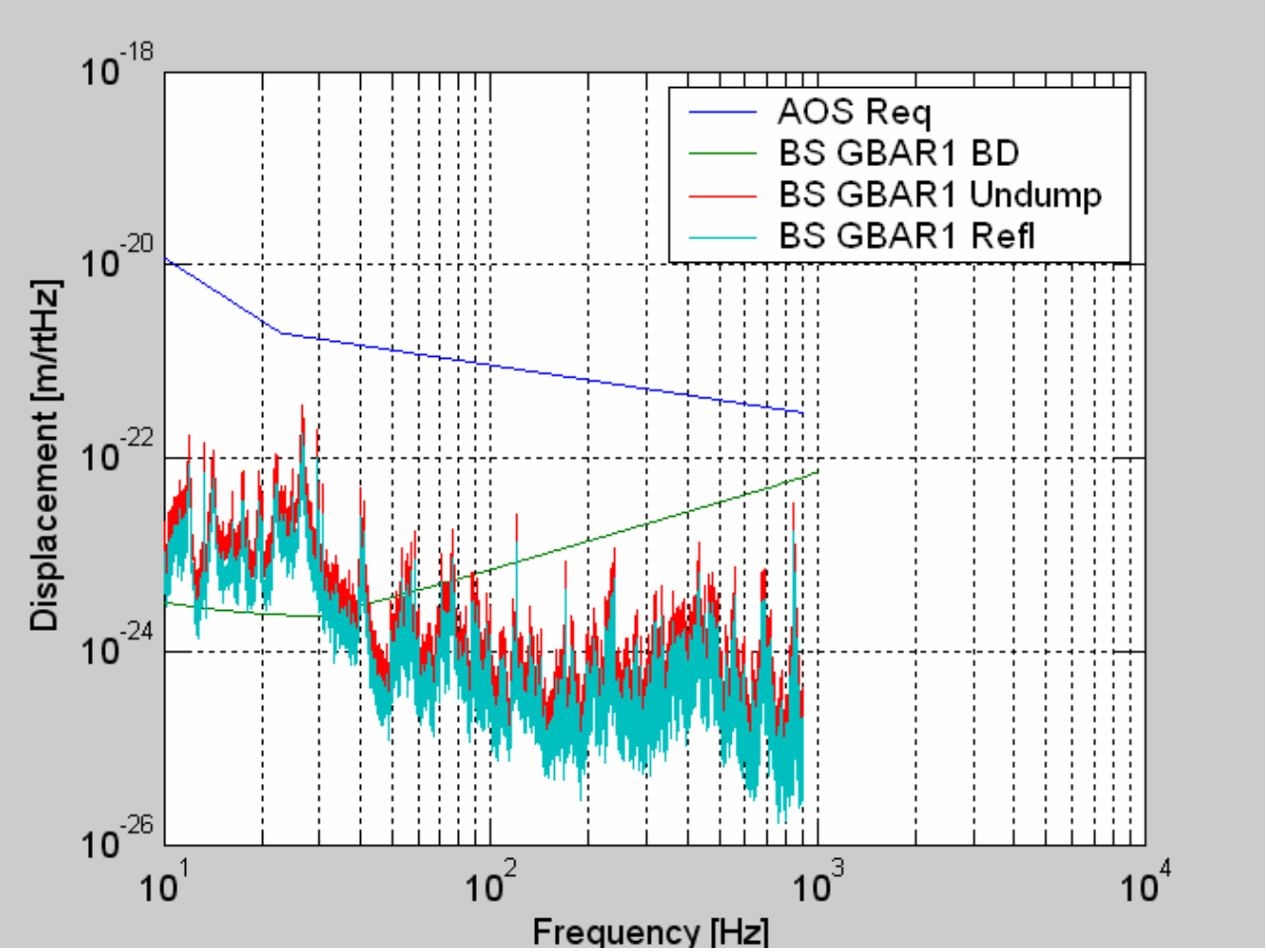

Figure 39: BS GBAR1 Beam Dump Scattered Light Displacement Noise

3.2.9.6 Stay Clear Zone

3.2.9.6.1 Clearance between Cavity Beam Dump and Recycling Cavity Beam

The Cavity Beam dump has a rectangular clear aperture, 218 mm horizontal by 249 mm vertical.

The clearances between the edges of the Cavity Beam Dumps and the vertical edge of the main beam in the recycling cavity are listed in Table 3.

These meet the requirement, 4.7 Clear Aperture Requirements.

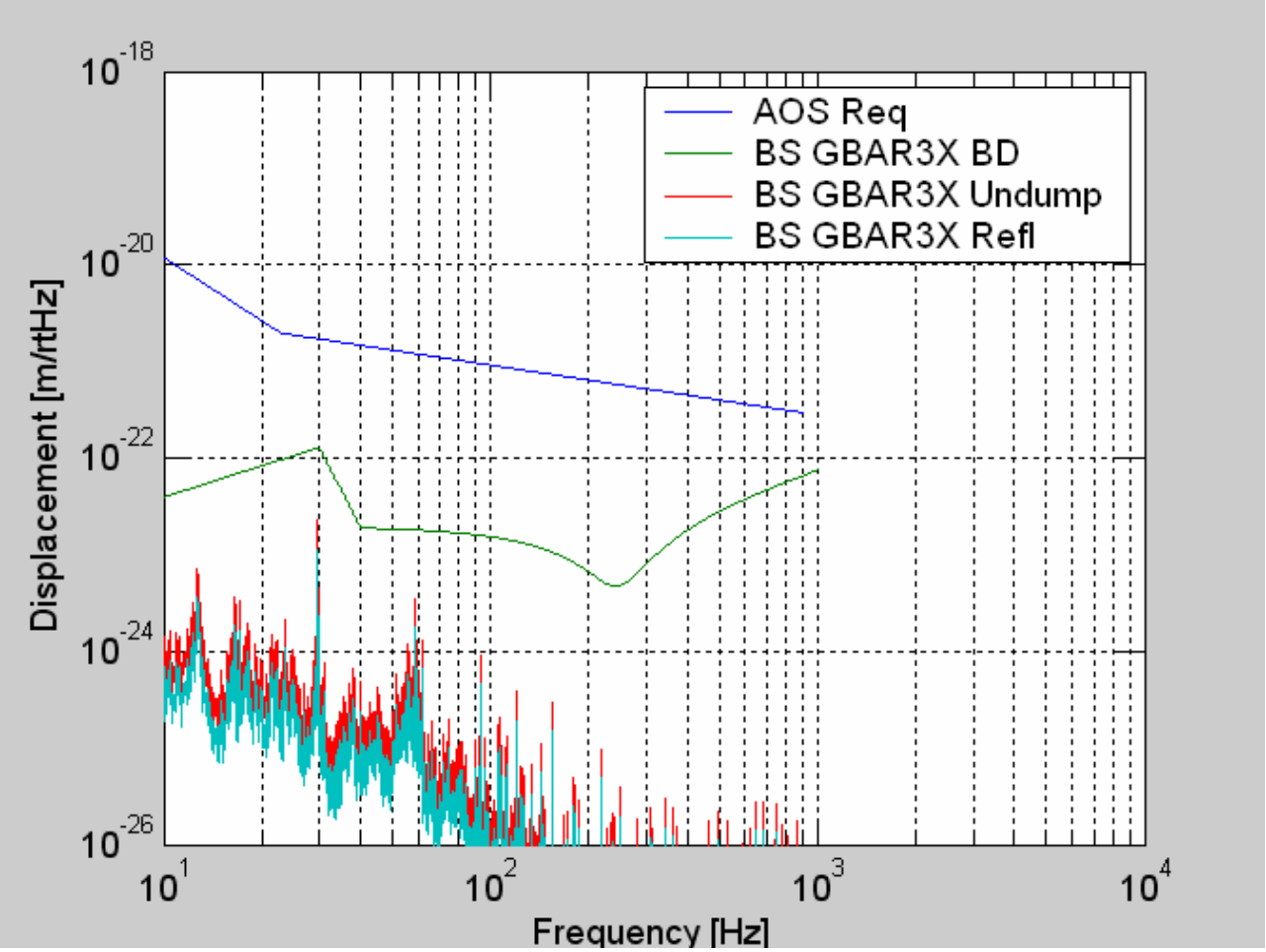

Figure 40: BS GBAR3X Beam Dump Scattered Light Displacement Noise

Table 3: Beam Dump Clearance

BEAM DUMP	CLEARANCE, mm
BSAR3	182
ITMXAR3	187
ITMXHR3	175
ITMYAR1	170
ITMYAR3	193
ITMYHR3	174

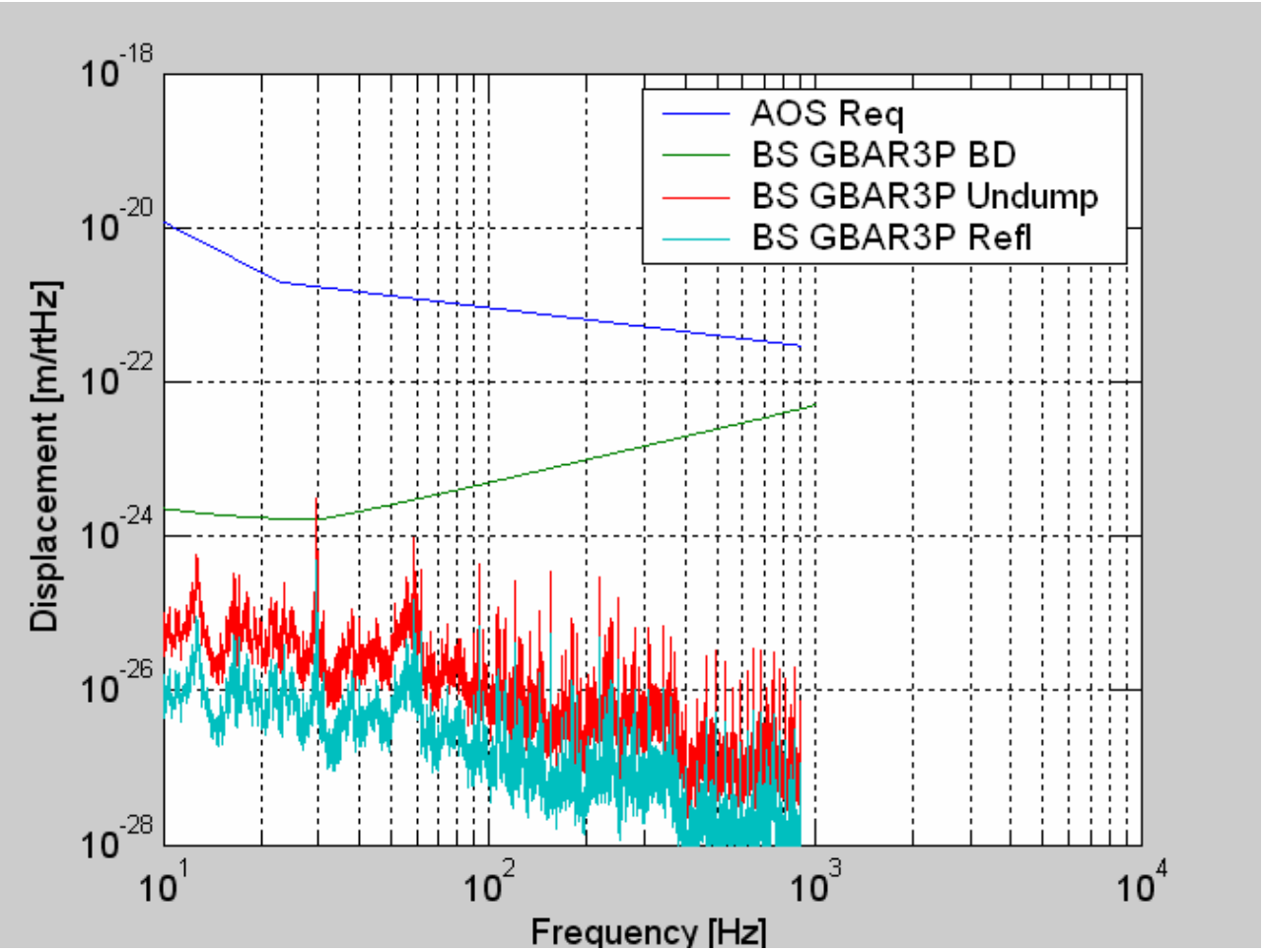

Figure 41: BS GBAR3P Beam Dump Scattered Light Displacement Noise

3.2.9.7 Beam Blocking

The 218 mm horizontal by 249 mm vertical clear aperture of the Cavity Beam Dump will allow < 100E-6 fraction of the ghost beam power to miss the beam dump.

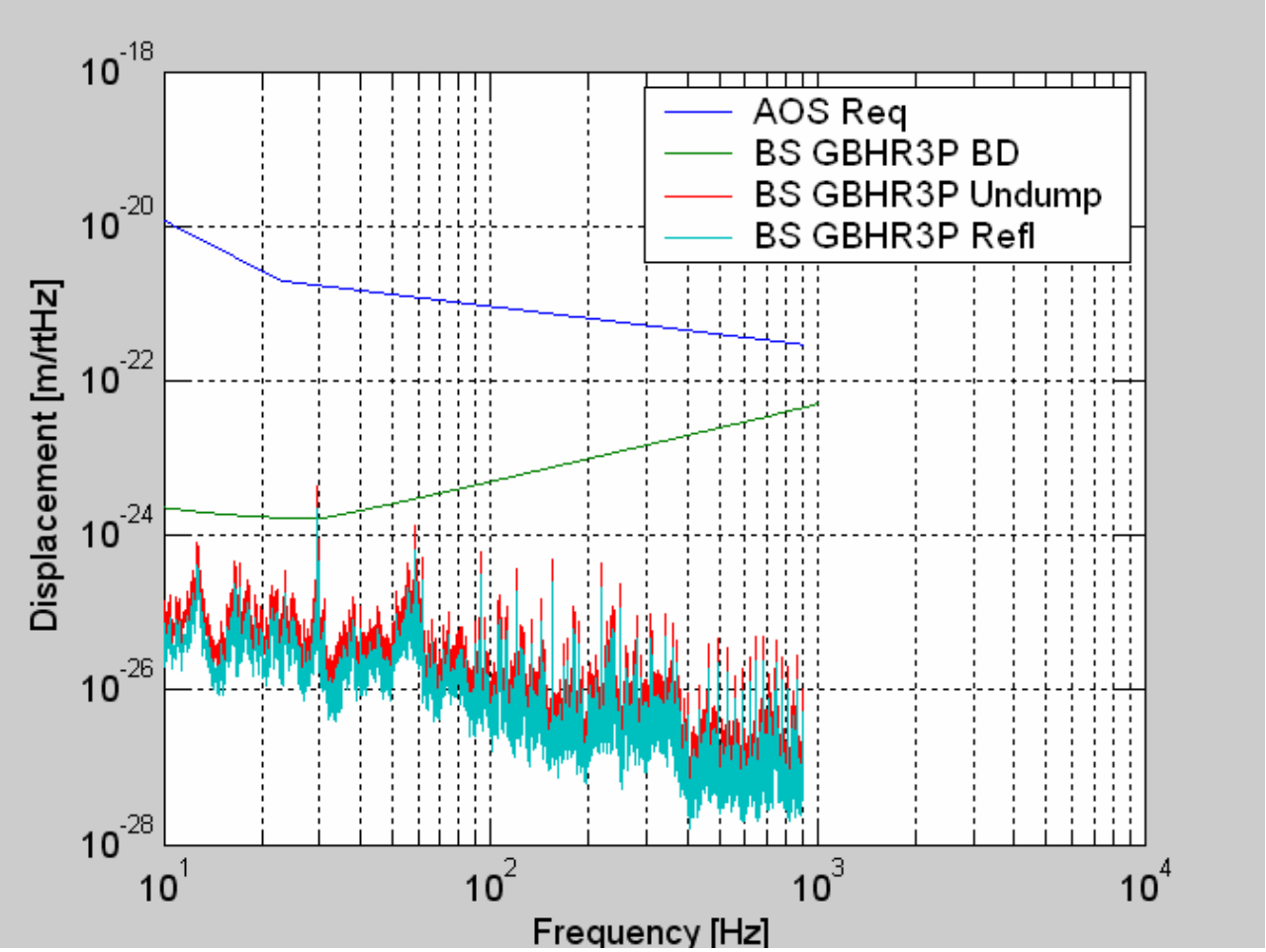

Figure 42: BS GBHR3P Beam Dump Scattered Light Displacement Noise

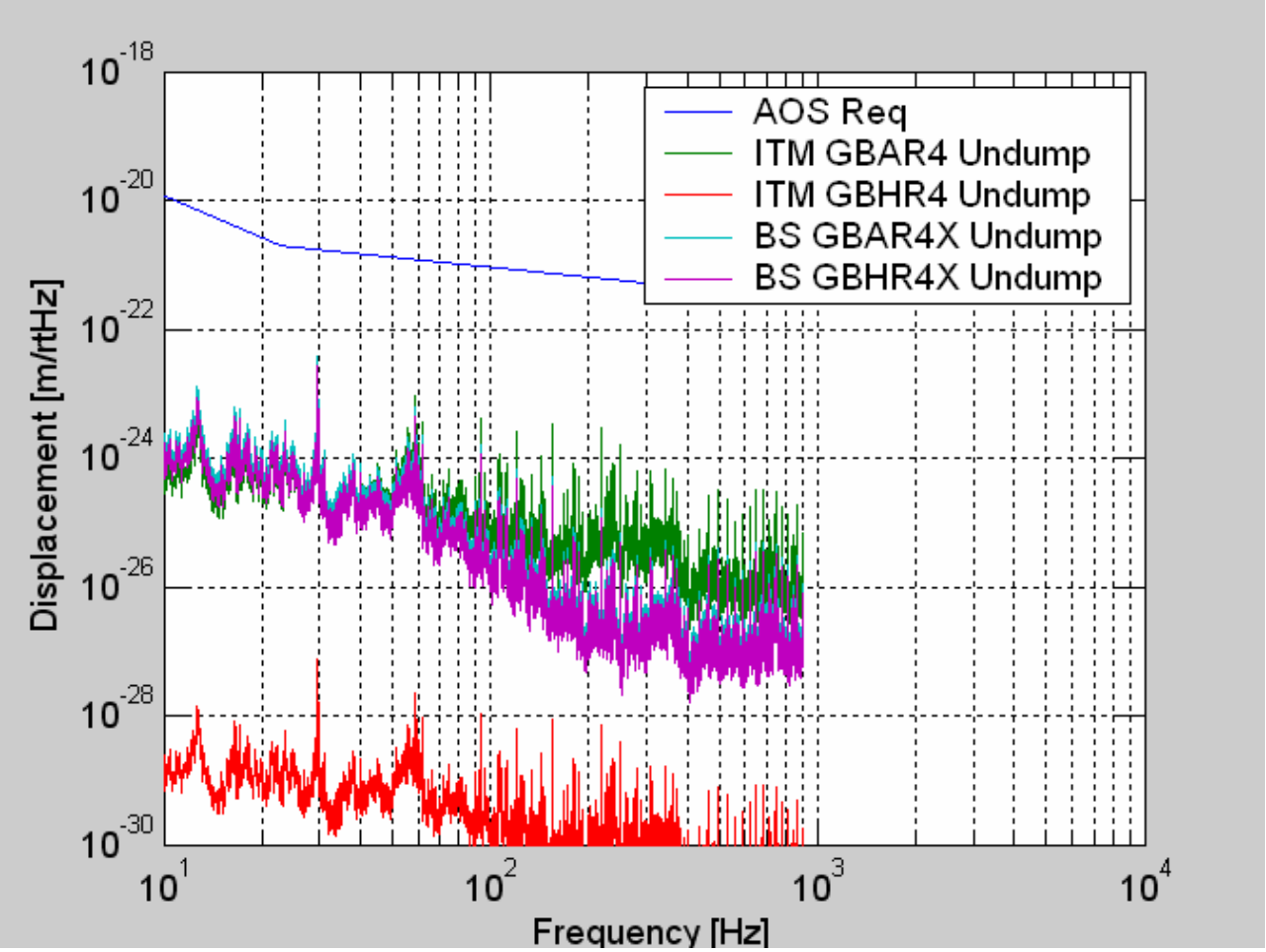

Figure 43: Un-dumped ITM GBAR4, ITM GBHR4, BS GBAR4X, and BS GBHR4X Scattered Light Displacement Noise

3.2.10 IO Baffle

An IO Baffle will be placed on the HR side of the PRM concentric with the main IFO beam, as shown in Figure 44: IO Baffle.

3.2.10.1 Beam Blocking

The baffle will extend above the HAM 3 optical table and will be wide enough to obscure the line of sight into the recycling cavity from any position on HAM 1, HAM 2 and before the baffle on HAM 3. The HAM3 table blocks the line of sight below the level of the table.

This will meet the requirement 4.4 IO Baffle Requirement.

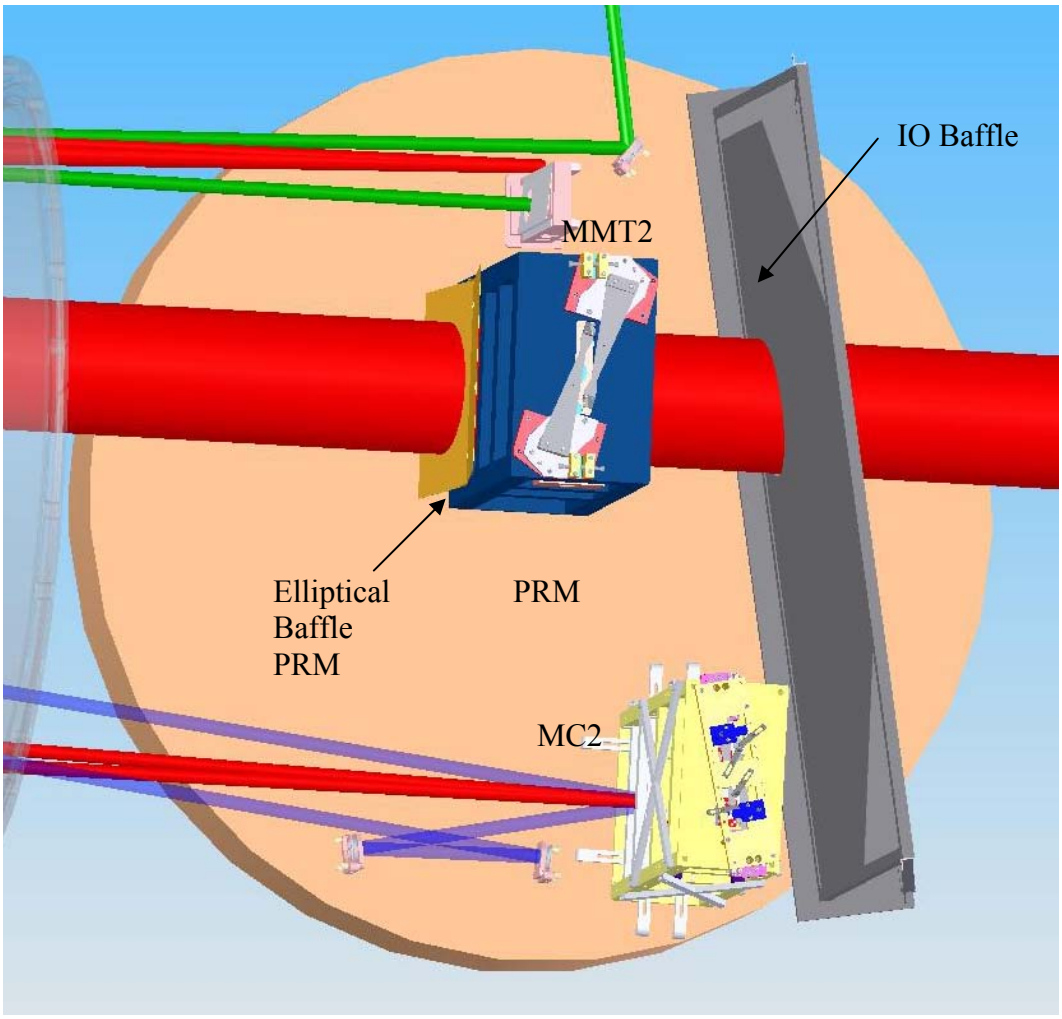

Figure 44: IO Baffle

3.2.10.2 Stay Clear Zone

The clear aperture diameter of the IO Baffle is 260 mm. This is 6 mm outside the centered clear aperture of the PRM, which is 249 mm.

The IO Baffle will be positioned within 2 mm of the center of the PRM.

This meets the requirements 4.7 Clear Aperture Requirements.

3.2.11 Cryopump Baffle

A concept for the suspended Cryopump Baffle is shown in Figure 45. It is a single pendulum suspended by springs from the circular, spool piece support ring. Eddy-current or elastomeric damping will be used to damp the pitch, yaw, and vertical motion.

The power scattered from the far COC at the opposite end of the arm cavity into the annular region bounded by the inner radius of the Cryopump Baffle and the beam tube radius is incident on the Cryopump Baffle. The incident power is given by

$$P_{cp} := P_a \cdot \int_{\theta_{cp}}^{\theta_{bt}} 2 \cdot \pi \cdot \theta \cdot BRDF_1(\theta)\, d\theta$$

The Initial LIGO pathfinder COC CSIRO, surface 2, S/N 2 was used to estimate the BRDF.

$$BRDF_1(\theta) := \frac{2755.12}{\left(1 + 8.50787 \cdot 10^8 \cdot \theta^2\right)^{1.23597}}$$

Where θ_{cp} is	9.612 E-5 rad
θ_{bt} is	1.327 E-4 rad
and, P_a is the arm power	8.339 E5 W
	P_{cp} = 2.8 W

3.2.11.1 Cryopump Blocking

The Cryopump Baffle will be placed inside the spool pieces closest to the cryopumps on the ITM side of the arms and the ETM side of the arms. It obscures the interior surfaces of the cryopump from the line of sight as viewed from the ITM and ETM HR surfaces and avoids backscattered light from the surfaces of the cryopump impinging on the ITM and ETM HR surfaces.

This meets the requirements: 4.5 Cryopump Baffle Requirement, and 4.7 Clear Aperture Requirements.

3.2.11.2 Cryopump Baffle Suspension

The Cryopump Baffle will be suspended from a single pendulum as shown in Figure 45.

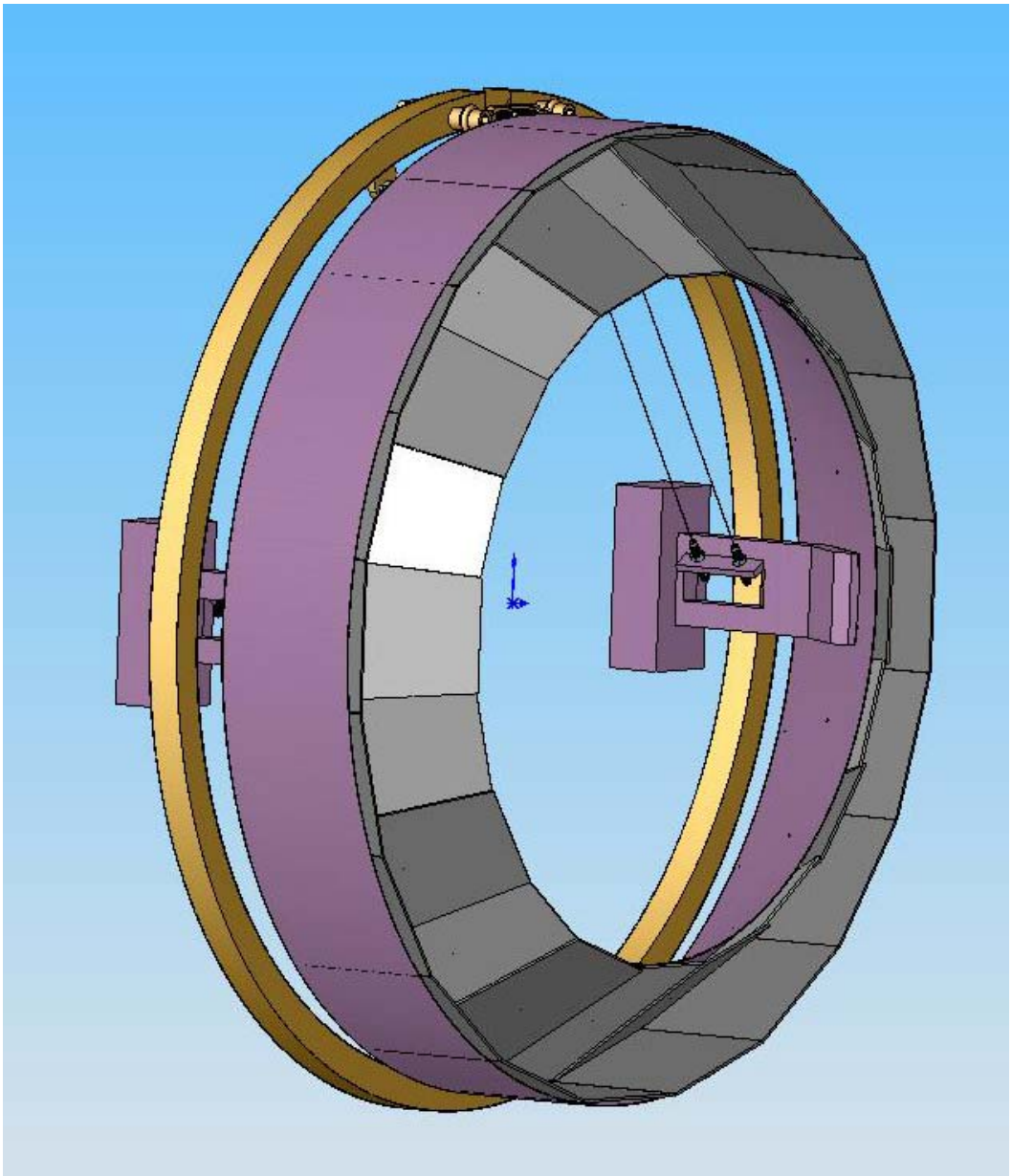

Figure 45: Conceptual Model of Suspended Cryopump Baffle

3.2.11.3 Cryopump Baffle Motion Requirements

Assuming a BRDF of 0.01 sr^{-1}, the minimum Cryopump Baffle motion attenuation requirements were determined using the scattered light model, and are shown in Figure 46. The actual pendulum response function will exceed the requirements.

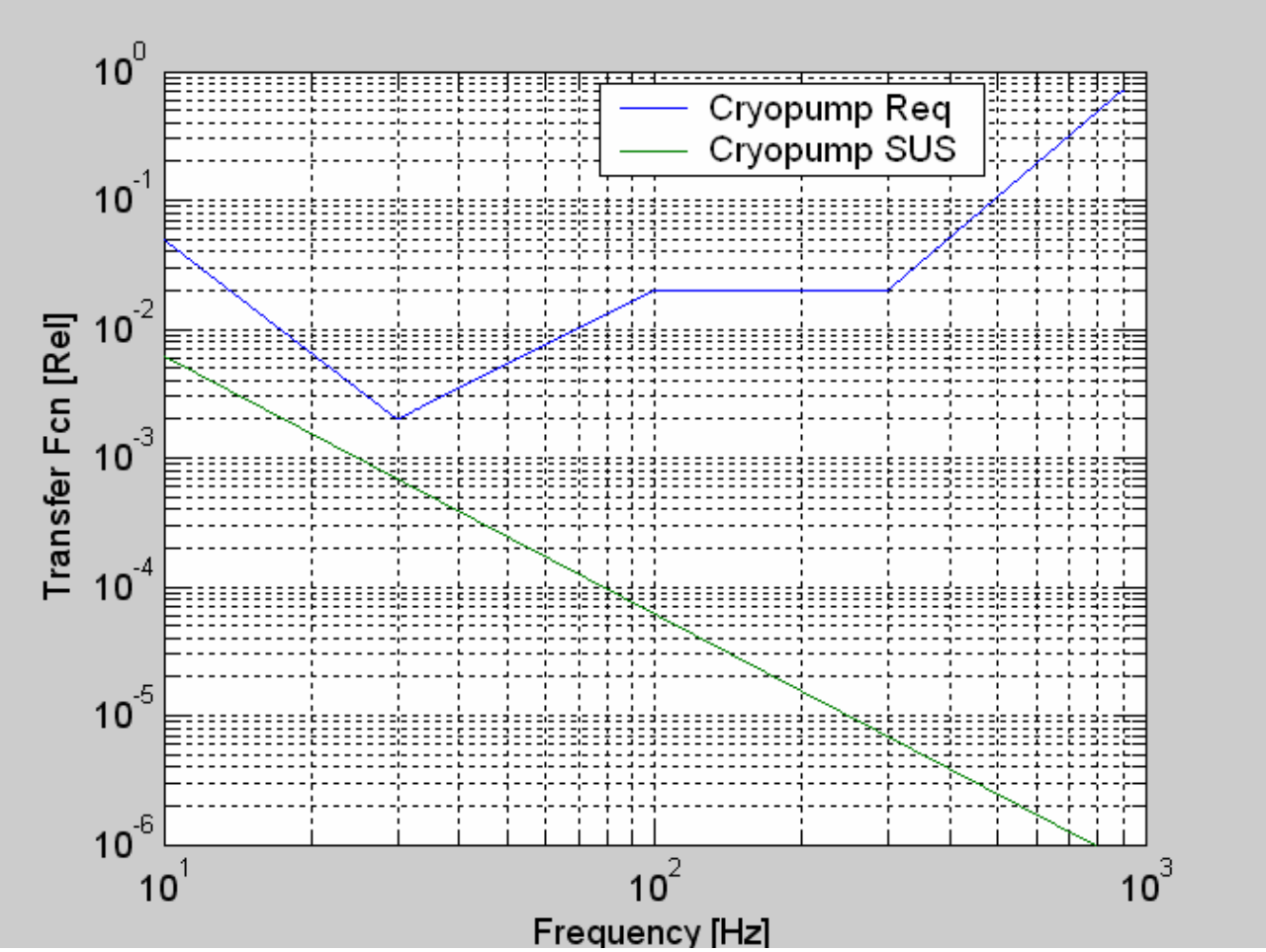

Figure 46: Cryopump Suspension Amplitude Response

3.2.11.4 Cryopump Baffle Surface BRDF

The Cryopump will be constructed of black glass with the surface inclined at an incidence angle of 56 deg; and therefore, is estimated to have a BRDF < 0.01 sr^{-1}. The edge of the hole in the baffle will be unpolished, with an estimated BRDF = 0.1 sr^{-1}

3.2.11.5 Cryopump Baffle Reflectivity

The light that is not absorbed by the Cryopump Baffle will reflect from the baffle surface onto the insides of the spool piece. There, it will scatter, reflect again from the Cryopump Baffle, and enter the IFO mode at the far COC.

The scattered light model was used to calculate the requirement for the reflectivity of the Cryopump Baffle. Assuming a BRDF of the spool piece wall of 0.1, the reflectivity of the Cryopump Baffle must is < 0.01.

This low reflectivity will be obtained by using multiple reflections from uncoated black glass inclined near Brewster's angle.

3.2.11.6 Seismic Motion of the Cryopump Scattering Surfaces

The light that reflects from the Cryopump Baffle will scatter from the spool piece wall, which has the seismic motion shown in Figure 17.

The surface and the unpolished edge of the beam hole of the suspended Cryopump Baffle have the seismic motion of the spool piece attenuated by the transfer function of the Cryopump Baffle suspension.

3.2.11.7 Scattered Light Displacement Noise of Suspended Cryopump Baffle

The scattered light displacement noise from the three Cryopump Baffle sources is shown in Figure 47.

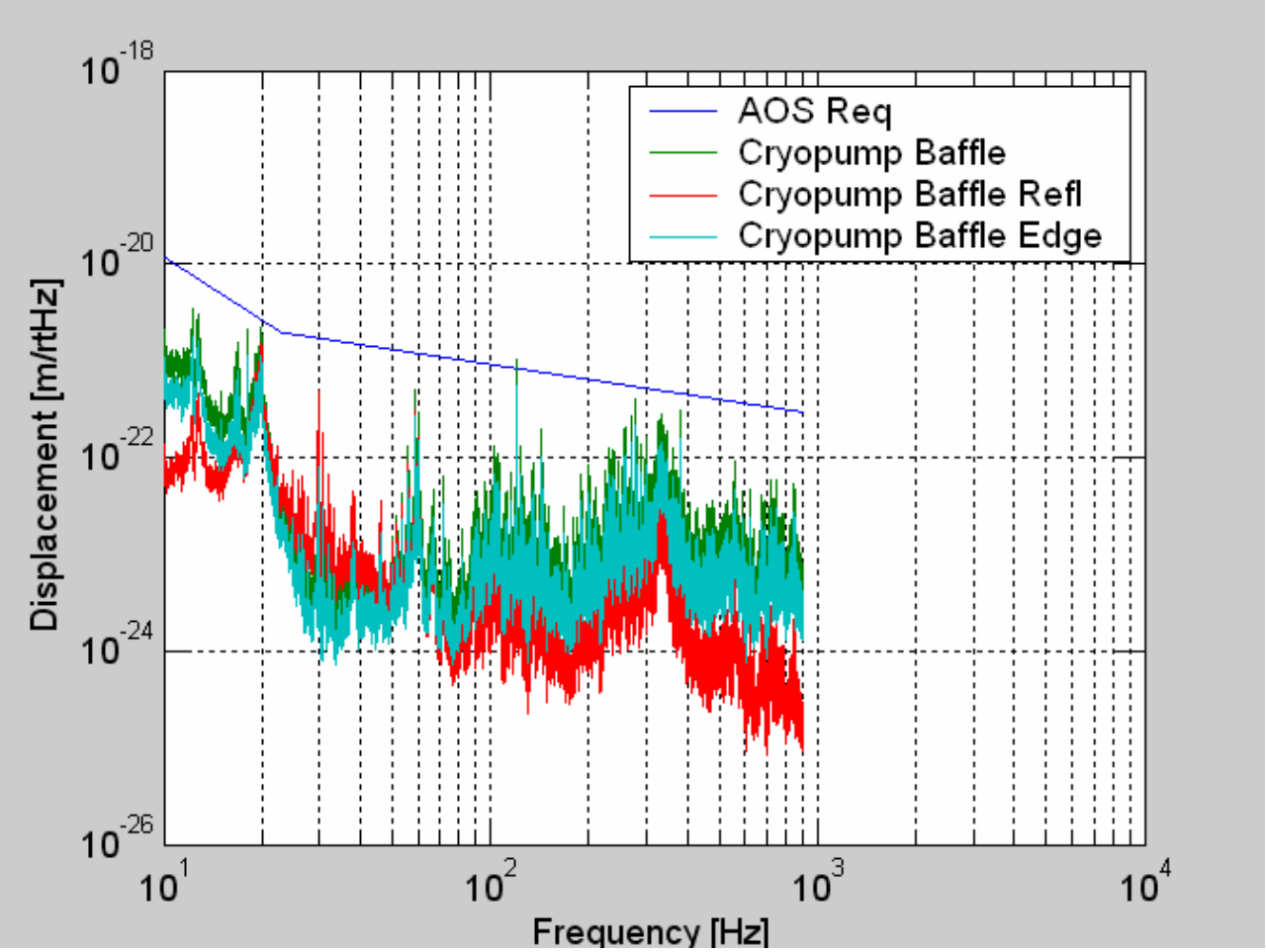

Figure 47: Scattered Light Displacement Noise of Suspended Cryopump Baffle

3.2.11.8 Fringe-wrapping of Cryopump Baffle Displacement Noise

The Cryopump Baffle has a pendulum resonance at approximately 0.8 Hz. The displacement noise at the odd harmonics of the motion due to fringe wrapping was calculated using the fringe wrap model, assuming a simple pendulum function with a Q = 1000 at the resonant frequency. The fringe wrapping does not cause excessive noise above 10 Hz, as shown in Figure 48.

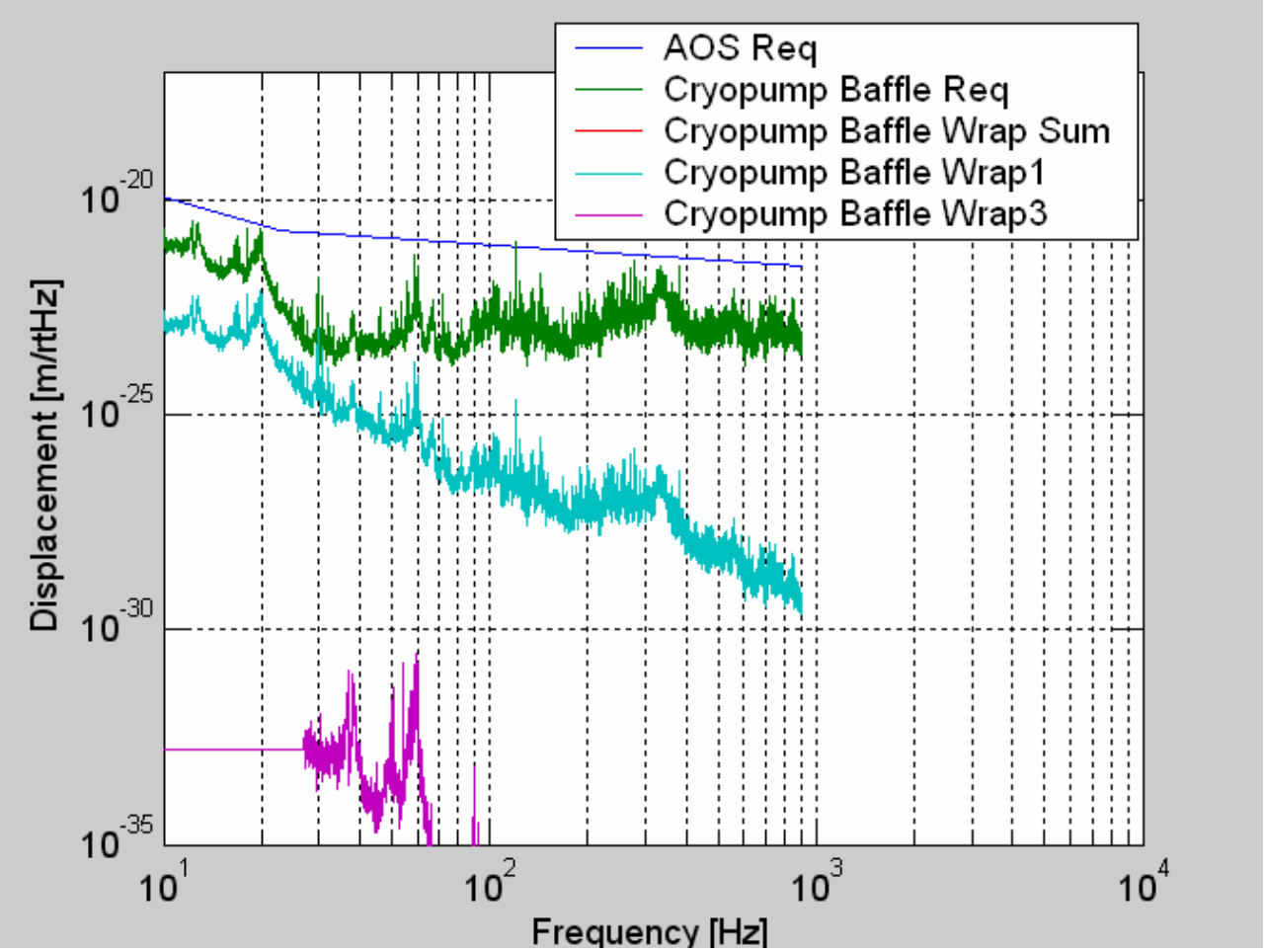

Figure 48: Cryopump Baffle Scattered Light Displacement Noise Caused by Fringe-wrapping

3.2.11.9 Stay Clear Zone

The clear aperture diameter of the Cryopump Baffle, 769 mm, is large enough to allow the folded and non-folded IFO beams of 315.4 mm diameter at the 1 ppm diameter to pass through without vignetting. The fractional geometric power loss of a w = 60 mm beam passing once through the Cryopump Baffle is 1.4E-8. With a 4 mm decentering of the baffle, the loss increases to 4E-8. This is negligible compared to the transmission loss through the ETM mirror.

This meets the requirement 4.7 Clear Aperture Requirements.

3.2.12 ETM Telescope Baffle

The ETM Telescope Baffle is mounted to the front of the ETM telescope, as shown in Figure 49. The baffle blocks all the transmitted light from the ETM except for the central region. The baffle will be constructed of black glass tilted at 10 deg with a high-efficiency AR coating. Most of the light will be absorbed by the baffle. Less than 0.0025 of the light incident on the baffle will be reflected at an angle toward the ETM. The reflected light will bounce back and forth between the ETM and the baffle until it eventually hits the chamber walls.

The ETM Telescope Baffle will be mounted concentrically with the optical axis of the ETM Telescope within 0.5 mm. The 160 mm diameter aperture in the baffle is the same as the clear aperture of the ETM Telescope.

This will meet the requirement 4.7 Clear Aperture Requirements.

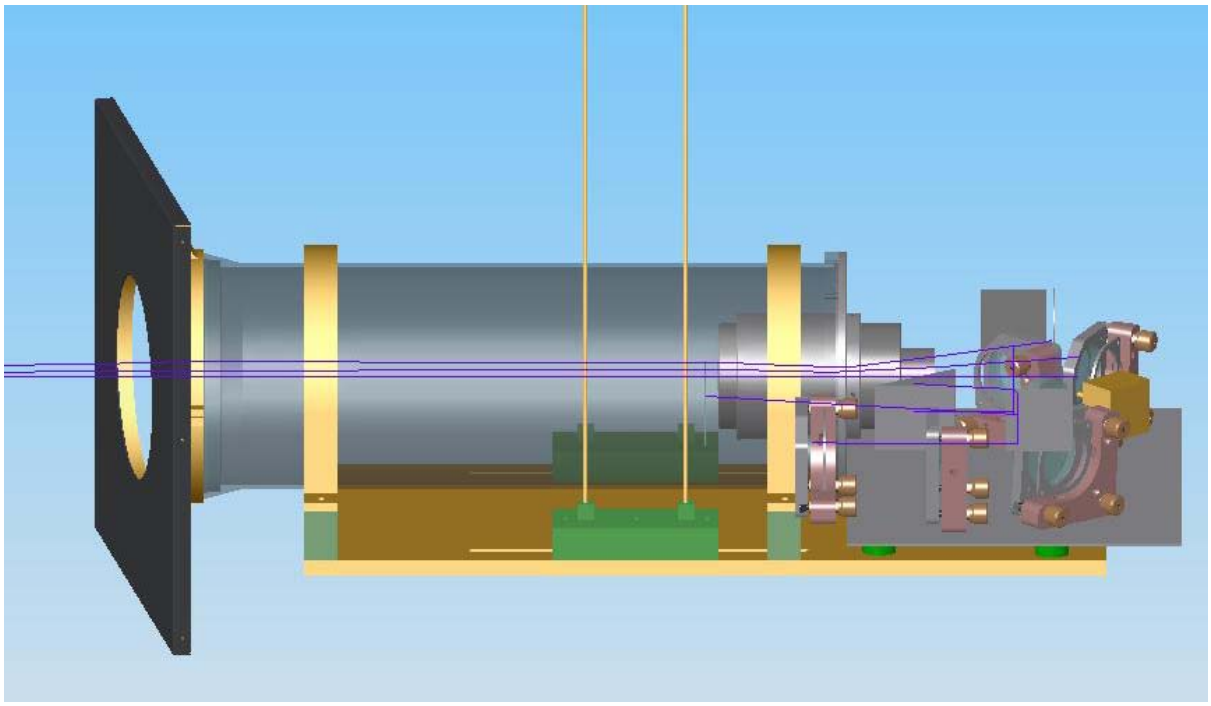

Figure 49: ETM Telescope Baffle

3.2.12.1 ETM Telescope Baffle Motion Requirements

The motion requirement for the ETM Telescope Baffle was determined using the scattered light model. The ETM Telescope Baffle requires no further motion isolation than that provided by the BSC optical table seismic requirement.

3.2.12.2 ETM Telescope Baffle Surface BRDF

The ETM Telescope Baffle will be constructed of black glass with the surface inclined at an incidence angle of 10 deg; the BRDF of the baffle is expected to be < 0.1 sr^-1. The hole in the baffle will be unpolished, with an assumed BRDF = 0.1 sr^{-1}.

3.2.12.3 ETM Telescope Baffle Reflectivity

The light that is not absorbed by the ETM Telescope Baffle will reflect from the baffle surface onto the insides of the vacuum chamber. There, it will scatter from the chamber, reflect again from the ETM Telescope Baffle, and enter the IFO mode.

The requirement for the reflectivity of the ETM Telescope Baffle was calculated using the scattered light model. The reflectivity of the ETM Telescope Baffle must be < 0.0025. This requirement will be met by using black glass with a high efficiency AR coating.

3.2.12.4 Seismic Motion of the ETM Telescope Baffle Scattering Surfaces

The light that reflects from the ETM Telescope Baffle will scatter from the vacuum chamber, which has the seismic motion shown in Figure 17.

3.2.12.5 Scattered Light Displacement Noise of Suspended ETM Telescope Baffle

The scattered light noise from the three ETM Telescope Baffle sources is shown in Figure 50.

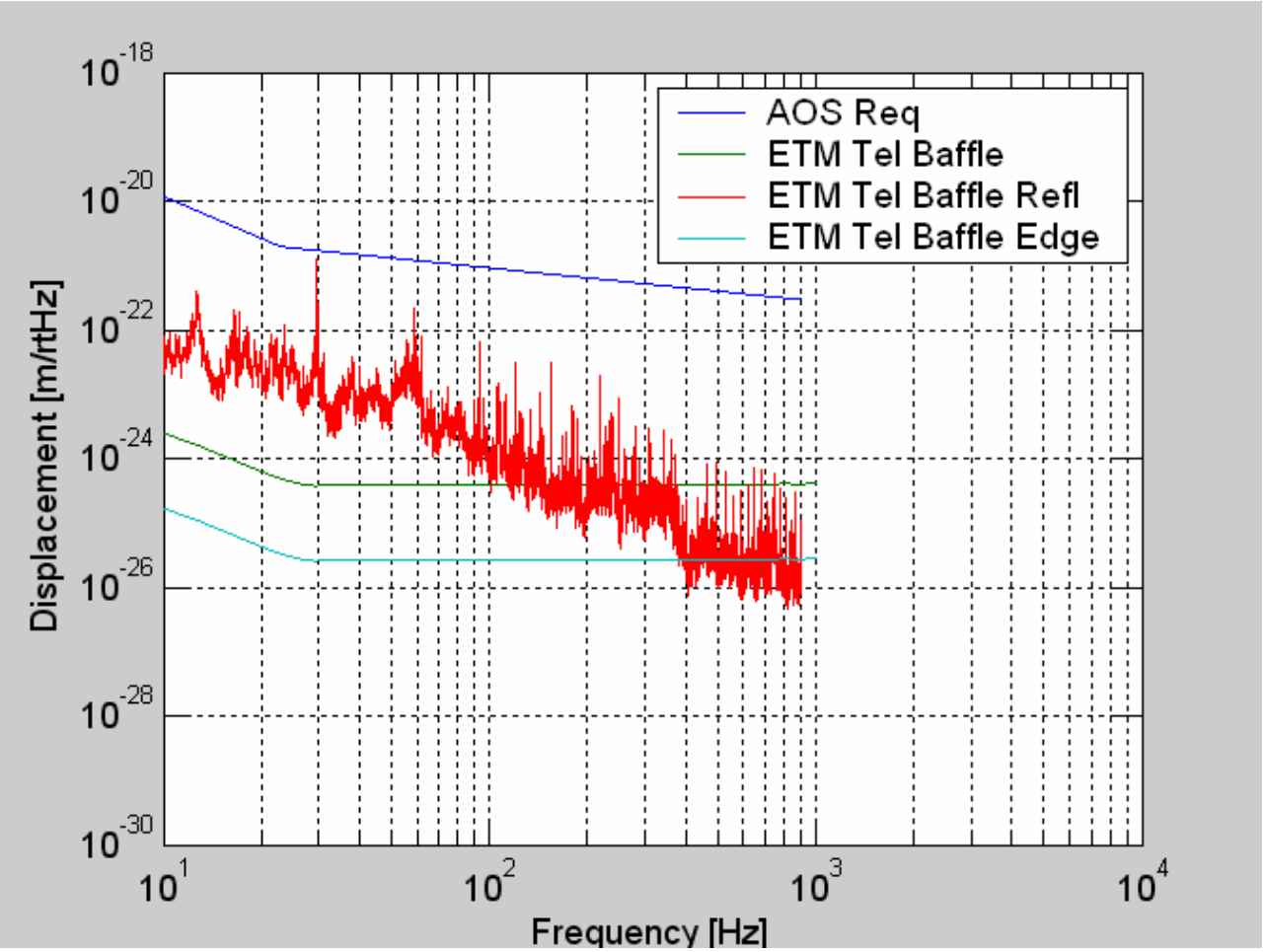

Figure 50: Scattered Light Displacement Noise of ETM Telescope Baffle

3.3 Stray Light Control Physical Characteristics

3.3.1 Faraday Isolator

Table 4: Faraday Isolator Characteristics

Parameter	**Value**
Configuration	Single Faraday isolator
Wavelength	1064 nm
Clear Aperture	20 mm
Rotator material	TGG crystal
Rotator crystal wedge angle front and back surface	1 deg
Total wavefront distortion	<1 λ @ 633 nm
Rotator transmissivity across clear aperture	>97 %
Input/output polarizer	Calcite, air-spaced Brewster's angle
Polarizer transmissivity per surface	>99.9 %
Half-wave rotation plate	Zero-order quartz

Table 5 : Faraday Isolator Suspension Characteristics

Parameter	**Value**
Frame	Modified LOS
Suspension	Four wire marionette
Amplitude response	See Figure 9
Damping	Elastomeric
Height adjustment	manual
Yaw adjustment	manual
Pitch adjustment	Remote, Pico Motor

3.3.2 Arm Cavity Baffle

Table 6: Arm Cavity Baffle Characteristics

Parameter	**Value**
Aperture diameter	346 mm

Parameter	Value
Outer diameter blockage	>850 mm
Material	Black Glass (#12 grade welder's glass)
BRDF	<0.001 sr^-1
Reflectivity	<0.01
Weight	TBD kg

Table 7: Arm Cavity Baffle Suspension

Parameter	Value
Frame	Aluminum frame
Suspension	Two wire, suspended from HEPI stage "0"
Amplitude response	See Figure 14, Figure 15, Figure 16
Damping	Elastomeric, Q < 1000

3.3.3 Elliptical Baffle

3.3.3.1 ITM Elliptical Baffle

Table 8: ITM Elliptical Baffle Characteristics

Parameter	Value
Suspension	Single pendulum SUS from BSC optical table or HEPI stage "0"
Damping	Elastomeric, Q < 1000
Aperture major diameter	249 mm
Aperture minor diameter	218 mm
Material	Black Glass (#12 grade welder's glass)
BRDF	<0.01 sr^-1
Reflectivity	<0.001
Weight	TBD kg

3.3.3.2 PRM Elliptical Baffle

Table 9: PRM Elliptical Baffle Characteristics

Parameter	Value
Suspension	Attached to PRM frame
Damping	none
Aperture major diameter	249 mm
Aperture minor diameter	218 mm
Material	Oxidized stainless steel
BRDF	<0.01 sr^-1
Reflectivity	<0.30
Weight	TBD kg

3.3.4 Manifold Baffle

Table 10: Manifold Baffle

Parameter	Value
Suspension	Mounted to manifold wall
Damping	none
Aperture	570 mm radius
Outer diameter	930 mm
Material	Oxidized stainless steel
BRDF	<0.01 sr^-1
Reflectivity	< 0.30
Weight	TBD kg

3.3.5 Brewster's Window

Table 11: Brewster's Window Characteristics

Parameter	Value
Clear aperture diameter	60 mm @ 56 deg incidence
Wavefront distortion	<0.14 λ @ 633 nm
BRDF @ 56 deg incidence	< 5E-6 sr^-1

Parameter	Value
Reflectivity	<4E-4
Diameter of substrate	172 mm
Thickness	25.4 mm
Material	Grade A fused silica, super polished
Attachment to Flange	O-ring seal

3.3.6 OMMT

Table 12: OMMT M2 Characteristics

Parameter	Value
Mirror scattering loss	< 500 ppm
BRDF @ 0.016 rad incidence	<3E-3 sr^-1
Suspension	SOS suspension
Damping	OSEM, Q < 10
Clear aperture	75 mm diameter
Weight	TBD kg

3.3.7 ITMX, ITMY, and BS Beam Dump

Table 13: Cavity Beam Dump Characteristics

Parameter	Value
Suspension	Single pendulum SUS from HEPI stage “0”
Damping	Elastomeric, Q < 1000
Aperture	218 mm horizontal x 249 mm vertical
Material	Black Glass (#12 grade welder’s glass)
BRDF	<0.001 sr^-1
Reflectivity	< 0.005
Weight	TBD kg

3.3.8 IO Baffle

Table 14: IO Baffle Characteristics

Parameter	Value
Mounting	HAM table clamp
Aperture diameter	260 mm
Outer diameter blockage, segment above HAM table	1537 mm
Material	Polished, oxidized stainless steel
Weight	TBD kg

3.3.9 Cryopump Baffle

Table 15: Cryopump Baffle Characteristics

Parameter	Value
Location	Corner Station-- x arm, y arm End Station-- x arm, y arm
Suspension	Single pendulum
Aperture diameter	769 mm
Outer diameter	1133 mm
Material	Black Glass (#12 grade welder's glass)
BRDF	<0.01 sr^-1
Reflectivity	<0.01
Weight	TBD

3.3.10 ETM Telescope Baffle

Table 16: ETM Telescope Baffle Characteristics

Parameter	Value
Aperture diameter	160 mm
Outer dimensions	340 mm x 340 mm
Material	Black Glass (#12 grade welder's glass)
BRDF	<0.1 sr^-1

Parameter	Value
Reflectivity	<0.0025
Weight	TBD

3.4 Stray Light Control Interface Definitions

3.4.1 Interfaces to other LIGO detector subsystems

3.4.1.1 Mechanical Interfaces

The beam dumps will attach to the optical tables or be suspended from the HEPI stage "0" in the HAM and BSC chambers, without interfering with the COC mirror structures. Earthquake stops will attach to the chamber wall.

The ITM Elliptical Baffle will hang from the BSC optics table or from the HEPI stage "0" and will have earthquake stops attached to the chamber wall.

The PRM Elliptical Baffle will mount directly to the PRM SUS structure.

The Arm Cavity Baffles will hang from the ITM and ETM HEPI stage "0"and will have earthquake stops attached to the chamber wall.

The Cryopump Baffle will be suspended from a mounting ring that is held in position inside the spool piece by means of compressive forces.

The Manifold Baffle will be held in position inside the manifold by means of compressive forces.

3.4.1.2 Electrical Interfaces

3.4.1.2.1 Suspended Baffles and Beam Dumps

All the suspended baffles and beam dumps are passively damped and will require no electrical interfaces.

3.4.1.2.2 Faraday Isolator

The Faraday Isolator will be suspended from a modified LOS, and appropriate electronic control signals to the Pico Motor will be used for pitch steering.

3.4.1.3 Optical Interfaces

The Cavity Beam Dumps will intercept the ghost beams while maintaining adequate clearance from the main recycling cavity beams.

The PRM elliptical baffle will intercept the main beam incident from the IO input mode matching telescope with a clear aperture slightly larger on all sides than the limiting aperture that is determined by the geometric shadow of the PRM and the BS.

3.4.1.4 Stay Clear Zone

3.4.1.4.1 Arm Cavity Baffle

The aperture of the Arm Cavity Baffle will be 346 mm, which is larger than the diameter of the ITM and ETM COC. The aperture will be concentric with the COC within 4 mm.

3.4.1.4.2 ITMX, ITMY, and BS Beam Dump

The Cavity Beam Dumps will have a stay clear zone of >30 mm from the elliptical edges of the main recycling cavity beam.

3.4.1.4.3 Cryopump Baffle

The Cryopump Baffle will be concentric to the spool piece diameter within 4 mm. The clearance between the 1 ppm edge of the main beam and the centered Cryopump Baffle aperture will be > 7 mm.

3.4.1.4.4 ETM Telescope Baffle

The clear aperture diameter of the ETM Telescope Baffle is 160 mm, which is the same as the clear aperture of the ETM telescope. The ETM Telescope Baffle will be concentric with the entrance aperture of the ETM telescope to within 0.5 mm.

3.4.1.4.5 Elliptical Baffle

The clear aperture of the Elliptical Baffle is 2 mm larger on all sides than the limiting clear aperture of the PRM and the BS. The Elliptical Baffle will be concentric with the centerline of the IFO main beam between the BS and the ITM within 2 mm.

3.4.1.4.6 IO Baffle

The clear aperture of the IO Baffle is 260 mm, which is larger than the diameter of the PRM. The IO Baffle will be concentric with the PRM within 2 mm.

3.4.2 Interfaces external to LIGO detector subsystems

There are no interfaces external to the LIGO detector.

3.5 Stray Light Control Reliability

All Stray Light Control baffles and beam dumps are passive and are expected to have 100% availability. The MTBF is expected to be equal to the life of the IFO.

The Faraday Isolator will be suspended by a modified LOS. The typical MTBF of an LOS will apply TBD.

3.6 Stray Light Control Maintainability

The following components are susceptible to failure:

1) Pico Motor
2) Suspension wires

If either of these components fails, the Faraday Isolator suspension assembly will be removed from the vacuum chamber and repaired. The physical location of the suspension will be preserved by means of alignment fixtures. The pointing angle of the Faraday Isolator will be reproduced by means of the initial alignment procedure.

Spare components will be stocked during initial installation for the replacement of long lead-time items such as mirrors.

3.7 Stray Light Control Environmental Conditions

3.7.1.1.1.1 Natural Environment

3.7.1.1.1.1.1 Temperature and Humidity

The SLC assemblies are designed to operate in the high vacuum environment of the IFO and in the controlled LVEA environment during installation.

Table 17 Environmental Performance Characteristics

Operating	Non-operating (storage)	Transport
+20C to +25C, 20-70% RH, non- condensing	0C to +60C, 10-90% RH, non-condensing	0C to +60C, 10-90% RH, non- condensing

3.7.1.1.1.1.2 Atmospheric Pressure

The Brewster's window will function with a differential pressure of 1 atmosphere under normal atmospheric pressure conditions.

3.7.1.1.1.1.3 Seismic Disturbance

The suspended SLC assemblies and the assemblies mounted to the vacuum chambers will withstand ground seismic disturbances.

3.7.1.1.1.2 Induced Environment

3.7.1.1.1.2.1 Electromagnetic Radiation

NA

3.7.1.1.1.2.2 Acoustic

NA

3.7.1.1.1.2.3 Mechanical Vibration

NA

3.8 Stray Light Control Transportability

All items will be transportable by commercial carrier without degradation in performance. As necessary, provisions will be made for measuring and controlling environmental conditions (temperature and accelerations) during transport and handling. Special shipping containers, shipping and handling mechanical restraints, and shock isolation will be utilized to prevent damage. All containers will be movable for forklift. All items over 100 lbs. that must be moved into place within LIGO buildings will have appropriate lifting eyes and mechanical strength to be lifted by cranes.

4 Stray Light Control Design and Construction

The design and construction of the Stray Light Control subsystem allow adequate cleaning, either on site or at an appropriate outside vendor, and will fit inside the vacuum baking ovens on site.

4.1.1.1 Materials and Processes

The materials and processes used in the fabrication of the Stray Light Control subsystem will be compatible with the LIGO approved materials list.

Metal components will have quality finishes on all surfaces, suitable for vacuum finishes. Aluminum components used in the vacuum will not have anodized surfaces.

4.1.1.1.1 Materials

A list of currently approved materials for use inside the LIGO vacuum envelope can be found in LIGO Vacuum Compatible Materials List (LIGO-E960022). All fabricated metal components exposed to vacuum will be made from stainless steel, copper, or aluminum. Other metals are subject to LIGO approval. Pre-baked viton (or fluorel) may be used subject to LIGO approval. All materials used inside the vacuum chamber will comply with LIGO Vacuum Compatibility, Cleaning Methods and Procedures (LIGO-E960022-00-D).

The only lubricating films permitted within the vacuum are dry plating of vacuum compatible materials such as silver and gold.

4.1.1.1.2 Processes

4.1.1.1.2.1 Cleaning

All materials used inside the vacuum chambers will be cleaned in accordance LIGO-E960022-00-D or LIGO-E000007-00, and Specification Guidance for Seismic Component Cleaning, Baking, and Shipping Preparation (LIGO-L970061-00-D). To facilitate final cleaning procedures, parts will be cleaned after any processes that result in visible contamination from dust, sand or hydrocarbon films.

Materials will be joined in such a way as to facilitate cleaning and vacuum preparation procedures; i. e. internal volumes will be provided with adequate openings to allow for wetting, agitation and draining of cleaning fluids and for subsequent drying.

4.1.1.1.3 Component Naming

All components will be identified using the LIGO Naming Convention (LIGO-E950111-A-E). This will include identification (part or drawing number, revision number, serial number) physically stamped on all components, in all drawings and in all related documentation.

4.1.1.2 Stray Light Control Workmanship

All components will be manufactured according to good commercial practice.

4.1.1.3 Stray Light Control Interchangeability

Common elements with ordinary dimensional tolerances, will be interchangeable.

4.1.1.4 Stray Light Control Safety

This item will meet all applicable NSF and other Federal safety regulations, plus those applicable State, Local and LIGO safety requirements. A hazard/risk analysis will be conducted in accordance with guidelines set forth in the LIGO Project System Safety Management Plan LIGO-M950046-F, section 3.3.2.

4.1.1.5 Stray Light Control Human Engineering

NA

4.1.2 Stray Light Control Assembly and Maintenance

Assembly fixtures and installation procedures will be developed in conjunction with the Stray Light Control hardware design. These will include (but not be limited to) fixtures and procedures for:

- installation and assembly of beam dumps and baffles into the vacuum
- assembly of the in vacuum components in a clean room (class 100) environment

4.1.3 Stray Light Control Documentation

The documentation will consist of working drawings, assembly drawings, and alignment procedures

4.1.3.1 Stray Light Control Specifications

Specifications for the purchase of specialized components and assemblies such as Faraday isolator, optical mirrors, windows, and lenses will be developed.

4.1.3.2 Stray Light Control Design Documents

The following documents will be produced:

- LIGO Stray Light Control Preliminary Design Document (including supporting technical design and analysis documentation)
- LIGO Stray Light Control Final Design Document (including supporting technical design and analysis documentation)
- LIGO Stray Light Control Installation Procedures

4.1.3.3 Stray Light Control Engineering Drawings and Associated Lists

A complete set of drawings suitable for fabrication will be provided along with Bill of Material (BOM) and drawing tree lists. The drawings will comply with LIGO standard formats and will be provided in electronic format. All documents will use the LIGO drawing numbering system, be drawn using LIGO Drawing Preparation Standards, etc.

4.1.3.4 Stray Light Control Technical Manuals and Procedures

4.1.3.4.1 Procedures

Procedures will be provided for the installation, and final alignment of the Stray Light Control elements.

4.1.3.5 Stray Light Control Documentation Numbering

All documents will be numbered and identified in accordance with the LIGO documentation control numbering system LIGO document TBD

4.1.3.6 Stray Light Control Test Plans and Procedures

All test plans and procedures will be developed in accordance with the LIGO Test Plan Guidelines, LIGO document TBD.

4.1.4 Stray Light Control Logistics

The design will include a list of all recommended spare parts and special test equipment required.

4.1.5 Stray Light Control Precedence

The relative importance of the positioning of the beam dumps and baffles will be as follows:

1) satisfy the stay clear requirements
2) align the baffles and beam dumps with the centers of the ghost beams

4.1.6 Stray Light Control Qualification

N/A

5 Quality Assurance Provisions

This section includes all of the examinations and tests to be performed in order to ascertain that the fabricated SLC elements conform to the requirements in section 3.

5.1 General

5.1.1 Responsibility for Tests

AOS will conduct tests to verify the as-delivered performance specifications of the sub-system.

5.1.2 Special Tests

5.1.2.1 Engineering Tests

TBD

5.1.2.2 Reliability Testing

No reliability testing is anticipated.

5.1.3 Configuration Management

Configuration control of specifications and designs will be in accordance with the LIGO Detector Implementation Plan.

5.2 Quality conformance inspections

Design and performance requirements identified in this specification and referenced specifications will be verified by inspection, analysis, demonstration, similarity, test or a combination thereof per the Verification Matrix, Appendix 1 (TBD). Verification method selection shall be specified by individual specifications, and documented by appropriate test and evaluation plans and procedures. Verification of compliance to the requirements of this and subsequent specifications will be accomplished by the following methods or combination of methods:

5.2.1 Inspections

Manufactured parts with LIGO identification numbers or marks will be inspected to determine conformity with the procurement specification.

Witness samples will be acceptable proof of the properties of HR and AR coatings applied to the optical surfaces.

5.2.2 Demonstration

The required attenuation characteristics of the assembled Faraday isolator will be demonstrated before installation.

The resonance and damping characteristics of the suspended beam dumps and baffles will be demonstrated before installation.

5.2.3 Test

Appropriate tests will be implemented to verify the specifications of the purchased components. TBD

6 Preparation for Delivery

Packaging and marking of equipment for delivery will be in accordance with the Packaging and Marking procedures specified herein.

6.1 Preparation

- Vacuum preparation procedures as outlined in E960022-B LIGO Vacuum Compatibility, Cleaning Methods and Qualification Procedures will be followed for all components intended for use in vacuum. After wrapping vacuum parts as specified in this document, an additional, protective outer wrapping and provisions for lifting shall be provided.
- Electronic components will be wrapped according to standard procedures for such parts.

6.2 Packaging

Procedures for packaging will ensure cleaning, drying, and preservation methods adequate to prevent deterioration, appropriate protective wrapping, adequate package cushioning, and proper containers. Proper protection will be provided for shipping loads and environmental stress during transportation, hauling and storage. The shipping crates used for large items will use for guidance military specification MIL-C-104B, Crates, Wood; Lumber and Plywood Sheathed, Nailed and Bolted. Passive shock witness gauges will accompany the crates during all transits.

For the viewports, the shipping preparation will include double bagging with Ameristat 1.5TM plastic film (heat sealed seams as practical, with the exception of the inner bag, or tied off, or taped with care taken to insure that the tape does not touch the cleaned part). The bag will be purged with dry nitrogen before sealing.

6.3 Marking

Appropriate identification of the product, both on packages and shipping containers; all markings necessary for delivery and for storage, if applicable; all markings required by regulations, statutes, and common carriers; and all markings necessary for safety and safe delivery will be provided.

Identification of the material will be maintained through all manufacturing processes. Each component will be uniquely identified. The identification will enable the complete history of each component to be maintained (in association with Documentation “travelers”). A record for the optical lever support structures will indicate all weld repairs and fabrication abnormalities.

The specification for marking will state that marking fluids, die stamps and/or electro-etching is not permitted. A vibratory tool with a minimum tip radius of 0.005" is acceptable for marking on surfaces that are not hidden from view. Engraving and stamping are also permitted.

7 Appendix A—Scattered Light Noise Theory

7.1.1 Scattered Light Noise Theory

7.1.1.1 Scattered Light Requirement

A DARM signal is obtained when the differential arm length is modulated as a result of a gravity wave strain. The DARM signal was calculated in reference T060073-00 Transfer Functions of Injected Noise, and is defined by the following expression:

$$V_{signal} := DARM \cdot L \cdot h_{SRD} \cdot \sqrt{P_0}$$

Where L is the arm length, h_{SRD} is the minimum SRD gravity wave strain spectral density requirement, P_0 is the input laser power into the IFO, and DARM is the signal transfer function.

In a similar manner, an apparent signal (scattered light noise) occurs when a scattered light field with a phase shift is injected into the IFO at some particular location, e.g. through the back of the ETM mirror. The scattered light noise is defined by the following expression:

$$V_{noise} := SNXXX \cdot \delta_{SN} \cdot \sqrt{P_{SNi}}$$

P_{SNi} is the scattered light power injected into the IFO mode, δ_{SN} is the phase shift of the injected field, and SNXXX is the noise transfer function for that particular injection location.

The phase shift spectral density of the injected field due to the motion of the scattering surface is given by

$$\delta_{SNi} := \frac{4 \cdot \pi \cdot x_s}{\lambda}$$

where x_s is the spectral density of the horizontal motion of the scattering surface.

In general, the different scattering sources are not coherent and must be added in quadrature. The requirement for scattered light displacement noise can be stated with the following inequality:

$$\sqrt{\sum_{i=1}^{n} \left(\frac{SNXXX}{DARM} \cdot \frac{4 \cdot \pi \cdot x_s}{\lambda} \cdot \sqrt{\frac{P_{SNi}}{P_0}} \right)^2} < \frac{1}{10} \cdot L \cdot h_{SRD}$$

7.1.1.2 Scattered Power into the IFO

The light power scattered into the interferometer from the ith source is calculated as follows:

$$P_{SNi} := P_{in} \cdot BRDF \cdot \Delta\Omega \cdot \frac{w_{IFO}^2}{w_{SN}^2} \cdot T$$

Where P_{in} is the power incident on the scattering surface, BRDF is the fraction of incident light that is scattered per unit solid angle, $\Delta\Omega$ is the solid angle subtended by the mode inside the IFO arm, w_{IFO} is the beam waist of the mode inside the arm, w_{SN} is the beam waist of the beam incident on the scattering surface, and T is the transmissivity of the path from the scattering surface to the injection point in the IFO.

The effective solid angle increases whenever the IFO beam waist has been transformed to a smaller waist by an AOS telescope or some other focusing element in the ISC detection system, because the product of solid angle and beam waist cross-sectional area is proportional to the total radiant flux, which is an optical invariant. Therefore, as the area of the beam waist decreases the solid angle increases proportionally.

7.1.1.2.1 Output Faraday Isolator Scatter

The power incident on the Faraday isolator is given by

$$P_{FIin} := P_0 \cdot G_{AS}$$

G_{AS} is the dark port signal ratio.

The light power scattered into the IFO from the five surfaces before the Faraday rotator magnet is given by

$$P_{FIs} := 5 \cdot P_{FIin} \cdot BRDF_{FI} \cdot \Delta\Omega_{IFO} \cdot \frac{w_0^2}{w_{FI}^2}$$

7.1.1.2.2 Arm Cavity Baffle Surface Scatter

The power incident on each of the arm cavity baffles is given by

$$P_{ACin} := f_{sCOCac} \cdot \frac{P_0}{2} \cdot G_{RC} \cdot G_{AC}$$

where G_{RC} is the recycling cavity power gain and G_{AC} is the arm cavity gain, and f_{sCOCac} is the fractional scattered power from the arm cavity that hits each Arm Cavity Baffle.

The light power scattered from each Arm Cavity Baffle into the mode cross section and re-scattered by the far COC into the IFO mode is given by

$$P_{ACs} := P_{ACin} \cdot BRDF_{AC} \cdot \frac{\pi \cdot w_0^2}{L^2} \cdot BRDF_{COC} \cdot \Delta\Omega_{IFO}$$

7.1.1.2.3 Arm Cavity Baffle Edge Scatter

The power incident on the edges of each arm cavity baffle is given by

$$P_{ACEin} := f_{sCOCace} \cdot \frac{P_0}{2} \cdot G_{RC} \cdot G_{AC}$$

where $f_{sCOCace}$ is the fractional scattered power from the arm cavity that hits the edge of each Arm Cavity Baffle.

The light power scattered into the IFO is given by

$$P_{ACEs} := P_{ACEin} \cdot BRDF_{ACE} \cdot \frac{\pi \cdot w_0^2}{L^2} \cdot BRDF_{COC} \cdot \Delta\Omega_{IFO}$$

7.1.1.2.4 Arm Cavity Baffle Reflected Light

The power reflected from the Arm Cavity Baffle and incident on the vacuum manifold wall is given by

$$P_{ACRin} := f_{sCOCac} \cdot \frac{P_0}{2} \cdot G_{RC} \cdot G_{AC} \cdot R_{AC}$$

where R_{AC} is the net reflectivity of the baffle.

This light will scatter from the wall, reflect from the Arm Cavity Baffle toward the far COC, and finally scatter from the COC into the mode of the IFO. The scattered power is given by

$$P_{ACRs} := P_{ACRin} \cdot BRDF_{VAC} \cdot R_{AC} \cdot \frac{\pi \cdot w_0^2}{L^2} \cdot BRDF_{COC} \cdot \Delta\Omega_{IFO}$$

7.1.1.2.5 ITM Elliptical Baffle Surface Scatter

When the IFO arm cavity is on resonance, the power exiting the arm cavity into the recycling cavity through the ITM is exactly twice the power incident on the ITM from the recycling cavity side. The two counter-propagating beams are exactly 180 degrees out of phase and they interfere at the surface of the ITM. The resultant beam, with a power equal to the recycling cavity arm power, appears to reflect from the ITM back into the recycling cavity.

However, in the actual LIGO IFO the recycling cavity beam has a truncated Gaussian profile with an elliptical shape. Beyond the edges of the sharp elliptical boundary, the Gaussian shaped beam exiting from the arm cavity will strike the elliptical baffle with twice the irradiance of the recycling cavity beam.

The Gaussian irradiance parameter, P_{0itm}, of the beam exiting the ITM is twice the irradiance parameter, P_{0rc}, of the recycling cavity beam.

$$P_{0itm} := 2 \cdot P_{0rc}$$

The exitance function from the ITM is given by

$$I_{ITM}(x, y) := 2 \cdot \frac{P_{0itm}}{\pi \cdot w^2} \cdot e^{-2 \cdot \left(\frac{x^2 + y^2}{w^2} \right)}$$

and the irradiance function inside the recycling cavity arm is given by

$$I_{rc}(x,y) := 2\cdot\frac{P_{0rc}}{\pi\cdot w^2}\cdot e^{-2\cdot\left(\frac{x^2+y^2}{w^2}\right)}$$

The total power exiting from the ITM is

$$P_{itm} := \int_0^R I_{itm}(r)\cdot 2\cdot\pi\cdot r\,dr$$

$$P_{itm} = 2.1084\times 10^3$$

The total power from the exiting ITM beam that passes through the elliptical baffle is

$$P_{ell} := 4\cdot\int_0^b\int_0^{a\cdot\sqrt{1-\frac{y^2}{b^2}}} I_{ITM}(x,y)\,dx\,dy$$

Then, the power that hits the elliptical baffle from the ITM side is the difference

$$P_{ellbaf} := P_{itm} - P_{ell}$$

$$P_{ellbaf} = 1.4\ \text{W}$$

The light power scattered from the Elliptical Baffle into the IFO mode at the far COC is given by

$$P_{ells} := P_{ellbaf}\,BRDF_{ellbaf}\,T_{itm}\cdot\frac{\pi\cdot w_0^2}{L^2}$$

where T_{itm} is the transmissivity of the ITM mirror.

7.1.1.2.6 ITM Elliptical Baffle Edge Scatter

The elliptical baffle is inclined 10 deg vertically. This causes the elliptical boundary of the back surface of the hole to be displaced vertically, exposing a crescent border around the lower half of the baffle.

For a baffle of thickness t, the vertical displacement of the back surface of the hole is given by

$$\Delta y := t\cdot\sin\left(10\cdot\frac{\pi}{180}\right)$$

The power from the ITM that traverses the front surface of the lower half of the baffle is given by

$$P_{ellef} := 2 \cdot \int_0^b \int_0^{(a)\cdot\sqrt{1-\frac{y^2}{b^2}}} I_{ITM}(x,y)\,dx\,dy$$

The power from the ITM that traverses the back surface of the lower half of the baffle is given by

$$P_{elleb} := 2 \cdot \int_0^{b-\Delta y} \int_0^{(a)\cdot\sqrt{1-\frac{(y-\Delta y)^2}{(b)^2}}} I_{ITM}(x,y)\,dx\,dy$$

The power hitting the edge is the difference

$$P_{elledge} := P_{elleb} - P_{ellef}$$

$$P_{elledge} = 0.018\ W$$

The light power scattered into the IFO at the far COC is given by

$$P_{elledges} := P_{elledge} \cdot BRDF_{elledge} \cdot T_{itm} \cdot \frac{\pi \cdot w_0^2}{L^2}$$

Where $BRDF_{elledge}$ is the scattering property of the elliptical baffle edge.

7.1.1.2.7 ITM Elliptical Baffle Reflected Light

The power reflected from the Elliptical Baffle and incident on the vacuum manifold wall is given by

$$P_{ellbafRin} := P_{ellbaf} \cdot R_{ellbaf}$$

where R_{ellbaf} is the reflectivity of the baffle surface.

The light will scatter from the wall, reflect from the Elliptical Baffle, and transmit through the ITM into the mode of the IFO at the far COC. The scattered power is given by

$$P_{elleRs} := P_{ellbafRin} \cdot BRDF_{VAC} \cdot R_{ellbaf} \cdot T_{itm} \cdot \frac{\pi \cdot w_0^2}{L^2}$$

7.1.1.2.8 PRM Elliptical Baffle

The light incident on the PRM Elliptical Baffle from the PRM mirror side is given by

$$P_{prmellin} := \eta_{prmell} P_{REFL}$$

where P_{REFL} is the input power reflected from the PRM and η_{prmell} is the fraction of the REFL beam power that is intercepted by the PRM Elliptical Baffle.

The power scattered into the IFO mode in the recycling cavity is given by

$$P_{prmells} := P_{prmellbaf} BRDF_{prmellbaf} T_{prm} \cdot \frac{\pi \cdot w_0^2}{L^2}$$

7.1.1.2.9 ITM Wide-Angle Scatter

7.1.1.2.9.1 Scattering from the manifold chamber walls

The arm cavity baffle will block most of the wide-angle scattered light from point defects in the ITM except for the light that goes through the beam tube holes in the baffle. The scattered light passing through the holes and incident onto the ITM Manifold walls is given by

$$P_{manwin}(\alpha) := P_{ac} \cdot BRDF_{cocwide}(\alpha, \theta) \cdot \Delta\Omega_{acb}$$

where, P_{ac} is the power circulating in the arm, $BRDF_{cocwide}$ is the wide-angle Lambertian scatter function for the ITM, and $\Delta\Omega_{acb}$ is the solid angle subtended by the two holes in the arm cavity baffle.

$$BRDF_{cocwide}(\alpha, \theta) := \frac{\alpha \cdot \cos(\theta)}{\pi}$$

The power scattered back to the surface of the ITM into the area of the mode is given by

$$P_{manwsitm}(\alpha) := P_{manwin}(\alpha) \cdot BRDF_{wall} \frac{\pi \cdot w_0^2}{L_w^2}$$

And the power scattered into the IFO mode is given by

$$P_{manwsifos}(\alpha) := P_{manwsitm}(\alpha) \cdot BRDF_{cocwide}(\alpha, \theta) \cdot \Delta\Omega$$

7.1.1.2.9.2 Retro-reflection from the ITM Manifold Spool Piece

The power incident on the spool piece at the end of the ITM manifold is given by

$$P_{manspin}(\alpha) := P_{ac} \cdot BRDF_{cocwide}(\alpha, \theta) \cdot \Omega_{sp}$$

$$\Omega_{sp} := \frac{A_{sp}}{L_{sp}^{2}}$$

is the solid angle subtended by the frontal area A_{sp} of the spool-piece, located a distance L_{sp} from the ITM.

Assuming that all this power is retro-reflected back to the ITM surface, the power scattered from the ITM into the IFO mode is given by

$$P_{mansprifos}(\alpha) := P_{manspin}(\alpha) \cdot BRDF_{cocwide}(\alpha, \theta) \cdot \Delta\Omega$$

7.1.1.2.9.3 Scatter from ITM Manifold Baffle

A baffle will be placed at the end of the manifold to intercept the light that would have hit the surface of the spool piece. The power incident on the Manifold Baffle is

$$P_{manbafin}(\alpha) := P_{manspin}(\alpha)$$

The power scattered back to the ITM into the area of the mode is given by

$$P_{manbafsitm}(\alpha) := P_{manbafin}(\alpha) \cdot BRDF_{baf} \cdot \frac{\pi \cdot w_0^{2}}{L_{sp}^{2}}$$

where $BRDF_{baf}$ is the BRDF of the baffle.

And the power scattered into the IFO mode is given by

$$P_{manbafifos}(\alpha) := P_{manbafsitm}(\alpha) \cdot BRDF_{cocwide}(\alpha, \theta) \cdot \Delta\Omega$$

7.1.1.2.9.4 ETM Manifold Baffle

A manifold baffle will also be placed in the manifold near the ETM. The calculation for the wide-angle scattered light from the ETM onto the manifold walls and from the ETM Manifold Baffle is similar as that for the ITM, with the appropriate length between the ETM and the ETM manifold spool-piece.

7.1.1.2.10 Brewster's Window

7.1.1.2.10.1 AS2 Brewster's Window

The power incident on the AS2 Brewster's window is given by

$$P_{AS2} := P_0 \cdot G_{AS}$$

where G_{AS} is the fractional input power that exits the antisymmetric port.

The light power scattered into the IFO mode from the two surfaces of the AS2 Brewster's window is given by

$$P_{ASBrews} := 2 \cdot P_{AS2} \cdot BRDF_{Brew} \cdot \Delta\Omega_{IFO} \cdot \frac{w_0^2}{w_{FI}^2} \cdot T_{FI}$$

where T_{FI} is the reverse transmissivity of the Faraday Isolator, and w_{FI} is the beam waist radius after the OMMT.

7.1.1.2.10.2 AS2 Brewster's Window Reflection

The reflected power incident on the AS2 Brewster's window nozzle is given by

$$P_{BrewRin} := 2 \cdot P_{AS2} \cdot R_{Brew}$$

where R_{Brew} is the Fresnel reflectivity of the Brewster's window surface.

The light power scattered into the IFO mode from the AS2 Brewster's window nozzle is given by

$$P_{BrewRs} := P_{BrewRin} BRDF_{nozzle} \Delta\Omega_{IFO} \cdot \frac{w_0^2}{w_{FI}^2} \cdot R_{Brew} \cdot T_{FI}$$

7.1.1.2.10.3 ITMX PO Brewster's Window

The power incident on the ITMX PO Brewster's window is given by

$$P_{ITMPO} := P_0 \cdot \frac{G_{AC}}{2} \cdot R_{ITMAR}$$

The light power scattered into the IFO mode from the two ITMX PO Brewster's window surfaces is given by

$$P_{ITMPOBrews} := 2 \cdot P_{ITMPO} \cdot BRDF_{Brew} \cdot \Delta\Omega_{IFO} \cdot \frac{w_0^2}{w_{ITMPO}^2}$$

7.1.1.2.10.4 BS PO Brewster's Window

The power incident on the BS PO Brewster's window is given by

$$P_{BSPO} := P_0 \cdot G_{AC} \cdot \left(1 - R_{BSHR}\right)^2 \cdot R_{BSAR}$$

The light power scattered into the IFO mode from the two BS PO Brewster's window surfaces is given by

$$P_{BSPOBrews} := 2 \cdot P_{BSPO} \cdot BRDF_{Brew} \cdot \Delta\Omega_{IFO} \cdot \frac{w_0^2}{w_{BSPO}^2}$$

7.1.1.2.11 Output Mode Matching Telescope, OMMT

The power incident on OMMT2 is given by

$$P_{OMMT2in} := P_0 \cdot G_{AS}$$

The light power scattered into the IFO mode from the OMMT2 mirror is given by

$$P_{OMMT2s} := P_{OMMT2in} \cdot BRDF_{OMMT2} \cdot \Delta\Omega_{IFO} \cdot \frac{w_0^2}{w_{FI}^2}$$

7.1.1.2.12 Cavity Beam Dumps

7.1.1.2.12.1 Un-dumped Cavity Beam Dump Beam

The power in the portion of the ghost beam that misses the Cavity Beam Dump is given by

$$P_{mbd} := f_{mbd} \cdot P_{GB}$$

where f_{mbd} is the fraction of the ghost beam that misses the beam dump, and P_{GB} is the power in the ghost beam.

The power that scatters from the chamber wall into the IFO mode is given by

$$P_{mbds} := P_{mbd} \cdot BRDF_{wall} \cdot \Delta\Omega_{IFO} \cdot T_{GB}$$

where T_{GB} is the transmissivity of the return path to the point where the ghost beam originated.

7.1.1.2.12.2 ITMYAR1

The power incident on ITMYAR1 Beam Dump is given by

$$P_{ITMAR1} := \frac{P_0}{2} \cdot G_{RC} \cdot R_{ITMAR}$$

The light power scattered into the IFO from the ITMY Beam Dump is given by

$$P_{ITMAR1s} := P_{ITMAR1} \cdot BRDF_{BD} \cdot \Delta\Omega_{IFO} \cdot R_{ITMAR}$$

7.1.1.2.12.3 ITMAR3

The power incident on ITMAR3 Beam Dump is given by

$$P_{ITMAR3} := \frac{P_0}{2} \cdot G_{RC} \cdot \left(1 - R_{ITMAR}\right)^2 \cdot R_{ITMHR}^2 \cdot R_{ITMAR}$$

The light power scattered into the IFO from the ITMY Beam Dump is given by

$$P_{ITMAR3s} := P_{ITMAR3} \cdot BRDF_{BD} \cdot \Delta\Omega_{IFO} \cdot \left(1 - R_{ITMAR}\right)^2 \cdot R_{ITMHR}^2 \cdot R_{ITMAR}$$

7.1.1.2.12.4 ITMHR3

The power incident on ITMHR3 Beam Dump is given by

$$P_{ITMHR3} := \frac{P_0}{2} \cdot G_{RC} \cdot \left(1 - R_{ITMAR}\right) \cdot R_{ITMHR} \cdot R_{ITMAR} \cdot \left(1 - R_{ITMHR}\right)$$

The light power scattered into the IFO from the ITMY Beam Dump is given by

$$P_{ITMHR3s} := P_{ITMHR3} \cdot BRDF_{BD} \cdot \Delta\Omega_{IFO} \cdot \left(1 - R_{ITMAR}\right) \cdot R_{ITMHR} \cdot R_{ITMAR} \cdot \left(1 - R_{ITMHR}\right)$$

7.1.1.2.12.5 BSAR1

The power incident on the BSAR1 beam dump is given by

$$P_{BSAR1in} := P_0 \cdot G_{RC} \cdot R_{BSAR}$$

The light power scattered into the IFO from the BS GBAR1 beam dump is given by

$$P_{BSAR1s} := P_{BSAR1in} BRDF_{BD} \cdot \Delta\Omega_{IFO} \cdot R_{BSAR}$$

7.1.1.2.12.6 BSAR3X

The power incident on the BSAR3X beam dump is given by

$$P_{GBAR3Xin} := P_0 \cdot G_{RC} \cdot \left(1 - R_{BSHR}\right) \cdot R_{BSAR} \cdot R_{BSHR} \cdot \left(1 - R_{BSAR}\right)$$

The light power scattered into the IFO from the BS GBAR3X beam dump is given by

$$P_{GBAR3Xs} := P_{GBAR3Xin} BRDF_{BD} \cdot \Delta\Omega_{IFO} \cdot \left(1 - R_{BSAR}\right) \cdot R_{BSHR} \cdot R_{BSAR} \cdot \left(1 - R_{BSHR}\right)$$

7.1.1.2.12.7 BSAR3P

The power incident on the BSAR3P beam dump from the two coincident beams is given by

$$P_{BSAR3Pin} := \frac{P_0}{2} \cdot G_{RC} \cdot \left[\left(1 - R_{BSAR}\right)^2 \cdot R_{BSHR}^2 \cdot R_{BSAR} + \left(1 - R_{BSHR}\right) \cdot R_{BSAR} \cdot R_{BSHR} \cdot \left(1 - R_{BSAR}\right)\right]$$

The light power scattered into the IFO from the BSAR3P beam dump is given by

$$P_{BSAR3Ps} := P_{BSAR3Pin} \cdot BRDF_{BD} \cdot \Delta\Omega_{IFO} \cdot \left(1 - R_{BSAR}\right)^2 \cdot R_{BSHR}^2 \cdot R_{BSAR}$$

7.1.1.2.12.8 BSHR3P

The power incident on the BSHR3P beam dump from the two coincident beams is given by

$$P_{BSHR3Pin} := \frac{P_0}{2} \cdot G_{RC} \cdot \left[\left(1 - R_{BSHR}\right)^2 \cdot R_{BSAR} + \left(1 - R_{BSHR}\right) \cdot R_{BSAR} \cdot R_{BSHR} \cdot \left(1 - R_{BSAR}\right)\right]$$

The light power scattered into the IFO from the BSHR3P beam dump is given by

$$P_{BSHR3Ps} := P_{BSAR3Pin} \cdot BRDF_{BD} \cdot \Delta\Omega_{IFO} \cdot \left(1 - R_{BSHR}\right)^2 \cdot R_{BSAR}$$

7.1.1.2.12.9 ITMAR4

The power incident on the ITMAR4 beam dump is given by

$$P_{ITMAR4} := \frac{P_0}{2} \cdot G_{RC} \cdot \left(1 - R_{ITMAR}\right)^2 \cdot R_{ITMHR}^3 \cdot R_{ITMAR}^2$$

The light power scattered into the IFO from the ITMAR4 beam dump is given by

$$P_{ITMAR4s} := P_{ITMAR4} \cdot BRDF_{BD} \cdot \Delta\Omega_{IFO} \cdot \left(1 - R_{ITMAR}\right)^2 \cdot R_{ITMHR}^3 \cdot R_{ITMAR}^2$$

7.1.1.2.12.10 ITMHR4

The power incident on the ITMHR4 beam dump is given by

$$P_{ITMHR4} := \frac{P_0}{2} \cdot G_{RC} \cdot \left(1 - R_{ITMAR}\right) \cdot R_{ITMHR}^2 \cdot R_{ITMAR}^2$$

The light power scattered into the IFO from the ITMHR4 beam dump is given by

$$P_{ITMHR4s} := P_{ITMAR4} \cdot BRDF_{BD} \cdot \Delta\Omega_{IFO} \cdot \left(1 - R_{ITMAR}\right) \cdot R_{ITMHR}^2 \cdot R_{ITMAR}^2$$

7.1.1.2.12.11 BSAR4X

The power incident on the BSAR4X beam dump is given by

$$P_{BSAR4Xin} := P_0 \cdot G_{RC} \cdot \left(1 - R_{BSHR}\right) \cdot R_{BSAR}^2 \cdot R_{BSHR}^2 \cdot \left(1 - R_{BSAR}\right)$$

The light power scattered into the IFO from the ITMHR4 beam dump is given by

$$P_{BSAR4Xs} := P_{BSAR3Xin} \cdot BRDF_{BD} \cdot \Delta\Omega_{IFO} \cdot \left(1 - R_{BSAR}\right) \cdot R_{BSHR}^2 \cdot R_{BSAR}^2 \cdot \left(1 - R_{BSHR}\right)$$

7.1.1.2.12.12 Cryopump Baffle

The power incident on the Cryopump Baffle is given by

$$P_{cp} := \eta_{lcp} \cdot P_{ac}$$

where η_{lcp} is the scattered loss ratio from the arm power to the Cryopump Baffle surface.

The light power scattered into the IFO from the Cryopump Baffle is given by

$$P_{cps} := P_{cp} \cdot BRDF_{cp} \cdot \pi \cdot \frac{w_0^2}{L^2} \cdot BRDF_{COC} \cdot \Delta\Omega_{IFO}$$

The power reflected by the Cryopump Baffle and incident on the spool piece wall is given by

$$P_{cpr} := R_{cpb} \cdot P_{cp}$$

where R_{cpb} is the reflectivity of the Cryopump Baffle.

The light power scattered into the IFO from the wall is given by

$$P_{cprs} := P_{cpr} \cdot BRDF_{wall} \pi \cdot \frac{w_0^2}{L^2} \cdot R_{cpb} \cdot BRDF_{COC} \cdot \Delta\Omega_{IFO}$$

The power incident on the Cryopump Baffle edge is given by

$$P_{cpeg} := \eta_{lcpeg} \cdot P_a$$

where η_{lcpeg} is the scattered loss ratio from the arm power to the Cryopump Baffle edge surface.

The light power scattered into the IFO from the Cryopump Baffle edge is given by

$$P_{cpegs} := P_{cpeg} \cdot BRDF_{cpeg} \cdot \pi \cdot \frac{w_0^2}{L^2} \cdot BRDF_{COC} \cdot \Delta\Omega_{IFO}$$

7.1.1.2.12.13 ETM Telescope Baffle

The power incident on the ETM Telescope Baffle is given by

$$P_{etmbaf} := P_a \cdot T_{etm} \cdot \eta_{etmbaf}$$

where P_a is the power in the arm cavity, T_{etm} is the transmissivity of the ETM mirror, and η_{etmbaf} is the fractional power that hits the ETM Telescope Baffle.

The light power scattered into the IFO from the ETM Telescope Baffle is given by

$$P_{etmbafs} := P_{etmbaf} BRDF_{etmbaf} T_{etm} \pi \cdot \frac{w_0^2}{L^2}$$

The power reflected by the ETM Telescope Baffle and incident on the chamber wall is given by

$$P_{etmbafr} := R_{etmbaf} \cdot P_{etmbai}$$

where R_{etmbaf} is the reflectivity of the ETM Telescope Baffle.

The light power scattered into the IFO from the wall is given by

$$P_{etmbafrs} := P_{etmbafr} \cdot BRDF_{wall} \cdot R_{etmbaf} \cdot T_{etm} \cdot \pi \cdot \frac{w_0^2}{L^2}$$

The power incident on the ETM Telescope Baffle edge is given by

$$P_{etmbafeg} := P_a \cdot T_{etm} \cdot \eta_{etmbafeg}$$

where $\eta_{etmbafeg}$ is the scattered loss ratio from the arm power to the ETM Telescope Baffle edge surface.

The light power scattered into the IFO from the ETM Telescope Baffle edge is given by

$$P_{etmbafegs} := P_{etmbafeg} \cdot BRDF_{etmbafeg} \cdot T_{etm} \cdot \pi \cdot \frac{w_0^2}{L^2}$$

7.1.1.2.13 Fringe-Wrapping

In the small phase-shift approximation the temporal DARM signal (noise) due to light scattered into the IFO mode is

$$S_{SN}(t) := SNXXX \cdot E_{SN} \cdot \frac{4 \cdot \pi}{\lambda} \cdot x_g \cdot A_{SEIi} \cdot \sin\left(2 \cdot \pi \cdot f_0 \cdot t\right)$$

The motion of the scattering surface is written as the underlying ground seismic motion, x_g , times the motion amplitude transfer function of the scattering surface, A_{SEIi} .

The amplitude displacement spectral density is given by the following expression with the transfer coefficient calculated by Hiro (T060073-00 Transfer Functions of Injected Noise)

$$S_{SN}\left(f_0\right) := SNXXX \cdot E_{SN} \cdot \frac{4 \cdot \pi}{\lambda} \cdot x_g\left(f_0\right) \cdot A_{SEIi}$$

When the horizontal displacement of the scattering surface exceeds λ/8, the amplitude of the noise no longer increases at the frequency of the scattering surface motion, but becomes non-sinusoidal and is up-converted to noise at odd harmonics of the scattering surface motion frequency. This phenomenon is called fringe-wrapping.

$$S_{SN}(t) := SNXXX \cdot E_{SN} \cdot \sin\left(\frac{4 \cdot \pi}{\lambda} \cdot x_g \cdot A_{SEIi} \cdot \sin\left(2 \cdot \pi \cdot f_0 \cdot t\right)\right)$$

We will assume that the transfer functions SNXXX are valid for large phase-shift signals.

This time function is represented exactly by the Bessel series expansion in odd harmonics of the scattering surface frequency, f_0, with amplitudes given by the Bessel functions of integral order $n=m_n$ and argument θ.

$$S_{SN}(t) := S_B(\theta, t)$$

$$S_B(\theta, t) := 2 \cdot \sum_n \left(Jn(m_n, \theta) \cdot \sin(2 \cdot \pi \cdot m_n \cdot f_0 \cdot t) \right)$$

$$\theta := \frac{4 \cdot \pi}{\lambda} \cdot x_g \cdot A_{SEI}$$

$$m_n := 2 \cdot n - 1$$

At the onset of fringe-wrapping, a significant distortion of the noise temporal waveform has already occurred, as shown in Figure 51, with the generation of up-converted noise at odd harmonics of the surface motion. The actual time signal and the Bessel function representation of the time signal are plotted in the figure and agree exactly.

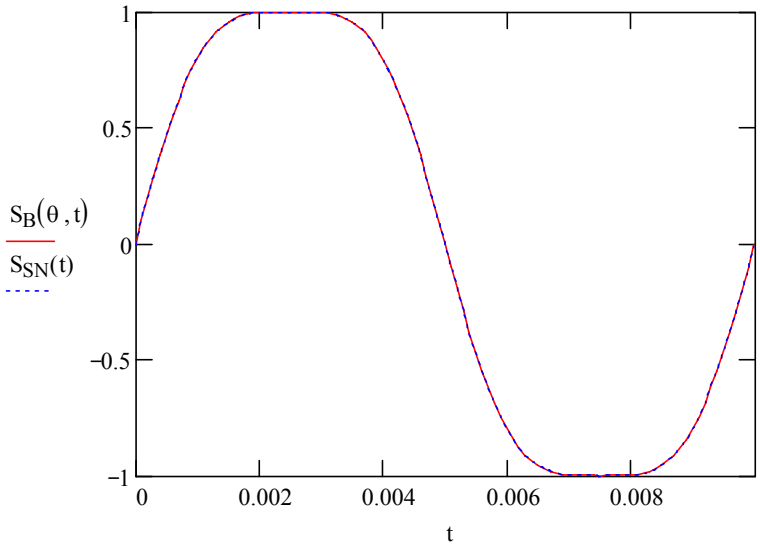

Figure 51: Noise Waveform at the Onset of Fringe-Wrapping, λ/8

If the displacement of the scattering surface is increased to λ/4, the fringe-wrapping becomes clearly visible, as shown in Figure 52. The fundamental and the third harmonic contribute most of the noise, as seen by the coefficients of the Bessel functions in the adjacent table.

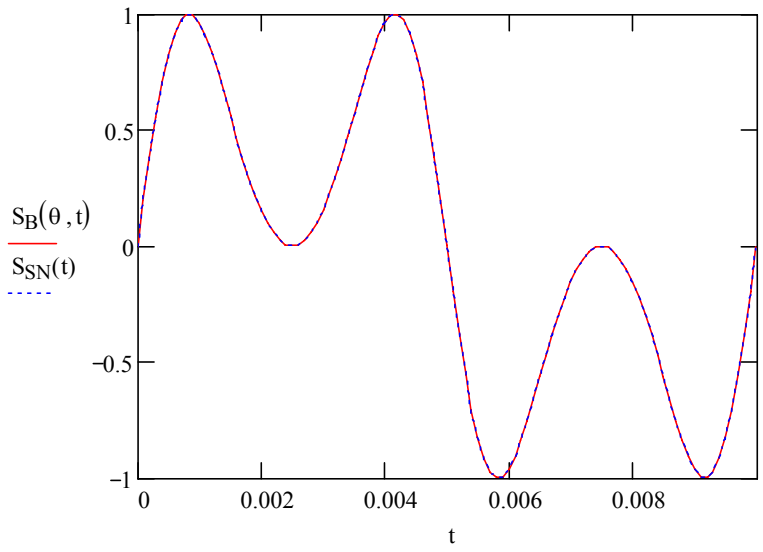

m =

	0
0	0
1	1
2	3
3	5
4	7
5	9
6	11
7	13
8	15
9	17
10	19
11	21

$Jn(m_n, \theta) =$

0.285
0.333
0.052
$3.42 \cdot 10^{-3}$
$1.25 \cdot 10^{-4}$
$2.925 \cdot 10^{-6}$
$4.767 \cdot 10^{-8}$
$5.728 \cdot 10^{-10}$
$5.287 \cdot 10^{-12}$
$3.868 \cdot 10^{-14}$
0

Figure 52: Displacement Noise waveform with Fringe-wrapping, λ/4

The displacement spectral density, m/rt Hz, of the fringe-wrapped signal (noise) at an up-converted frequency is given by the Bessel function series

$$S_{SNsum}(f) := E_{SN} \cdot SNXXX \cdot 2 \cdot \sum_n \left| Jn\left(m_n, \theta\left(\frac{f}{m_n}\right)\right)\right|$$

Note that the Bessel function phase is evaluated by using the motion of the surface at the lower frequency that corresponds to an odd multiple of the up-converted frequency.

7.1.1.2.13.1 Damped Pendulum Example

Assume that the scattering surface is suspended from a damped, simple pendulum with resonant frequency = 1 Hz, Q = 1000; and the displacement spectral density of the suspension point x_g is 1E-7 m/ rt Hz.

The amplitude response of the pendulum is given by

$$A_{SEI}(f) := \left| \frac{1}{1 + i \cdot \frac{f}{Q \cdot f_0} - \left(\frac{f}{f_0}\right)^2} \right|$$

The calculated noise displacement spectral density is shown in Figure 53. The displacement phase of the fundamental disturbance is shown in red, shifted upwards slightly in the graph for clarity. Additional displacement noise caused by fringe-wrapping is evident at the 3rd and 5th harmonics of the fundamental disturbance. The total displacement noise is shown in cyan.

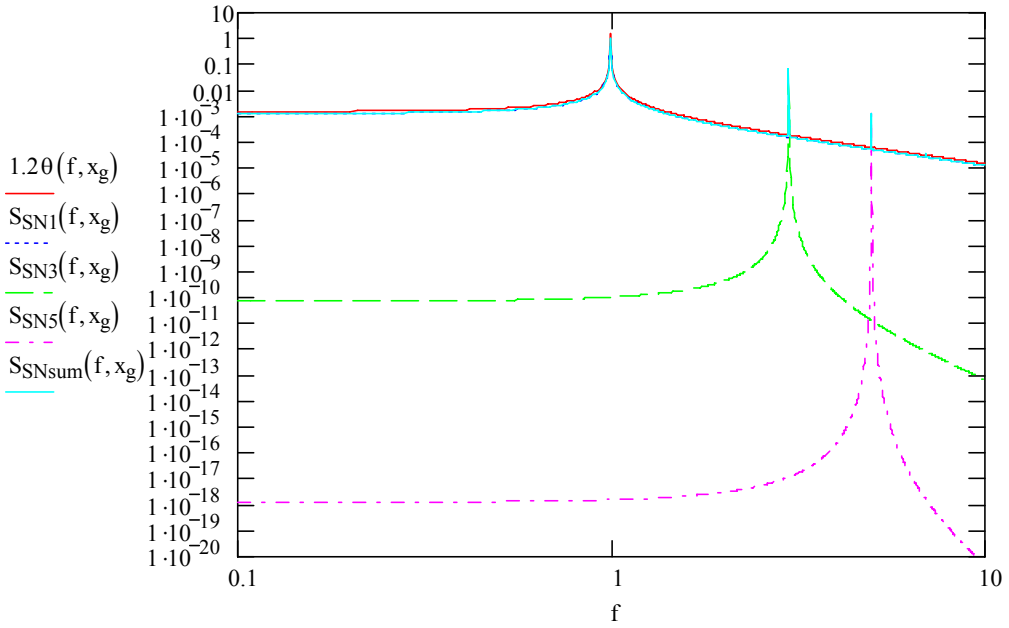

Figure 53: Scattered Light Displacement Noise Caused by Fringe-wrapping

7.1.1.3 Scattered Light Parameters

The IFO parameters that were used for the scattered light calculations are listed in Table 18.

Table 18: IFO parameter values used for scattered light calculation

PARAMETER	VALUE
IFO_length	4.00E+03
IFO_beamwaist	1.15E-02
IFO_beam_waist_RC	6.00E-02
beam_radius_ITM	6.00E-02
beam_waist_photodetector	5.00E-03
beam_radius_Faraday	2.10E-03
beam_radius_OMC	5.00E-04
lambda	1.06E-06
IFO_diffraction_angle	2.95E-05
IFO_solid_angle	2.72E-09
laser_power	1.25E+02
recycling_cavity_power_gain	1.69E+01
reflected_port_power_ratio	1.00E-03

PARAMETER	VALUE
dark_port_signal_ratio	1.08E-03
recycling_cavity_power	2.11E+03
arm_cavity_power	8.34E+05
ETM_transmitted_power	1.25E+01
reflected_port_power	1.25E-01
dark_port_power	1.35E-01
ITM_transmissivity	5.00E-03
ITM_HR	9.95E-01
ETM_transmissivity	1.50E-05
ETM_Reflectivity	1.00E+00
PRM_AR_reflectivity	5.00E-04
PRM_transmissivity	2.12E-01
SRM_AR_reflectivity	5.00E-04
SRM_HR_reflectivity	9.60E-01
SRM_transmissivity	4.00E-02
diameter_ETM	3.40E-01
diameter_ITM	3.40E-01
diameter_PRM	2.85E-01
diameter_SRM	2.85E-01
diameter_MMT3	2.85E-01
Radius_Inner_Cryo	3.85E-01
Radius_Edge_Cryo	3.88E-01
Radius_Beam_Tube	5.31E-01
area_arm_cav_baffle	6.95E-01
length_armcavbaf_wall	4.40E+00
manifold_wall_length	1.40E+01
manifold_wall_angle	6.64E-02
Radius_Inner_Spoolpiece	5.70E-01
Radius_Outer_Spoolpiece	9.30E-01
Spoolpiece_length	2.80E+01
Spoolpiece_frontal_area	1.70E+00
Spoolpiece_solid_angle	2.16E-03
Area_Arm_Cav_Baf_Hole	9.08E-02
Length_Arm_Cav_Baf	1.00E+00

PARAMETER	VALUE
Solid_Angle_COC_Wide_Angle	1.82E-01
AP2_lens_focal_length	1.00E-01
lens_AR_reflectivity	2.50E-03
scatter_loss_Brewster_window	4.00E-05
incident_angle_Faraday_crystal	1.70E-02
back_transmission_Faraday_Isolator	1.00E-03
Faraday_Tranmission	9.00E-01
transmission_ETM_path	1.00E-02
BRDF_elliptical_baffle_edge	1.00E-01
BRDF_ETM_Tel_Baffle_Edge	1.00E-01
BRDF_chamber_walls	1.00E-01
BRDF_Nozzle	1.00E-01
BRDF_photodetector	1.00E-03
BRDF_ITMX_PO_steer_mirror	1.00E-05
BRDF_COC_30urad	1.94E+03
BRDF_elliptical_baffle	1.00E-02
BRDF_arm_cav_baffle	1.00E-03
BRDF_cryopump_baffle	1.00E-02
BRDF_cryopump_baffle_edge	1.00E-01
BRDF_Brewster_window	5.00E-06
BRDF_beam_dump	1.00E-03
BRDF_ETM_Tel_Baffle	1.00E-01
BRDF_ETM_Tel_Baffle_Edge	1.00E-01
BRDF_lens	1.00E+03
BRDF_Faraday	4.92E-04
BRDF_manifold_baffle	1.00E-02
BRDF_OMMT2	3.00E-03
BRDF_Faraday	4.92E-04
BRDF_COC_wide_angle	4.76E-06
a	1.09E-01
b	1.23E-01
w	6.00E-02
h	1.23E-01
fraction_power_missed_ghost_beam	1.00E-04

PARAMETER	VALUE
fraction_power_ghost_beam	1.00E+00
N_Cryopump_Baffles	4.00E+00
N_Arm_Cavity_Baffle	4.00E+00
N_Elliptical_Baffle	2.00E+00
N_ETM_Tel_Baffle	2.00E+00
N_Manifold	4.00E+00
N_Surfaces_Faraday	5.00E+00
N_Surfaces_Brewster	2.00E+00
Scatter_Efficiency_Cryo_Baffle	3.32E-06
Scatter_Efficiency_Cryo_Baffle_Edge	8.85E-08
Scatter_Efficiency_AC_Baffle	8.79E-06
Scatter_Efficiency_AC_Baffle_Edge	4.20E-08
Scatter_Efficiency_Ellip_Baffle	6.65E-04
Scatter_Efficiency_Ellip_edge	8.54E-06
Scatter_Efficiency_ETM_Tel_Baffle	1.69E-01
Scatter_Efficiency_ETM_Tel_Baffle_edge	7.80E-04
Scatter_Efficiency_PRM_Ellip_Baffle	1.00E-06
Scatter_Efficiency_Wide_Angle	1.50E-05
cryopump_sus_length	4.00E-01
cryopump_sus_freq	7.88E-01
cryopump_sus_Q	1.00E+03
arm_cavity_baf_sus_length	8.00E-01
arm_cavity_baf_sus_freq	2.50E+00
arm_cavity_baf_sus_Q	1.00E+03
ellip_baf_sus_length	1.00E+00
ellip_baf_sus_freq	4.98E-01
ellip_baf_sus_Q	1.00E+03
cav_bd_sus_length	1.00E+00
cav_bd_sus_freq	4.98E-01
cav_bd_sus_Q	1.00E+02
Faraday_sus_length	4.00E-01
Faraday_sus_freq	7.88E-01
Faraday_sus_Q	1.00E+02
OMMT2_sus_length	2.50E-01

PARAMETER	VALUE
OMMT2_sus_freq	9.96E-01
OMMT2_sus_Q	1.00E+01
reflectivity_ellip_baffle	1.00E-03
reflectivity_arm_cav_baffle	1.00E-02
reflectivity_cryopump_baffle	1.00E-02
reflectivity_spoolpiece	5.00E-01
reflectivity_cavity_beam_dump	5.00E-03
Reflectivity_Brewster	4.00E-04
reflectivity_ETM_Tel_Baffle	2.50E-03
reflectivity_manifold_baffle	2.50E-01
Reflectivity_Faraday_AR	2.50E-03